STUDY ON CRACKING BEHAVIOR OF CONCRETE DUE TO REBAR CORROSION

TRAN Kim Khoa

STUDY ON CRACKING BEHAVIOR OF CONCRETE DUE TO REBAR CORROSION

By

TRAN Kim Khoa

A dissertation submitted to Nagoya University in a partial fulfillment of the requirements for the Degree of Doctor of Engineering

Department of Civil Engineering
Graduate School of Engineering, Nagoya University
JAPAN

March, 2012

ACKNOWLEDGEMENTS

Foremost, I would like to express my deepest gratitude to Prof. Hikaru NAKAMURA, my principal advisor, for his invaluable guidance, continuous support and encouragement throughout my study in Nagoya University. He has also given me an inspiration in the science research, especially in the field of the concrete structure. Surely, without his supports and patient, the dissertation has never been completed. I would like to thank Prof. Minoru KUNIEDA for his invaluable comments and advices during my research in the concrete structure laboratory. I also wish to express my sincere thanks to the other examination committee members including Prof. Yoshito ITOH and Prof. Yuichi UCHIDA for their valuable comments and advices. I am very grateful to the kindness, continuous helps and the friendship of Dr. Naoshi UEDA during my study in the laboratory. I also want to thank the former and the current students of the concrete structure laboratory for their helps and supports on my study and my daily life in Japan. I would like to thank the laboratory of Pro. ITOH for providing the laser equipment for my study. The supports from the staff of Graduate School of Engineering are also much appreciated.

I would like to thank Nikken Sekkei Civil Engineering Ltd. for their supports to my study and my family during our stay in Japan. I would like to thank the seniors and the staff of the company for their kindness and valuable helps.

I gratefully acknowledge NGK Insulators Ltd. for providing me a scholarship for my study in Japan. Their finance support is very much appreciated.

I want to thank our families in Vietnam for their supports, understanding and encouragements to my own family during the time we stay in Japan. I am also grateful to the helps from the Japanese and Vietnamese friends in Nagoya during our stay here.

Last but not least, behind the accomplishment, I would like to express my deep thanks to my parents, Mr. TRAN Duc Duong and Mrs. NGUYEN Thi Kheo for their love, trust and hope on me. I want to extend my hearty appreciation to my dear wife, Mrs. LE Thi Anh Nguyet and our lovely daughter TRAN Kim Gia Binh for their endless loves, patient, continuous encouragement and supports in my life.

ABSTRACT

In recent years, cracking of concrete due to rebar corrosion has become a major deterioration behavior in concrete structures. Such cracking typically accelerates the corrosion and deterioration processes, and can involve spalling of the concrete cover. It is necessary to assess internal damage from observable surface conditions during maintenance procedures. Therefore, it is desirable to establish a prediction method that can qualitatively and quantitatively evaluate internal crack propagation behavior and the rebar corrosion amount from observing surface cracks.

In this study, crack propagation behavior due to rebar corrosion is evaluated both experimentally and analytically.

In the experiment, various specimens are tested by using electric means and the propagation of cracks is monitored. Surface crack widths are then measured and internal crack patterns are observed at several rebar corrosion amounts. In addition, deformation of the specimen surface is measured using a laser displacement meter to understand relationship between surface deformation and crack propagation.

In the analysis, crack propagation behavior was simulated using the Rigid-Body-Spring-Method (RBSM) with three-dimensional Voronoi particles. A three-phase material model including rebar, corrosion products layer and concrete is proposed. For the corrosion products layer, internal expansion pressure due to corrosion expansion is modeled by the initial strain problem and the properties of the corrosion products layer are recommended. Moreover, effects of penetration of corrosion products into cracks, local corrosion and local penetration of corrosion products into cracks

during the corrosion process are simulated and the effects are quantitatively evaluated. The applicability of the model is verified by comparison with the experimental results. As a result, the effects of modeling and the mechanism of crack propagation such as crack initiation, progress of surface crack width, propagation behavior of internal cracks and the effect of internal cracks on surface crack width are clarified.

Effects of several factors such as rebar diameter, concrete cover thickness, specimen size and local corrosion length of rebar on crack propagation behavior of the single-rebar specimens are investigated experimentally and analytically. It was found that the rebar diameter affects the crack initiation and propagation; the cover thickness affects the internal crack patterns; the specimen size affect the surface crack propagation and internal crack propagation; the local corrosion length of rebar induces three-dimensional cracking behavior and de-lamination phenomenon on concrete cover and in this case, concrete cover plays an important role on surface de-laminated area. However, only ratio of concrete cover to rebar diameter cannot evaluate or predict crack width propagation.

Moreover, the applicability of the analytical model is confirmed in terms of crack patterns, surface crack width and internal crack propagation due to multi-rebar corrosion by the experiments of beams having multi-rebars. A mechanism of crack propagation in concrete due to multi-rebar corrosion is analytically investigated. As a result, it is found that rebar spacing strongly affects crack patterns and crack propagation mechanism of concrete. Internal cracks are more dominant than surface cracks and the propagation of internal cracks combined with surface cracks may cause de-lamination of the concrete cover.

Table of contents

List of figures

Figure number and title **Page**

List of tables

1. INTRODUCTION

1.1 Background

In recent years, durability of aging concrete structures has become one of the critical topics for design of new structures, maintenance and reparation of existing concrete structures in all over the world (Ravindra et al., 2008). Degradation of concrete structures due to rebar corrosion has become a main concern of the structure durability (Maage et al., 1996). The degradation not only reduces the structure capacity but also influences the structure service life. That is, corrosion products of rebar cause expansion pressure to concrete around the rebar. And, the expansion pressure induces cracking. Once the cracking occurs, the serviceability of concrete structures decreases and spalling of cover concrete is often observed. Cracking of concrete due to rebar corrosion also causes acceleration of other deteriorations for the structures (**Figure 1.1**).

Moreover, rebar corrosion induced-deterioration takes a huge increase of cost in maintenance and reparation of concrete structures. **Table 1.1** shows cost examples related to reinforced concrete structures deteriorated by corrosion of reinforcement

(Tullmin, 2007).

Figure 1.1. Damage of a concrete bridge resulted from rebar corrosion

(*Source: JSCE*)

Corrosion of rebar in concrete is a very complex phenomenon. The corrosion of rebar in concrete occurs by an electrochemical process and causes a volume increase due to formation of corrosion products and then induces splitting-stress in concrete (**Figure 1.2**) (Bentur et al., 1997).

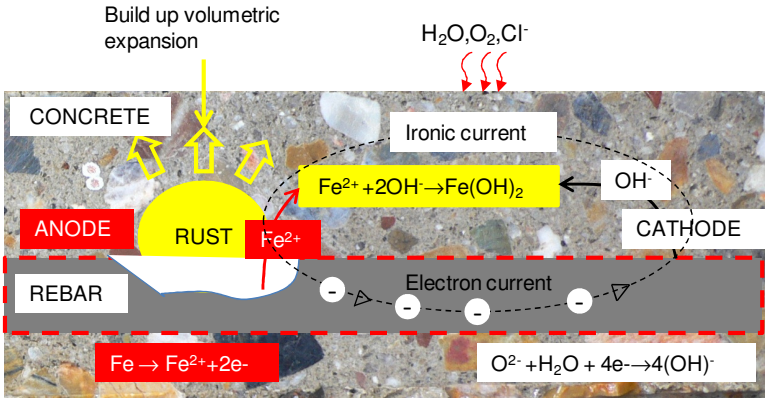

Figure 1.2. Electrochemical mechanism of rebar corrosion in concrete

Table 1.1. Cost examples related to damage of concrete structure due to rebar corrosion (*Source: http://www.corrosion-club.com/concretecosts.htm*)

Country/ City	**Structure type/ Damage type**	**Cost**	**Year of reference**
United States	Reinforced concrete bridges and car parks due to deicing salts	$325 million – $1 billion per year.	2000
United States	The estimated total cost to address bridge deficiencies in the United States depending on time taken to meet the objective.	$78 billion – $112 billion	1988
United Kingdom	Estimate of annual costs attributable to corrosion of reinforced concrete	£550 million.	
Toronto (Canada)	$110 million is to be spent by this city on the repair of roads, sidewalks and bridges in 2005 ...with a backlog of $235 million deferred due to budget constraints.	$110 million	2005

Although a significant number of researches on modeling the corrosion processes of steel in concrete have been performed, accurate life prediction for concrete structures is still difficult (Yunovich et al., 2002).

The deterioration of concrete structure due to rebar corrosion is normally divided into four main stages as shown in **Figure 1.3**. The initiation stage is defined as the time from initiation of the rebar corrosion until rebar corrosion induced stress in concrete exceeds the concrete tensile strength and cracks are initially formed in concrete. The propagation stage and the acceleration stage are defined when cracks propagate and join together when rebar corrosion amount increases. And, the deterioration stage is defined when cracks become large and they cause de-lamination or spalling of concrete cover. In this stage, corrosion induced cracks significantly degrade the capacity and service life of the concrete structure.

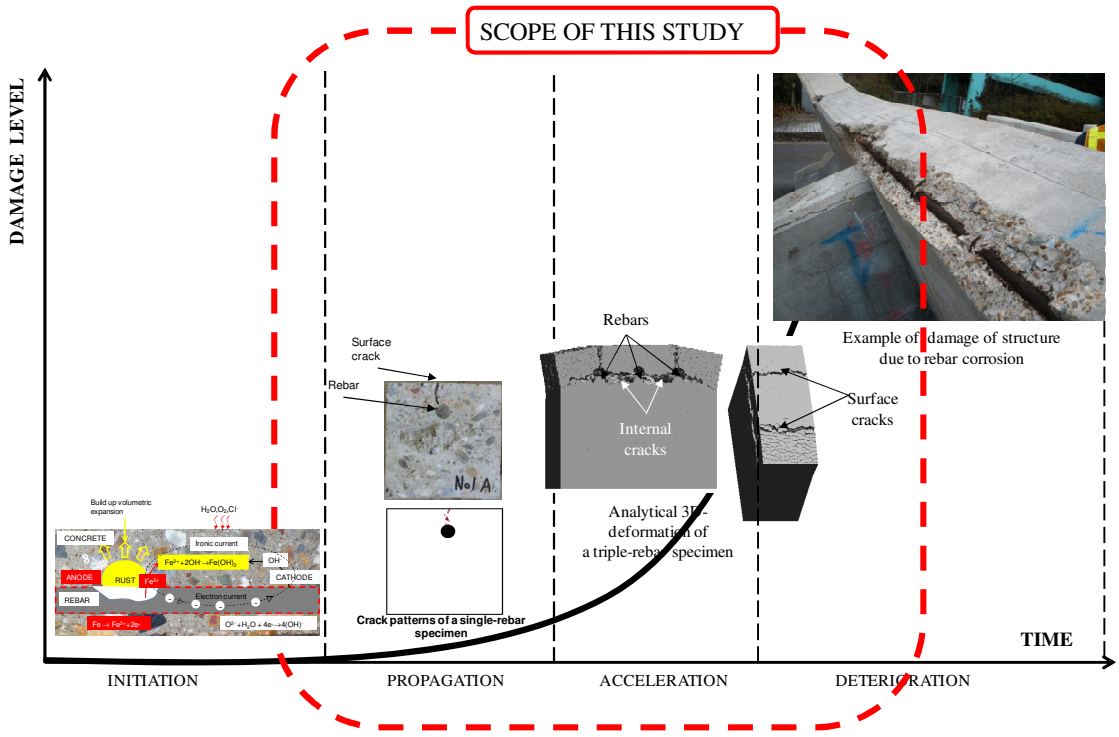

Figure 1.3. Deterioration stages of concrete structure due to rebar corrosion

Many researches were conducted in the initiation stage such as why rebar is corroded

in concrete and initiation of corrosion of rebar in concrete due to (1) breakdown of the passive layer on the rebar by chloride ions or (2) carbonation due to carbon dioxide reactions with the cement phase of the concrete (Bentur et al., 1997); effects of the chloride and oxygen permeation on corrosion of rebar in concrete (Maruya, 2003); macro-cell corrosion of reinforcement in concrete (Saraswathy, 2005); etc. In terms of design of new structures, current design standards and design regulations also stipulated some conditions to prevent or delay the crack initiation. Degradation of the structure capacity after the deterioration stage occurs was also evaluated (Yamamoto et al., 2002; Matsuo et al.,2008). On the other hand, the cracking behavior of concrete due to rebar corrosion in the later stages (i.e. the propagation, the acceleration stage and the structure deterioration stage) has not been studied throughout. Therefore, this study focuses on the stages from the crack initiation until the beginning of the deterioration stage due to rebar corrosion as indicated in **Figure 1.3**.

The motivation of this study is how to understand and how to evaluate cracking behavior of concrete due to rebar corrosion. Main points of the study can be summarized as follows:

- To evaluate crack propagation of concrete due to rebar corrosion.
- To evaluate factors affecting the cracking behavior due to rebar corrosion.
- To investigate the crack propagation in several conditions of concrete structures.
- To understand cracking mechanism of concrete due to rebar corrosion.

1.2 Problem statement and literature review

1.2.1 Problem statement

The corrosion process of rebar in concrete takes place in a long time and it is complex

and costly to carry out experiment for existing structures to evaluate corrosion induced cracking. Therefore, in order to design new structure properly, to evaluate and to maintain the existing structures adequately, it is desirable to establish a prediction method to understand and to evaluate cracking mechanism induced by rebar corrosion qualitatively and quantitatively. It is also necessary to predict the internal damage from the observable surface condition during maintenance process.

1.2.2 Literature review

Studies on the cracking behavior of concrete due to rebar corrosion reported in the literature are summarized as follows.

1.2.2.1 Experimental studies

In order to evaluate cracking behavior, electric accelerated corrosion test was usually conducted. Then, surface crack initiation and surface crack width propagation were measured (Alonso et al., 1998; Nguyen et al, 2006). However, in the experiment, crack evolution was measured by using a magnification lens (Alonso et al.) and a CCD camera (Nguyen et al, 2006) which might affect the accuracy of crack opening measurement. In this experiment, only one type of specimen size was tested so effects of specimen size or boundary were not known.

Internal crack patterns due to rebar corrosion considering different ratios of concrete cover thickness to diameter of reinforcing bar were observed by using the electric accelerated corrosion test (Tsutsumi et al., 1996) to verify the proposed criterion regarding the change of the internal crack patterns. However, the crack pattern around the threshold of the criterion was not very clear.

Some experiments were carried out to evaluate corrosion induced crack propagation in several conditions such as various ratios of concrete cover thickness to rebar diameter (Alonso et al., 1998). However, crack propagation was not discussed clearly.

Some researchers confirmed mechanical properties of corrosion products of reinforcement in concrete (Ouglova et al.,2006) but effects of the properties of corrosion products on cracking of concrete was not discussed.

1.2.2.2 Analytical studies

Several researchers developed corrosion internal expansion numerical models to simulate the internal expansion due to the rebar corrosion process in concrete. For example, Nguyen et al (2006) used finite-element-method thermal expansion model. Lundgren (2002) used finite-element-method interface element model, Toongoenthong and Maekawa (2005) used finite-element-method expansive material element model However, effects of corrosion products properties and other factors of the corrosion process on modeling of the crack propagation have not been clarified.

Surface crack propagation against rebar corrosion amount or rebar mass loss or rebar radius loss was also investigated experimentally and analytically (Alonso et al., 1998; Lundgren, 2002, Nguyen et al 2006). However, relationships between propagating surface and internal cracks, as well as the dependence of surface crack opening on internal cracking, are still unclear. Lundgren (2002) and Nguyen et al. (2006) could simulate qualitative behavior of the crack propagation of single rebar specimens reasonably but the quantitative behavior of the crack propagation such as crack with development were different from the test results.

Effect of penetration of corrosion products into cracks after cracking of concrete on

the internal expansion pressure was known and several simple models have been recommended (Toongoenthong and Maekawa, 2005; Val et al., 2009). However, assessment of the effect was not done quantitatively.

Some researchers found that corrosion products were not formed uniformly around the rebar section (Yuan, 2009). However, effect of local corrosion of the rebar section on the cracking behavior has not been reported in the literature.

Some researchers investigated crack propagation due to multi-rebar corrosion (Ahmed, 2007 and Murakami, 2008). However, joining of internal cracks and propagation of cracks due to multi-rebar corrosion were not evaluated and investigated in detail. Factors affecting the crack propagation in the case of multi-rebar corrosion were also not reported in the literature.

1.3 Study objective and research framework

1.3.1 Study objective

The aim of this study is to evaluate cracking behaviour of concrete due to rebar corrosion qualitatively and quantitatively. As discussed in the previous part, the corrosion process of rebar in concrete is complex, therefore, the corrosion induced cracking mechanism of concrete is also difficult to evaluate. In order to overcome this difficulty, both experiment and numerical analysis are selected as study methods in this research.

In the experiment, corrosion is induced by electrical means and the propagation of cracks is observed and measured. **Figure 1.4** shows a schematic of an electric corrosion test carried out in this study. **Figure 1.5** shows an electric accelerated corrosion test in laboratory. Various types of specimens are designed for particular purposes to

understand their behaviors and to verify the proposed analytical models. Surface crack widths are then measured; internal crack patterns, internal crack lengths, corrosion pattern of rebar are observed at several rebar corrosion amounts. In addition, deformation of specimen surface is measured using a laser displacement meter to understand a relationship between surface deformation and corrosion induced crack propagation. Based on the experimental results, behavior of the specimen can be predicted or generally understood.

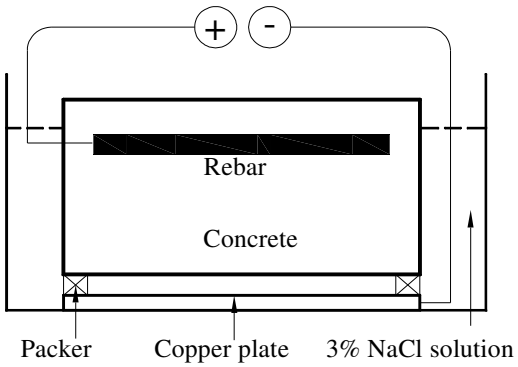

Figure 1.4. Schematic of an electric corrosion test

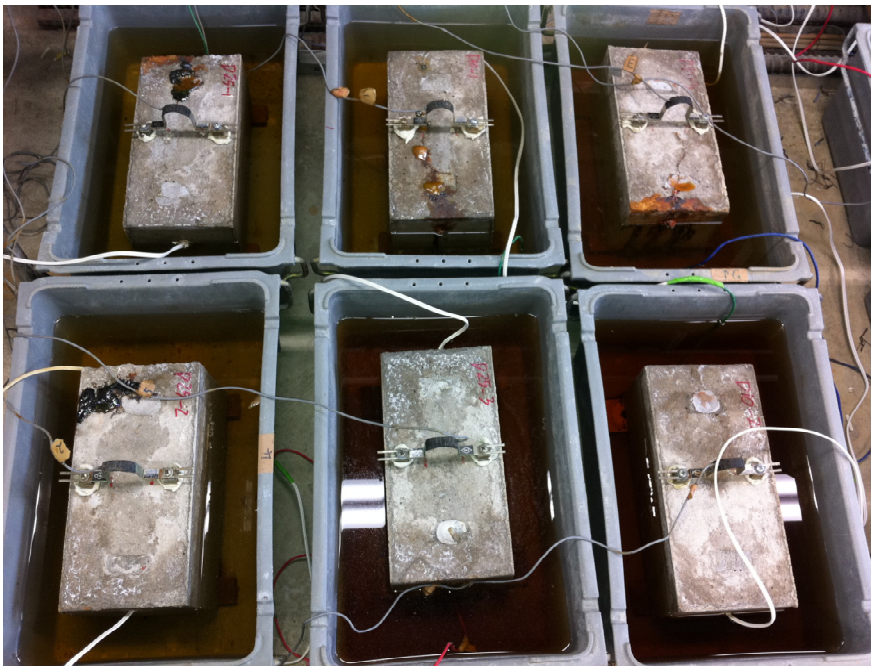

Figure 1.5. Electric accelerated corrosion test in laboratory

However, in order to throughout investigate the cracking behavior and the cracking mechanism as well as factors affecting the cracking mechanism, analytical method should be performed. Moreover, another merit of analytical method is that a parameter study could be conveniently performed. In the parameter study, various specimens could be analyzed to find out cracking behavior. It is clearly that the parameter study is not easy to perform using the experimental method.

In this study, crack propagation behavior can be simulated using 3D Rigid-Body-Spring-Model (RBSM), which is a discrete method for structural analysis with three-dimensional Voronoi particles. Recently, numerical methods utilizing advances in computer technology have become common in structural analysis for concrete structure. Several numerical analysis methods such as Finite Element Method, Boundary Element Method have been applied to evaluate mechanical behavior of concrete structures (Ngo and Scordelis, 1967; Ohtsu and Yosimura, 1997). Generally,

these methods can reasonably analyze global behavior of structure such as loading capacity or crack/strain formation and propagation. However, these methods are not convenient to obtain realistic damage status such as crack patterns, crack width and crack length propagation as well as to visualize damage patterns of the structure. Because of these reasons, Rigid- Body- Spring- Model (RBSM) method, which is based on discrete approach, is used as the structural analysis method in this study. **Figure 1.6** shows 3D-Voronoi particles definition of RBSM model.

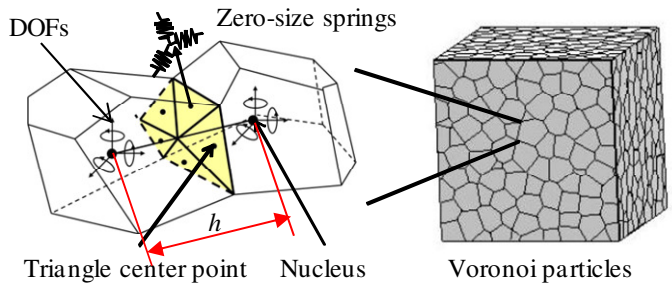

Figure 1.6. Voronoi particles definition of RBSM model

Moreover, modeling of corrosion expansion behavior is a key of the crack propagation analysis. Therefore, corrosion expansion model, local corrosion model of rebar section and penetration model of corrosion products into cracks are developed and combined with the RBSM analysis.

1.3.2 Research framework

Figure 1.7 shows a framework of the study, in which experimental method, numerical simulation and analytical parameter study will be used to perform six discussion cases concerning the cracking behavior of concrete due to rebar corrosion. In

each discussion case, specimens are designed to investigate the cracking behavior experimentally. The specimens were tested by using the electric accelerated corrosion test and then crack width propagation, surface and internal crack patterns, internal cracks width and lengths and corrosion amount of rebar are observed and obtained during the test. The specimens were simulated by the proposed analytical model. The analytical results were compared with the experimental results to confirm the applicability of the analytical method and analytical results such as crack propagation, 3D deformation, surface deformation, internal crack propagation are obtained to understand the cracking mechanism throughout. In order to investigate the cracking mechanism comprehensively and to identify factors affecting the cracking mechanism, the analytical parameter study was carried out for specimens with varied parameters. Contents of each discussion case are briefly explained in the next part of this chapter.

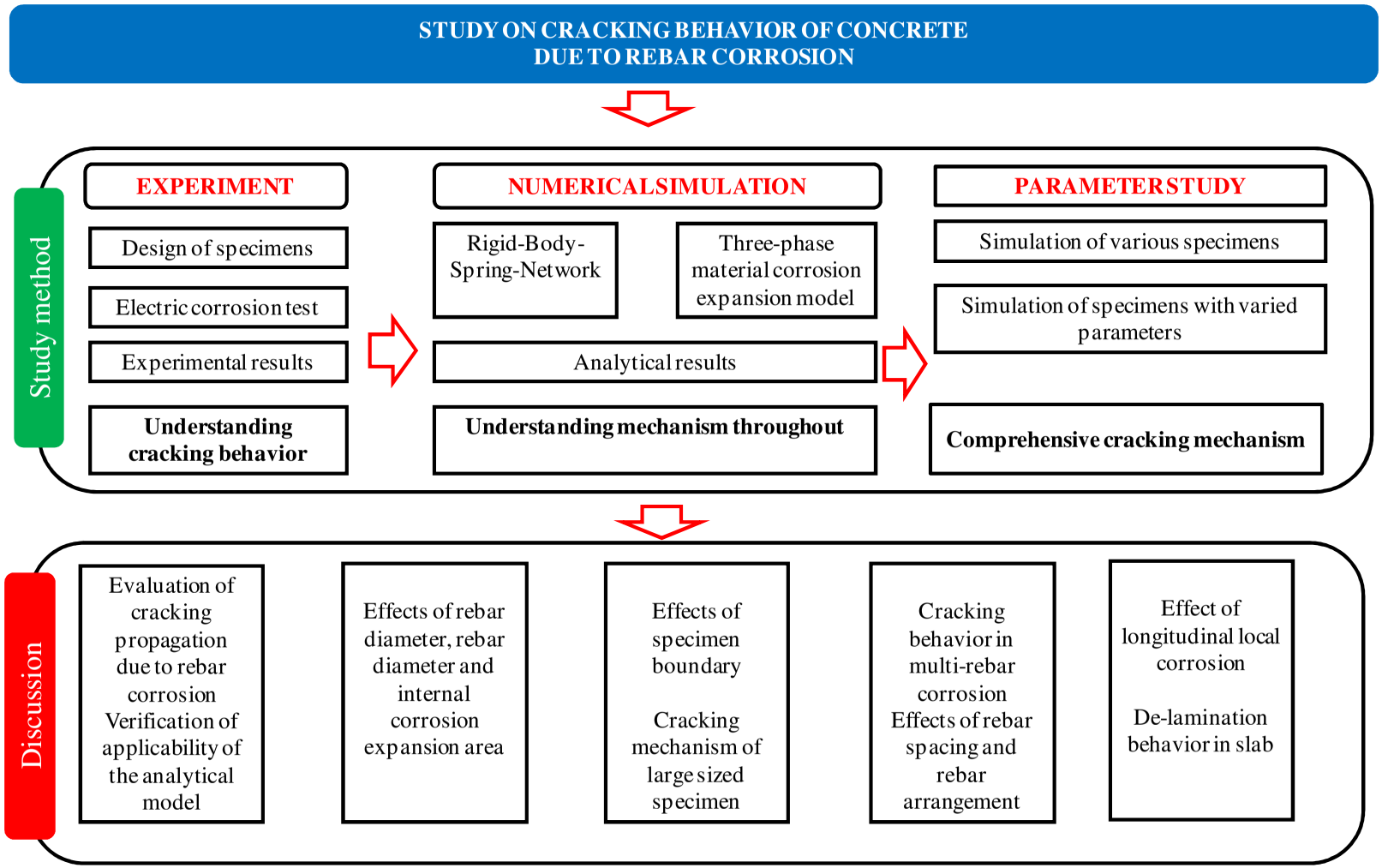

Figure 1.7. Framework of the study

1.4 Overview of the dissertation content

This part briefly introduces contents of the dissertation.

Chapter 1 is the introduction of the dissertation including background of the study, problem statement, literature review, study objectives and the framework of the study.

Chapter 2 presents the experimental method conducted in this study. In this chapter, a test procedure using electric means in the laboratory condition is explained. Specimen setting up and measurement of experiment are introduced. A table of specimens tested in this study is shown in this chapter.

Chapter 3 presents analytical development. In this chapter, details of Rigid-Body-Spring-Model (RBSM) method with random Voronoi particles and the concrete material models, which are used as structural analysis method in this study, are described. Another important part of this chapter is the development of the internal corrosion expansion model. In order to model the internal corrosion expansion, a three-phase material model including rebar, corrosion products and concrete. Details of the corrosion three-phase material model with mechanical properties of corrosion products are explained in this chapter. Several corrosion models such as sectional local corrosion or rebar, which is only a part of rebar section to be corroded and penetration of corrosion products in to cracks after cracking of concrete discussed in this chapter.

Chapter 4 discusses the surface crack propagation of a single-rebar specimen series with the specimen size of 150 mm width x 150mm height and concrete cover thickness as 30mm. In this chapter, crack propagation behavior is investigated both analytically and experimentally. In the experiment, the surface crack widths are measured and internal crack patterns and internal crack lengths/widths are observed at several rebar corrosion amounts. In addition, deformation of the specimen surface is measured using

a laser displacement meter to understand the relationship between surface deformation and crack propagation. Crack propagation behavior is simulated using the proposed RBSM method. Moreover, the effects of penetration of corrosion products into cracks, local corrosion and local penetration of corrosion products into cracks during the corrosion process are simulated and the effects are quantitatively evaluated. The applicability of the model is verified by comparison with the experimental results. As a result, the effects of modeling and the mechanism of crack propagation such as crack initiation, progress of surface crack width, propagation behavior of internal cracks and the effect of internal cracks on surface crack width are clarified in this chapter.

Chapter 5 discusses effects of rebar diameter and ratio of concrete cover thickness to rebar diameter on the cracking behavior of the specimens. In this chapter, various specimens having different rebar diameters and different ratios of concrete cover thicknesses to rebar diameters are investigated experimentally and analytically. The purpose of this chapter is to confirm internal crack patterns and crack width propagation of the specimens when these parameters vary. The results in this chapter are compared with the results of some previous researches. Moreover, rectangle internal corrosion expansion areas width changed dimensions are simulated to investigate effects of the expansion areas on the cracking behavior.

Chapter 6 investigates cracking behaviors of single-rebar specimens with different specimen sizes/boundaries. In this chapter, a series of single-rebar specimens are tested using the electric accelerated corrosion test and the experimental results such as surface crack propagation, internal crack patterns, internal crack lengths, etc are obtained during the test. The specimens are simulated and the analytical results are verified against the test results and effects of the specimen sizes or boundary conditions are discussed. A

analytical parameter study is also performed on various specimens having the same height and various widths and varied widths and heights to indentify which and how dimension affects the cracking behavior.

Chapter 7 investigates crack propagation in the case of multi-rebar corrosion. In this chapter, several multi-rebar corrosion specimens tested by the other researchers are used to verify the proposed analytical model in terms of internal crack patterns, surface crack propagation and internal crack propagation. Then, a an analytical parameter study is performed on multi-rebar corrosion specimens with varied rebar spacing to investigate effects of rebar spacing on crack patterns, crack propagation, crack joining and surface deformation of the concrete cover.

Chapter 8 investigates effects of longitudinal local corrosion rebar and 3D behavior of crack propagation as well as de-lamination behavior in a slab structure due to rebar corrosion. In this chapter, single rebar specimens having longitudinal local corrosion rebar is investigated experimentally and analytically. The local corrosion of rebar along the specimen length is also observed in the experiment and it shows 3D-behavior of the cracking in this case. This behavior is confirmed and clearly evaluated by the simulation results. Moreover, de-lamination behavior of a real- structure slab, which is a part of a slab structure of the expressway structure, is simulated and the simulation results well agree with the survey data. Then, an analytical parameter study on effect of concrete cover thickness on de-laminated area of the slab is performed and it confirms that the concrete cover thickness plays an important role in the propagation of internal cracks and spalling area of concrete surface of the slab. The local corrosion length of rebar is also an important parameter in order to evaluate area of potential de-laminated area in the analysis.

Chapter 9 includes summary and conclusion derived from this study as well as comments and suggestions for the maintenance process and future studies.

2. EXPERIMENT METHOD

2.1 Introduction

The corrosion process of rebar within concrete takes a very long time to occur and the nature of the corrosion of rebar inside concrete is an electrochemical process as discussed in Chapter 1. In order to obtain experimental results in this study, electric accelerated corrosion tests are carried out by using electric means. This chapter presents an experimental procedure, setting up of an electric accelerated corrosion test and measurement method in the laboratory condition and an outline of the specimens carried out in this study.

2.2 Experiment procedure

Figure 2.1 shows a flow chart of the experimental procedure conducted in the laboratory condition for an electric accelerated corrosion test which is used in this study. There four main stages in the experiment including specimen design, concrete casting,

electric accelerated corrosion test and observation after the test. The experimental results are observed and measured during these stages. Contents of each experimental stage are explained as follows.

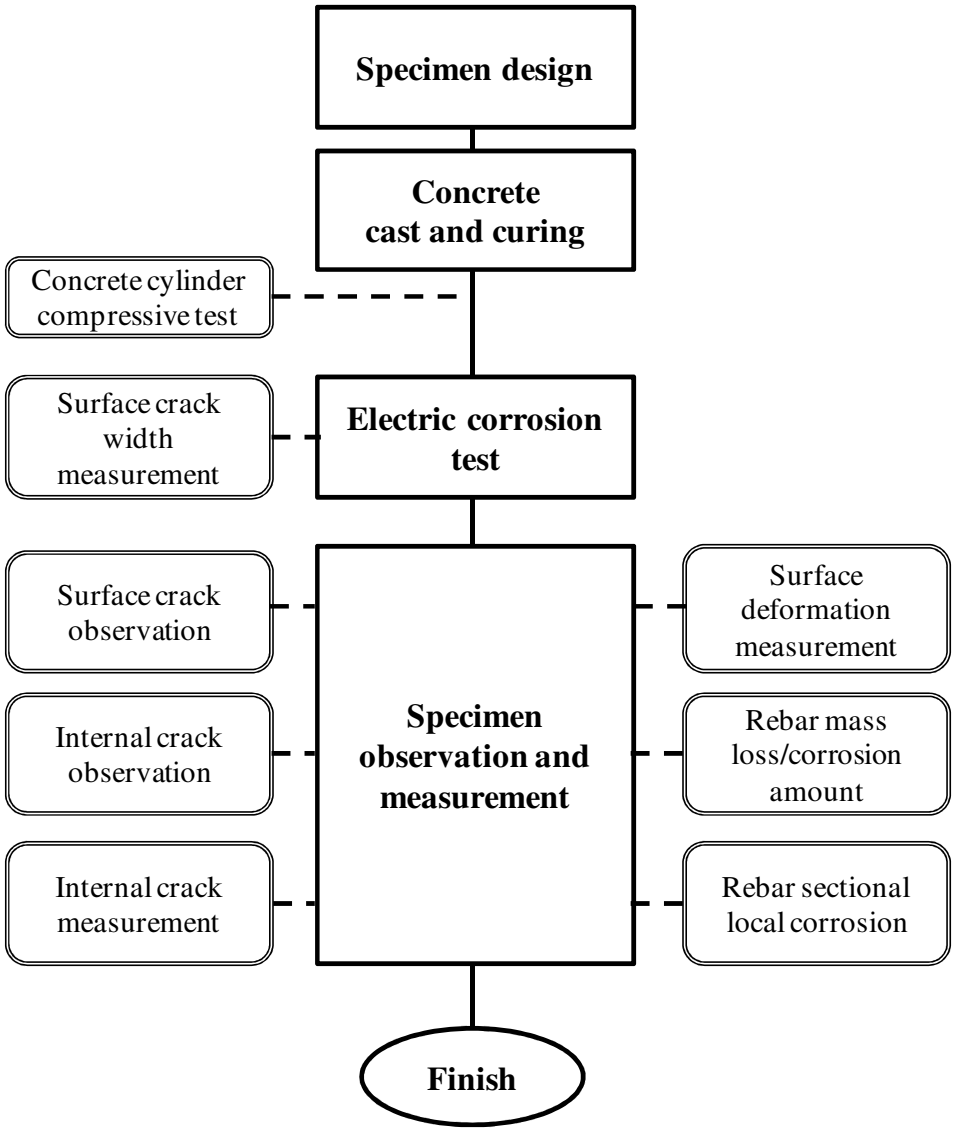

Figure 2.1. Experiment procedure in the laboratory condition

2.2.1 Specimen design

Before starting the experiment, concept of each specimen is carefully considered. The

concept of specimen is dependent on the purpose of the test, for example, what to be observed during the test, which behavior of specimen to be expected during the test, which effects to be investigated in the test, etc.

In this study, only single-rebar specimens are tested and **Figure 2.2** shows a typical setting dimension of a specimen. Single-rebar specimen is a fundamental case and other cases could be understood based on this type of specimen.

In the literature, several researchers also conducted electric corrosion test for single-rebar specimens (Tsutsumi et al., 1996; Alonso et al., 1998; Nguyen et al., 2006) to investigate and evaluate cracking behavior due to rebar corrosion. For example, Tsutsumi (1996) evaluated types of internal crack patterns based on the ratio of concrete cover to rebar diameter, Alonso (1998) investigated factors affecting the corrosion induced cracking such as concrete compressive strength, cover thickness, rebar diameter, etc, Nguyen (2006) observed deformation of single rebar specimen. In this study, several new test methods are used in order to observe the cracking behavior more precisely such as directly measuring surface crack during the test, measuring surface deformation, measuring internal cracks, etc. Specimen is also cut at two positions along the specimen length in order to observe variation along the specimen if any.

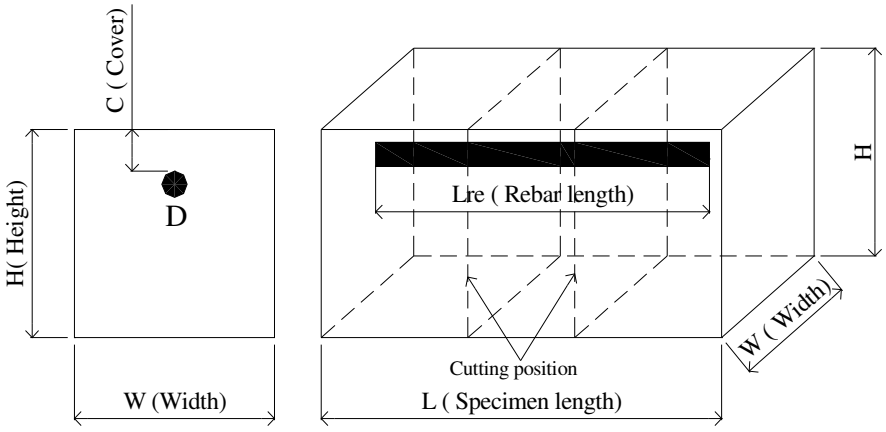

Figure 2.2. Typical setting dimensions of specimen

Table 2.1 shows a summary of specimens conducted in this study. Concept of each specimen series is explained as follows.

Specimen series 150*150-C30 is considered as a basic series in this study. Based on the experimental results of this series, main behaviors of the cracking mechanism can be understood and the test results of this series can be used to validate the proposed analytical model. Series 150*150-C7.5, 150*150-C15 and 150*150-C45 are tested to investigate effects of cover thickness and then effect of ratio of cover thickness to rebar diameter. Series 150*150-D10 and 150*150-D25 are tested investigate effects rebar diameter and then effect of ratio of cover thickness to rebar diameter. Series 300*150-C30, 250*250-C30, 400*400-C30 and 600*400-C30 are tested investigate effects of specimen sizes. Each specimen series includes numbers of specimens in order to enable observation of cracking behaviors at different rebar corrosion stages. Special rebar corrosion situations occurred in series 600*400-C30 are used to evaluate effect of longitudinal local corrosion of rebar. Beside the above specimens, other specimens conducted in the literature are used to validate the proposed analytical model in the case of multi-rebar corrosion in Chapter 7.

Table 2.1. Table of specimens conducted in this study (*Unit in mm*)

No.	Series name	W	H	L	D	C	Qty	Chapter	Concept
1	**150*150-C30**	150	150	300	19	30	6	4,5	Basic series
2	**150*150-C7.5**	150	150	300	19	7.5	4	5	Various cover thickness
3	**150*150-C15**	150	150	300	19	15	4	5	
4	**150*150-C45**	150	150	300	19	45	4	5	
5	**150*150-D10**	150	150	300	10	30	3	5	Various rebar dia.
6	**150*150-D25**	150	150	300	25	30	3	5	
7	**300*150-C30**	300	150	200	19	30	3	6	Various specimen size/ boundary
8	**250*250-C30**	250	250	200	19	30	1	6	
9	**400*400-C30**	400	400	200	19	30	6	6,8	
10	**600*400-C30**	600	400	300	19	30	3	6,8	

2.2.2 Concrete casting and curing

Table 2.2 shows a typical mixture proportion of concrete used for specimens in this study. **Figure 2.3** shows a typical specimen formwork set-up and direction of concrete casting. With this set-up, rebar is put within concrete and the concrete cover is cast with the best quality of concrete. After casting the concrete, the specimens are cured in a room at 20^{o}C until 28 day curing. Then, the electric corrosion test is conducted. Prior to the electric accelerated corrosion test, the concrete compressive strength is determined by the cylinder compression test.

Table 2.2. Typical mixture proportions of concrete

W/C (%)	s/a (%)	Unit content (kg/m^3)				
		Water	Cement	Sand	Aggregate	AE (liter/m^3)
56.5	44.0	166	294	779	990	1.18

Notes:
W/C is the water/cement weight ratio
s/a is the river sand/total aggregate volume ratio
AE is a water reducing agent admixture

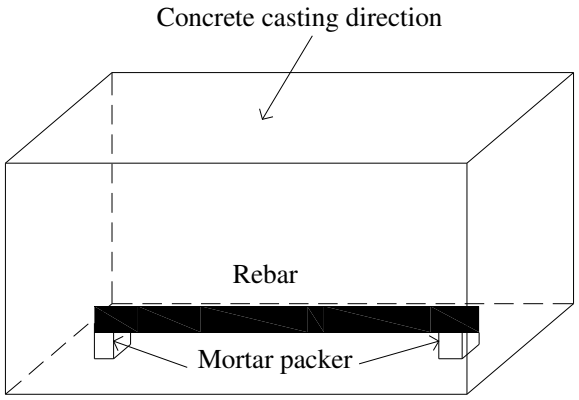

Figure 2.3. Typical specimen formwork set-up

2.2.3 Electric corrosion test

Figure 2.4 shows a schematic of the electric corrosion test. Specimen is immersed in a 3% NaCl solution in the beginning of the test. The NaCl solution provides source of ion Cl^- in the electric corrosion test. The rebar of the specimen is connected to the anode of the direct-current (DC) power source which acts as an anode in the electric corrosion circus. A copper plate immersed in the NaCl solution, which acts as a cathode, is connected to the cathode of the DC power source. The pore fluid in the concrete acts as electrotype. In the multi specimen test, specimens are connected together as shown in

Figure 2.4. The DC power source is set to keep the electric current constantly during the testing time. In the electric corrosion test, the accelerated current density is set at 900 μA/cm^2. This current density is relative large in order to obtain cracking due to rebar corrosion quickly (Alonso, 1998).

In order to measure surface crack propagation directly, the concrete cover is arranged on the upper side, i.e. concrete cover surface is higher than the level of NaCl solution in the electric corrosion test. Based on the researches reported in the literature, it is known that when rebar is corroded, surface crack may initiate and develop along the rebar (Tsutsumi, 1996). Therefore, during the electric corrosion test, surface crack width is recorded using a strain gauge type displacement transducer (PI gauge) and logged in a data logger as shown in **Figure 2.5**. The advantage of this method is the surface crack propagation can be measured precisely during the test which would be better than some methods using a magnification lens (Alonso, 1993) and a CCD camera (Nguyen, 2006) .

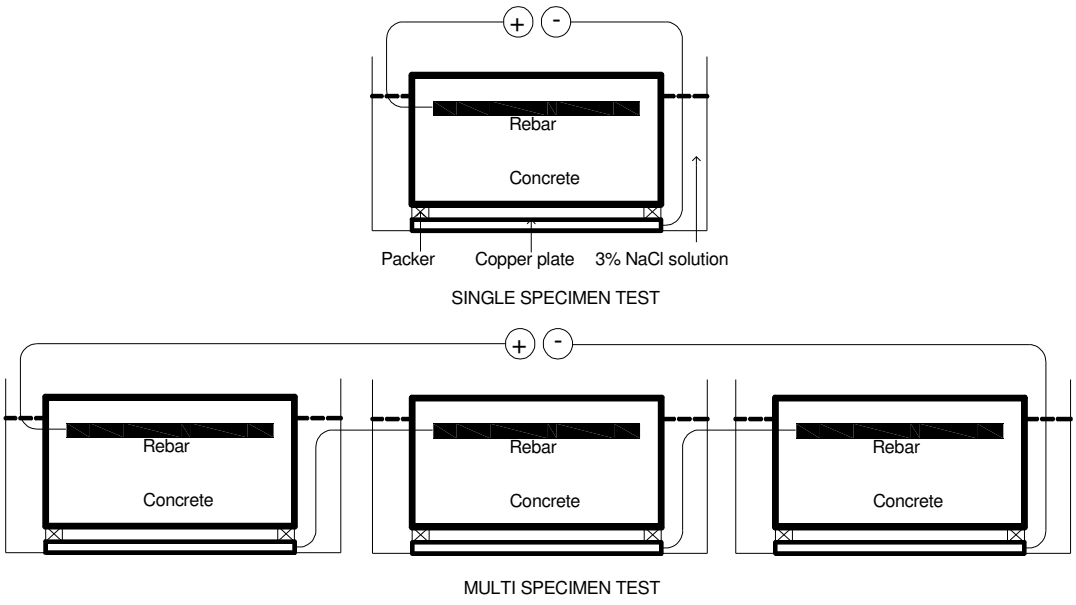

Figure 2.4. Schematic of electric accelerated corrosion test

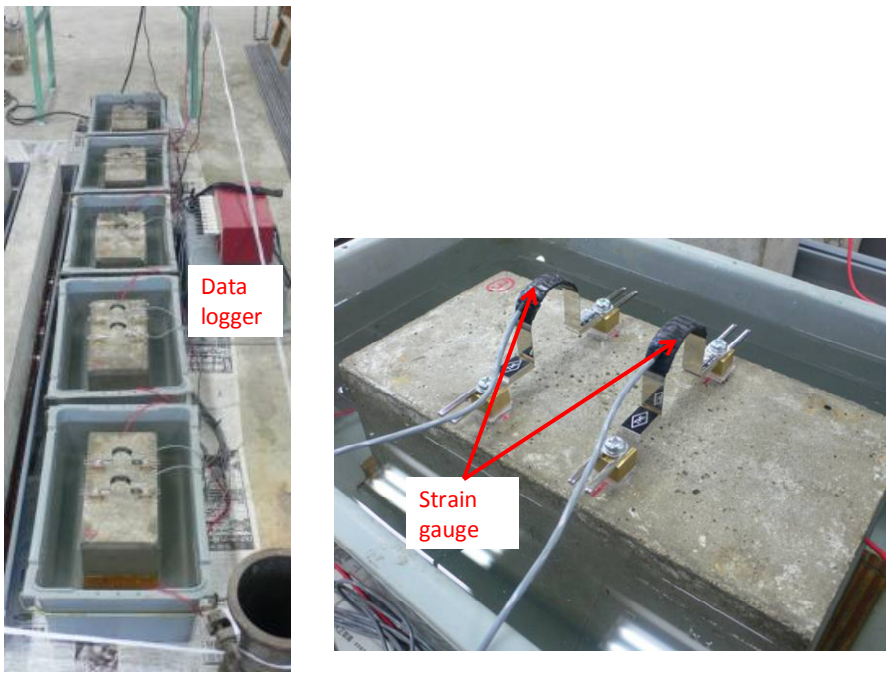

Figure 2.5. An example of electric accelerated test, series 150*150-C30

2.2.4 Specimen observation and measurement

The testing time is varied for each specimen to investigate cracking condition at several corrosion stages. When each specimen's test is completed, the electric corrosion test is terminated to observe the surface crack pattern, to measure surface deformation .Then, the specimen is cut at the positions shown in **Figure 2.2** by using a concrete cutting machine to enable internal measurement and observation such as internal crack patterns, internal crack widths and lengths; sectional rebar local corrosion and rebar mass loss.

2.2.4.1 Surface deformation measurement

When rebar is corroded, concrete cover is deformed due to internal expansion pressure and the tensile stress reaches maximum on the cover surface just above the rebar (Nguyen, 2006). In order to understand the relationship between crack

propagation and deformation of the specimen surface due to rebar corrosion, the vertical deformation of specimen surface is measured during the corrosion process using a laser displacement meter having an accuracy of 1μm. **Figure 2.6** shows an arrangement of measurement of surface deformation for series 150*150-C30. Due to the weight limitation of the laser equipment, only specimen series 150*150-C30 with a length of 200 mm was tested. The vertical deformation is measured along the measuring lines shown in **Figure 2.7**. The measured value of vertical deformation is conversed to the relative value with the assumption that vertical deformation is zero at the reference points as indicated in the **Figure 2.7**.

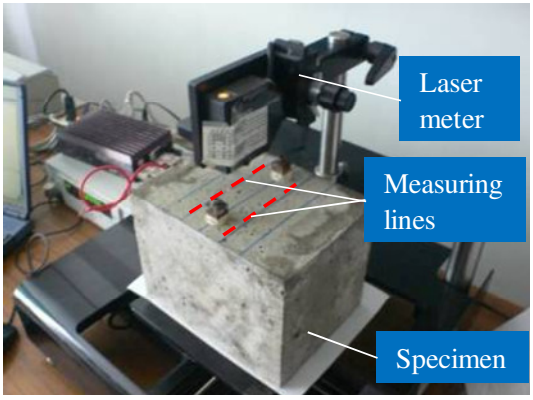

Figure 2.6. Laser displacement meter: measurement of surface vertical deformation

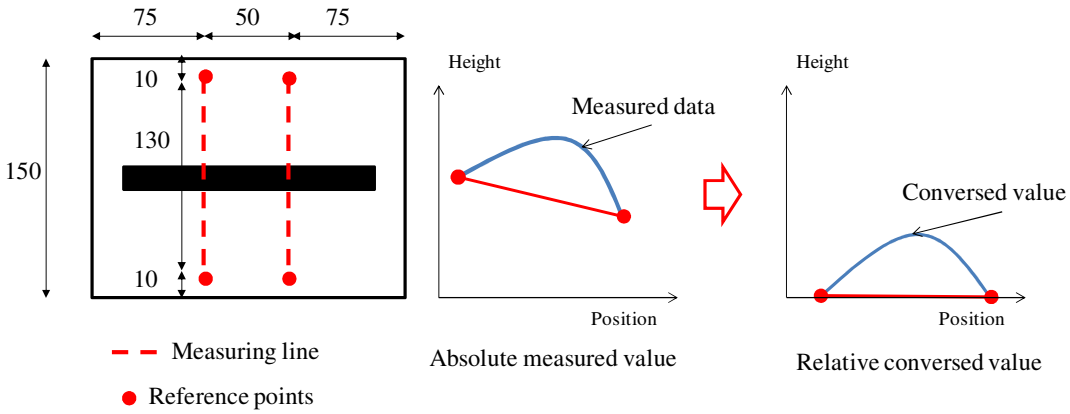

Figure 2.7. Vertical surface deformation measurement: conversion of measured data

Surface vertical deformation was measured at several surface crack width values monitored by the data logger during the electric corrosion process. In order to eliminate errors in the measurement using the laser equipment, a Fast Fourier Transform was conducted to remove the effects of imperceptible vibrations of the specimens and then an Inverse Fourier Transform was conducted to obtain surface deformation. Microwaves with frequencies of more than five wave periods in each 10 mm of length were eliminated in the process. Each specimen was measured at the beginning of the corrosion test (day 0) to obtain the initial surface levels. The difference between the initial surface level and the measurement level at each measurement time is the deformation of the specimen surface at the measuring time. For example, **Figure 2.8** shows surface deformations of specimens at minor surface crack widths and visible surface crack widths. Surface deformation depending on the surface crack width is measured in the experiment.

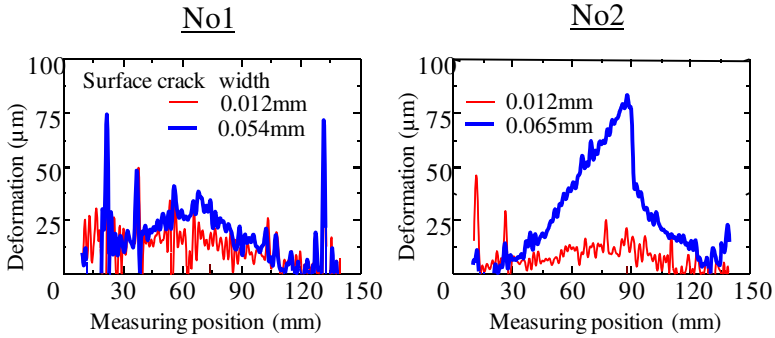

(a) Surface deformation corresponding to minor surface crack width

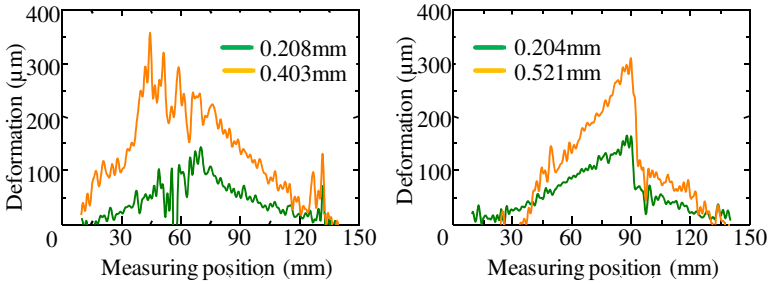

(b) Surface deformation corresponding to visible surface crack width

Figure 2.8. Experimental surface deformation of series 150*150-C30

2.2.4.2 Surface crack pattern observation

Surface crack pattern are observed as shown in **Figure 2.9**. Crack patterns are obtained at several stages of the test in order to observe crack propagation when rebar corrosion increases.

Figure 2.9. Typical surface crack pattern of series 150*150-C30

2.2.4.3 Measurement of rebar mass loss/ corrosion amount/ radius loss

After cutting the specimen, the rebar is cleaned using a steel brush and corrosion products are removed from the sound steel by immersing the rebar in a 10% ammonium citrate solution for 24 hours. After removing corrosion products from the rebar, the corroded rebar is weighted to indentify a remaining weight, M_1 (g), after the electric corrosion test. The difference between the initial weight of rebar, M_0 (g), determined before casting the concrete and the remaining weight after the corrosion test is a mass loss W (g) of the rebar for each specimen.

In some cases, a relationship between rebar mass loss W and the testing time t (hr) can be developed based on the testing data. For example, in the case of the specimen series 150*150, an empirical equation to calculate rebar mass loss could be derived as follows based on the testing data shown in **Figure 2.10**:

$$W = 0.235I.t \qquad (I \cdot t < 66\,\mathrm{A \cdot hr})$$

$$W = 0.617I \cdot t - 25.305 \quad (I \cdot t > 66\,\mathrm{A \cdot hr}) \qquad (2.1)$$

where W, I and t are rebar mass loss (g), electric current intensity (A) and testing time

(hr) respectively. The proposed empirical equation is in a bi-linear type due to the linear relationship between the rebar mass loss (W) and the composition of I and t ($I \cdot t$), according to the Faraday's law (Admed et al., 2007).

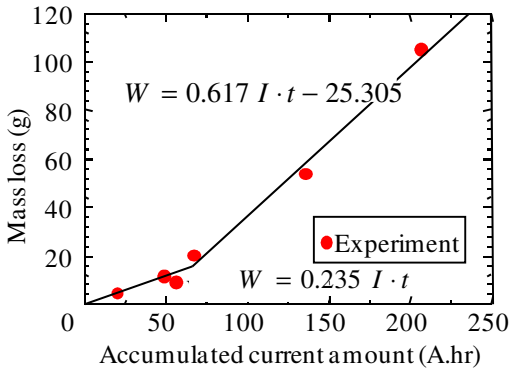

Figure 2.10. Mass loss and testing time relationship (series 150*150-C30)

Corrosion amount of the rebar, W_r (mg/cm^2), during the testing is determined by dividing the mass loss W (mg) by the wet surface area of the rebar S_{wet} (cm^2).

$$W_r = \frac{W}{\pi D \cdot L_{re}} \tag{2.2}$$

where D and L_{re} are initial rebar diameter (cm) and rebar length (cm), respectively.

Some researchers used rebar radius penetration, x (μm), or rebar corrosion ratio Δw (%) to represent corrosion level of the rebar (Alonso, 1993; Ahmed et al., 2007; and Murakami, 2008). Below is relationships between W_r and x or Δw:

With assumption that the rebar is uniformly corroded and a relationship between W_r and penetration depth x (mm) is as follows (Tran et al., 2010):

$$x = \frac{W_r}{\rho_s} \tag{2.3}$$

in which ρ_s is rebar density (7.85×10^3 mg/cm^3).

Percentage of radius loss, Δx (%), is defined:

$$\Delta x = \frac{2x}{D} \tag{2.4}$$

The relationship between the rebar corrosion ratio, Δw, and the corrosion amount W_r is as follows:

Definition of Δw:

$$\Delta w = \frac{M_0 - M_1}{M_0} \tag{2.5}$$

Definition of W_r:

$$W_r = \frac{M_0 - M_1}{\pi \cdot L_{re} \cdot D} \tag{2.6}$$

M_0 is the initial weight of the rebar:

$$M_0 = \pi \cdot \frac{D^2}{4} \cdot L_{re} \cdot \rho_s \tag{2.7}$$

From (2.5), (2.6) and (2.7):

$$\Delta w = \frac{W_r \cdot 4}{D \cdot \rho_s} \tag{2.8}$$

2.2.4.4 Internal crack pattern observation and measurement

Internal crack patterns are observed **Figure 2.11**. Internal crack patterns are obtained at several rebar corrosion amounts in order to observe crack propagation when rebar corrosion amounts increase.

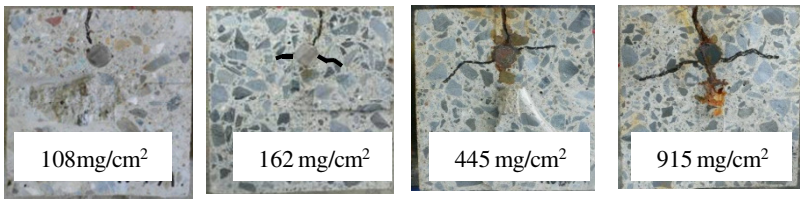

Figure 2.11. Internal crack patterns of series 150*150-C30

Internal cracks are measured in their length and their width. The internal crack length is horizontally measured from the rebar sides to the crack tips of internal visible cracks as shown in **Figure 2.12**. The internal crack width is measured by using a crack scale and crack width values are marked along internal cracks as shown in **Figure 2.12**.

Figure 2.12. Measuring internal crack length and width

2.2.4.5 Observation of rebar corroded sectional pattern

After cutting the specimen, actual rebar corroded pattern on the rebar section can be observed. In most of the cases in the experiment, rebars are not corroded uniformly around their sections and the part toward the concrete surface are much more corroded rather than the other part as shown in **Figure 2.13**.

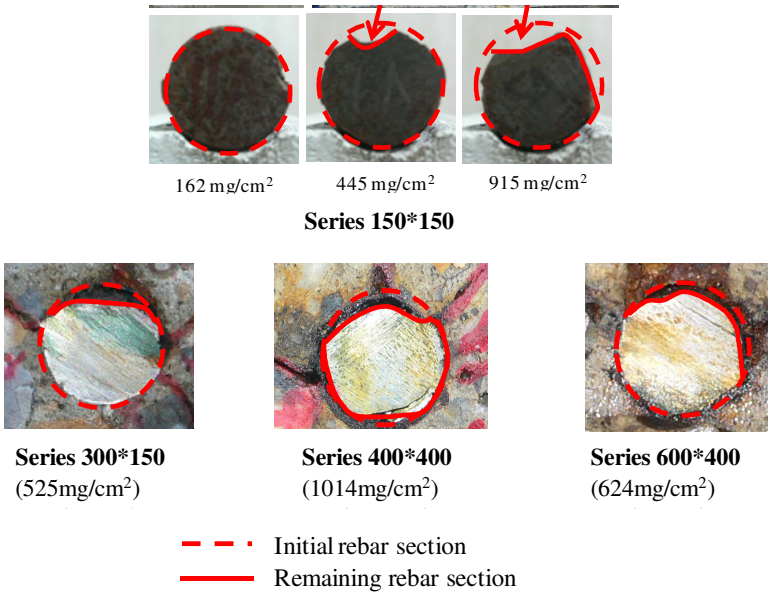

Figure 2.13. Sectional rebar corrosion patterns

2.3 Summary

This chapter presented the experimental method for the electric accelerated corrosion test in the condition of the laboratory. In this experimental method, several advanced testing methods such as direct measurement of surface crack propagation, surface deformation measurement, internal crack observation and measurement at several positions along the specimen, were applied in order to obtain the cracking behavior precisely in the test. Based on the experimental results, the cracking behavior of the specimens due to rebar corrosion will be understood and the experimental results will be used to validate analytical results in the next chapters.

3. ANALYTICAL MODEL

3.1 Introduction

Based on the advantages of the Rigid-Body-Spring Method (RBSM) as presented in Chapter 1 , the RBSM is selected as an structural analysis in this study combined with the corrosion expansion model. Since the RBSM analytical model for concrete structural analysis were published by some researchers (Bolander et al., 1998 and Saito, 1999), in this chapter, the content of RBSM method is briefly presented with the concrete material models used in the analysis. Moreover, in order to model the internal pressure expansion due to rebar corrosion, a three-phase material model including rebar, corrosion products layer and concrete is proposed and presented in this chapter. A merit of the three-phase material is that the properties of corrosion products layer such as initial thickness and elastic modulus can be directly input into the analytical. The modelling of the internal pressure expansion of the three-phase corrosion expansion is presented in this chapter and several corrosion models are also described.

3.2 Three- dimensional RBSM

The RBSM developed by Kawai and Takeuchi (1990) employs the discrete numerical analysis method. Analyses of concrete or concrete structures using the RBSM have been conducted by Ueda et al. (1988), Bolander and Saito (1998), Ishikawa et al. (2003) and Nagai et al. (2004).

The RBSM represents a continuum material as an assemblage of rigid particle elements interconnected by zero-length springs along their boundaries as shown in **Figure 3.1**. In this study, three-dimensional RBSM is used (Yamamoto et al., 2008). Each element has six degrees of freedom at the center points. The boundary between two elements is divided into triangles formed by the center and vertices of the boundary. At each center point of a triangle, three springs- one normal and two shear springs- are set. The analytical model is divided into elements using Voronoi random polygons. In a RBSM model, crack widths can be automatically measured during analysis so it is convenient to directly calculate the volume of cracks in the analysis. The three-dimensional analysis can simulate complex corrosion problems (Tran et al., 2011) such as longitudinal local corrosion along the length of rebar, pitting corrosion along the length of the rebar as well as the spalling behavior of concrete surface due to rebar corrosion. In these cases, a two-dimensional analysis cannot simulate reasonably.

In the analysis, a stiffness matrix is constructed based on the principle of virtual work, and the modified Newton-Raphson method is employed for the convergence algorithm. In the convergence process, displacements that cancel the unbalanced force of elements are added to the elements. The displacements are calculated using the stiffness matrix. Convergence of the model is judged when the ratio of Σ(Unbalanced force of element in the model)^2 to Σ(Applied force to element)^2 becomes less than 10^{-6}. When the model

does not converge at a given maximum iterative calculation number, the analysis proceeds to the next step (Ishikawa et al., 2003).

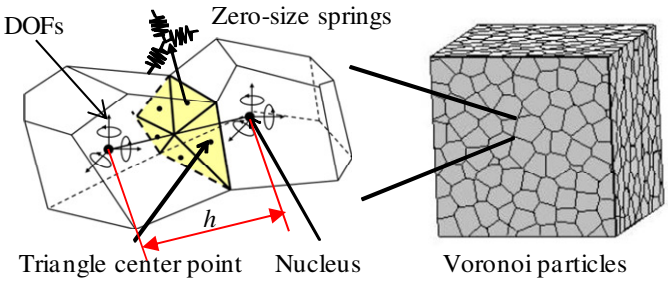

Figure 3.1. Voronoi particle definition of RBSM element

3.3 Concrete material model

Figure 3.2 shows the concrete material models that are used in the analysis.

The tensile behavior of concrete up to the tensile strength is modeled as linear elastic. A bilinear softening branch is assumed after cracking as shown, in which f_t is tensile strength, G_F is tensile fracture energy and h is distance between centers of the Voronoi elements.

In the compressive model, the stress-strain relationship is parabolic up to the compressive strength f'_c. The initial stiffness, E_c, is Young's modulus of concrete. After the peak, the softening branch exists until failure. G_{Fc} is compressive fracture energy and it is calculated as follows (Nakamura, 2001):

$$G_{Fc} = 8.8 \cdot \sqrt{f'_c} \tag{3.1}$$

Normal springs are set to represent the tensile and compressive properties of concrete. Strain of the normal springs is defined as follows:

$$\varepsilon = \frac{\Delta n}{h} \tag{3.2}$$

where ε is strain of the normal springs and Δn is normal relative displacement of elements of those springs.

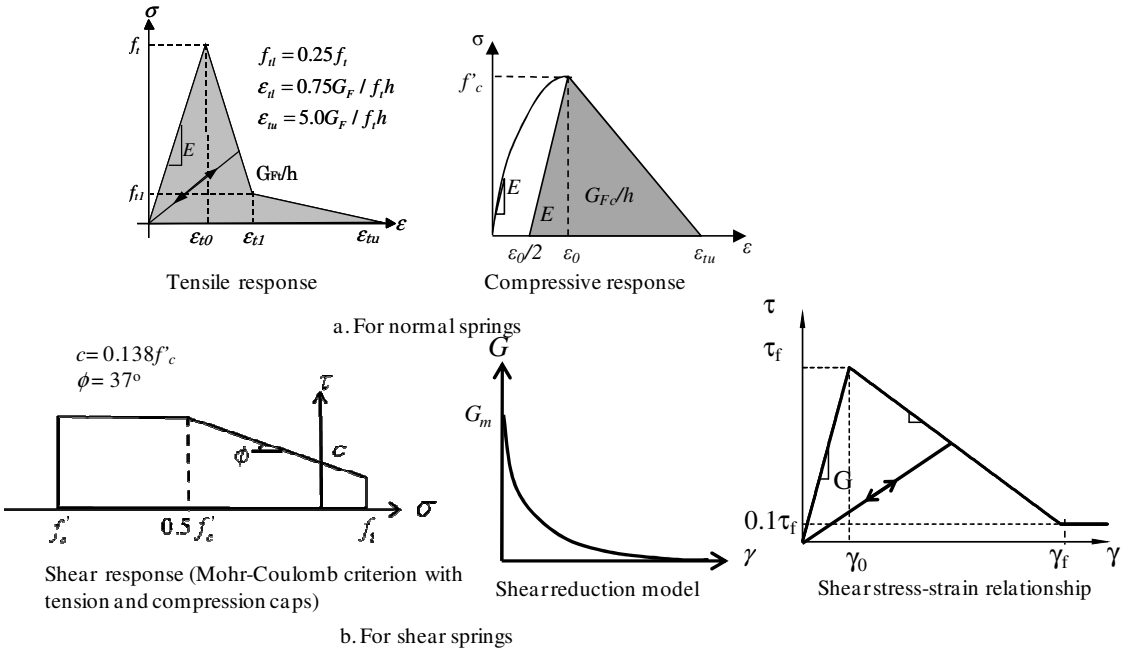

Figure 3.2. Concrete material model

Tangential (shear) springs represent the shear transferring- mechanism of concrete. Strain of the shear springs is defined as follows:

$$\gamma = \frac{\Delta s}{h} \tag{3.3}$$

where γ is strain of the shear springs and Δs is shear relative displacement of elements of those springs (Ishikawa et al., 2003).

The shear strength is assumed to follow the Mohr- Coulomb type criterion with the tension and compression caps, in which, c is cohesion and ϕ is internal friction and τ is shear stress. The shear-fracture criterion is expressed as follows (Ishikawa et al., 2003):

$$\frac{\tau^2}{\tau_f{}^2} \geq 1 \tag{3.4}$$

where

$$\tau_f = \begin{cases} c - \sigma \tan\phi, & \text{for} \quad \sigma \geq 0.5 f'_c \\ c - 0.5 f'_c \tan\phi, & \text{for} \quad \sigma < 0.5 f'_c \end{cases} \tag{3.5}$$

The shear transferring capacity at the cracked interface changes according to the crack opening. In order to take account of this effect, the shear stiffness is reduced by using a function of the strain normal to the crack as shown in the shear-reduction model in **Figure 3.2b**, in which G is the shear stiffness. Springs set on boundary behave elastically until stresses reach the τ_{max} criterion or the tensile strength f_t (Ishikawa et al., 2003). The shear stress-strain relationship is shown in **Figure 3.2b**. In the analysis, ultimate shear strain γ_f is assumed as 0.015.

Rebar is modeled as linear elastic in the analysis with the modulus of elasticity being 200 GPa.

Because mesh size of specimens in the case of corrosion is relatively small, the applicability of the RBSM method in the case of relatively small mesh size specimen is calibrated and it is confirmed by the experimental results of direct tension test, bending test and the cylinder compression test as described in Appendix A.

3.4 Corrosion expansion model

3.4.1 Modeling of corrosion internal expansion

In the RBSM model, the expansion of corrosion products is modeled as shown in **Figure 3.3**. A three-phase material model including rebar, corrosion products and concrete is applied in the analytical model. The merit of the model is that the properties of corrosion products such as thickness (H) and elastic modulus (E_r) are directly assumed. The model is also efficient in investigating the effects of corrosion products.

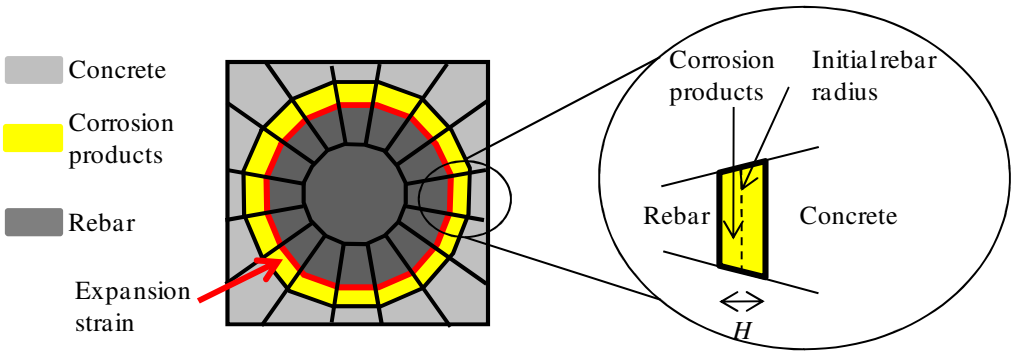

Figure 3.3. RBSM corrosion expansion model

The initial thickness of corrosion products layer (H) is kept to be constant during the analysis. This is a fictitious thickness used in the simulation in this study. The corrosion products layer is modeled by an elastic material model with unloading occurs to the origin. Due to nature of the corrosion process, we assume that internal expansion pressure is only activated in the normal direction, so strain is applied only to the normal springs located on the boundary between the corrosion products layer and the rebar. Strain in the corrosion product layer is determined (Lundgren, 2002):

$$\varepsilon_{cor} = \frac{U_{cor} - U}{H} \tag{3.6}$$

where U_{cor} is the real increase of the rebar radius corresponding to confinement of the concrete and U is the free increase of the rebar radius. On the other hand, shear stiffness of shears springs of the corrosion products layer is set nearly zero in the analysis to simulate free sliding of corrosion products layer in the shear direction.

Normal stress distribution in the corrosion products layer is determined based on the linear stress-strain relationship. Increment of a normal stress in the corrosion layer at each analysis step is determined as follows:

$$\Delta\sigma_{cor} = E_r(\Delta\varepsilon - \Delta\varepsilon_0) \tag{3.7}$$

in which, $\Delta\varepsilon = \frac{\Delta U_{cor}}{H}$ is increment of the total strain and $\Delta\varepsilon_0 = \frac{\Delta U}{H}$ is increment of the initial strain.

The internal expansion due to rebar corrosion is simulated using the initial strain problem with increment of initial strain in each analysis step is determined as Eq. (3.8) and it is an input data in the analysis.

$$\Delta\varepsilon_0 = \frac{\Delta U}{H} \tag{3.8}$$

in which, ΔU is an increment of the free increase U in each analysis step.

U is computed from the corrosion amount (W_r) as follows (Tran et al., 2011):

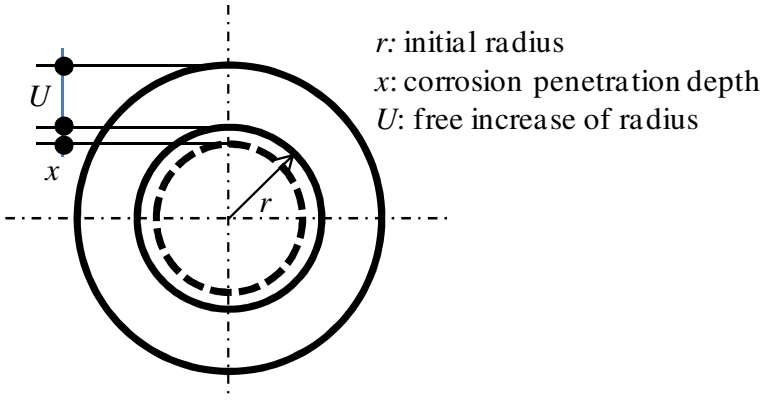

Figure 3.4. Physical dimensions of corrosion model

Based on **Figure 3.4**, the volume of steel loss is:

$$V_{loss} = L[\pi r^2 - \pi(r-x)^2] = \pi L[2r \cdot x - x^2] \approx 2\pi \cdot L \cdot r \cdot x \text{, since } x^2 \approx 0 \tag{3.9}$$

Volume of corrosion products:

$$V_{cor} = L[\pi(r+U)^2 - \pi(r-x)^2] \approx 2\pi L \cdot r(U+x) \qquad \text{since } x^2 \approx 0 \text{ and } U^2 \approx 0 \quad (3.10)$$

α_{cor} is the volume-expansion ratio of corrosion products, which depends on the corrosion products that are formed (Lundgren, 2002), in this study, it is assumed as 2.5 (Matsuo, 1997). As definition of α_{cor}:

$$\alpha_{cor} \cdot V_{loss} = V_{cor} \quad (3.11)$$

So,

$$\alpha_{cor} \cdot 2\pi L \cdot r \cdot x = 2\pi L \cdot r \text{ (U+x)} \quad (3.12)$$

Or

$$x = \frac{U}{\alpha_{cor} - 1} \quad (3.13)$$

W_r was defined in Chapter 2 and with Eq. (3.12) and Eq.(3.13):

$$W_r = \frac{\rho_s \cdot V_{loss}}{2\pi r \cdot L} = \rho_s \cdot x = \frac{\rho_s \cdot U}{\alpha_{cor} - 1}, \quad or \quad , U = \frac{W_r \cdot (\alpha_{cor} - 1)}{\rho_s} \quad (3.14)$$

in which, ρ_s is rebar density (= 7.85×10^3 kg/m^3 or 7.85×10^3 mg/cm^3).

3.4.2 Modeling of local corrosion

The chloride diffusivity coefficient through surface cracked concrete is much more than through sound concrete (Wang et al., 2008) As a result, a rebar is much more corroded around a part surrounded by un-cracked concrete or concrete with only minor cracks. **Figure 2.13** shows several actual corroded sectional patterns of the rebar after the electric corrosion test. Yaun and Ji (2009) also carried out the experiment of rebar corrosion and they found that the corrosion products only distributed in an elliptic shape on the half circumference of the rebar facing the concrete cover.

In this study, local corrosion of rebar after crack initiation is simply assumed as follows:

- Rebar is locally corroded when vertical cracks exceed 0.1 mm in width.
- The local corrosion model is assumed as a QUARTER corrosion model or a HALF corrosion model as shown in **Figure 3.6**. The observed corroded rebar sections after the electric tests appear similarly to these shapes.
- At the same corrosion amount, the total amount of corrosion products in the local corrosion model (S_L) is the same as that in the uniform model (S_u).
- Increment of initial strain in Eq. (3.8) is only applied over half or one- quarter of the model.

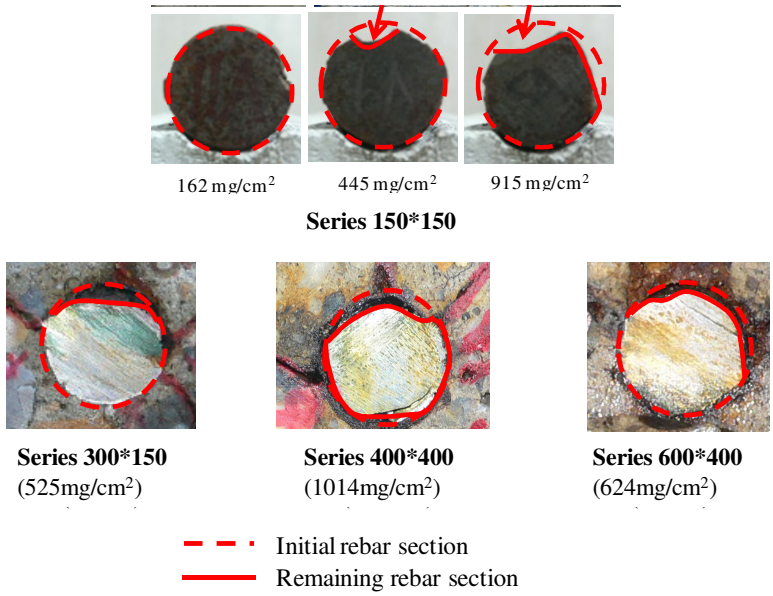

Figure 3.5. Actual corroded sectional patterns

Effects of the local corrosion of the rebar section on the cracking behavior will be discussed in Chapter 4.

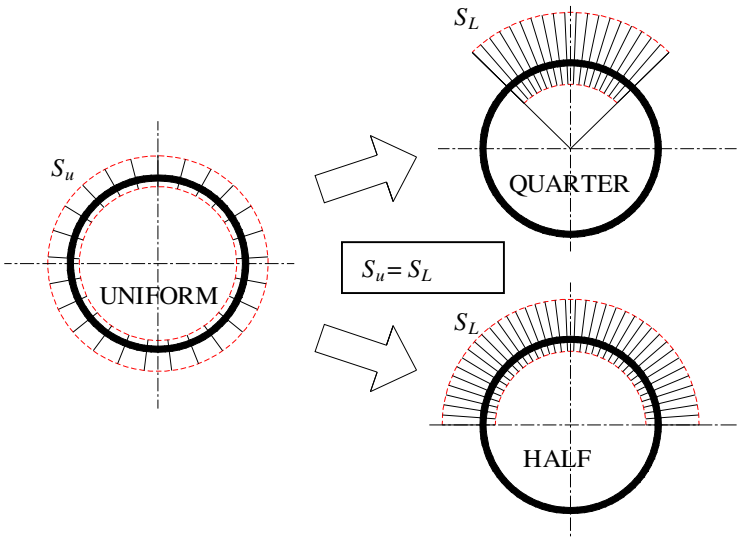

Figure 3.6. Modeling of local corrosion

3.4.3 Modeling of local penetration of corrosion products into cracks

During the corrosion process, it has been shown that corrosion products may penetrate into cracks after the concrete cracks and this effect may reduce the internal expansion pressure on concrete due to rebar corrosion (Val et al., 2009). From the experiment observation, the penetration of corrosion products into cracks could be observed and most of the corrosion products penetrated into vertical cracks in the concrete cover thickness as shown in **Figure 3.7**. The penetration of corrosion products into cracks can be diagrammatically modeled as in **Figure 3.8**. In this study, the effect of corrosion products penetrating into vertical cracks in the concrete cover is considered based on the observation from the tests. This effect can be simulated in the RBSM analysis. One of the advantages of the RBSM model is that crack widths and volume of the cracks can be calculated directly during the analysis. It is therefore convenient to calculate the reduction in volume of corrosion products that penetrated into cracks. The reduction in the internal expansion pressure caused by the penetration of corrosion

products into cracks is calculated by reducing the free increase *U*.

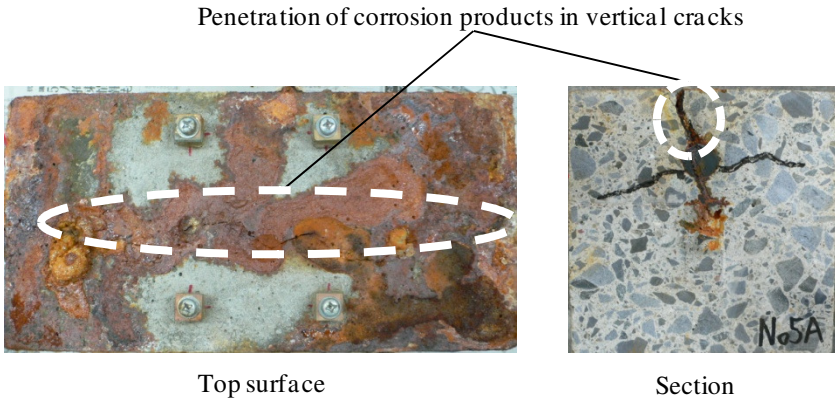

Figure 3.7. Penetration of corrosion products into cracks

The following assumptions were made when considering this effect in the analysis:

- Corrosion products can only penetrate into cracks if crack widths exceed the threshold value set for crack width. In this study, the threshold is assumed as 0.1 mm crack width.
- Corrosion products fully fill the volume of cracks.
- The free increase *U* is uniformly reduced around the rebar. When the local corrosion models are applied in the analysis, the HALF or the QUARTER corrosion model presented in section 3.4.2 is applied to re-distribute the internal corrosion expansion pressure.

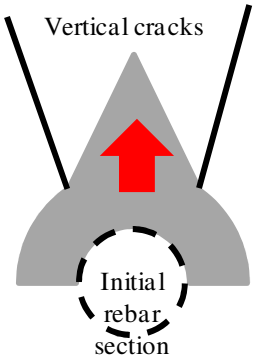

Figure 3.8. Image of penetration of corrosion products into cracks

With a free increase of U, the corresponding corrosion product volume corresponding with the U value is can computed from **Figure 3.4**:

$$V_{cor,U} = \left[\pi (r+U)^2 - \pi r^2 \right] L = \pi U (2r+U) L \tag{3.15}$$

as $U^2 \approx 0$, Eq. (3.15) can be approximated as

$$V_{cor,U} = 2\pi r \cdot U \cdot L \tag{3.16}$$

When the penetration of corrosion products into cracks is considered, the effective corrosion products volume $V_{cor,eff,U}$ is:

$$V_{cor,eff,U} = V_{cor,U} - V_{crk} \tag{3.17}$$

where V_{crk} is volume cracks computed in **Figure 3.9**, in which only the volume of vertical cracks is taken into account based on the observation of the test results.

If the effective free increase is U_{eff}, U_{eff} can be determined from V_{crk} based on Eqs. (3.16) and (3.17) as follows:

$$U_{eff} = U - \frac{V_{crk}}{2\pi r L} \tag{3.18}$$

or, in terms of increment value at an analysis step:

$$\Delta U_{eff} = \Delta U - \frac{\Delta V_{crk}}{2\pi . r . L} \tag{3.19}$$

in which, ΔU_{eff} is effective increment of the free increase and ΔV_{crk} is increment of volume of cracks computed in **Figure 3.9**.

The effect of the penetration of corrosion products into cracks is accounted for during the analysis. Increment of initial strain in Eq.(3.8) at an analytical step is reduced by ΔU_{eff} in Eq.(3.19).

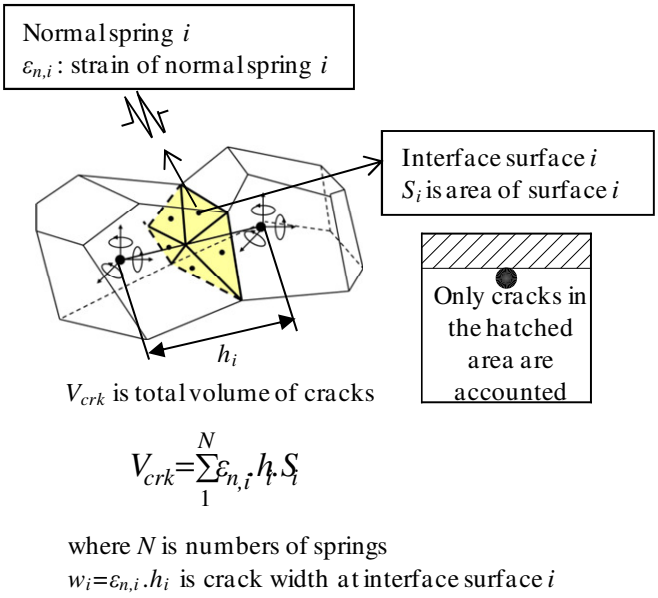

Figure 3.9. Computation of crack volume in the analysis

3.5 Summary

This chapter presented the analytical method based on 3D- RBSM method combined with a three-phase material corrosion expansion model including rebar, corrosion products layer and concrete. The concrete material model used in the analysis was presented in this chapter. Several corrosion models such as local corrosion models on the rebar section and the penetration of corrosion products into cracks after cracking for concrete were developed in order to simulate the rebar corrosion process in several

conditions as per the observation for the electric corrosion test. And, the merit of the analytical model is that several effects on the rebar corrosion process in concrete can be directly modeled in the analysis.

4. EVALUATION OF CRACKING BEHAVIOR AND APPLICABILITY OF ANALYTICAL MODEL

4.1 Introduction

In this chapter, crack propagation behavior due to rebar corrosion of the series 150*150-C30 is investigated both analytically and experimentally.

In the experiment, the procedure presented in Chapter 2 is carried out. That is, surface crack widths are measured, internal crack patterns are observed and internal cracks are measured at several rebar corrosion amounts. In addition, deformation of the specimen surface is measured using a laser displacement meter to understand a relationship between surface deformation and crack propagation, etc.

In the analysis, crack propagation behavior is simulated using the proposed RBSM analytical model presented in Chapter 3. Properties of the corrosion products layer such as the initial thickness and elastic modulus are recommended for the analytical model.

These recommended values are also compared with the experimental values reported in the literature. Moreover, effects of elastic modulus of corrosion products, effects of penetration of corrosion products into cracks, local corrosion model on the rebar section during the corrosion process are simulated and the effects are quantitatively evaluated. The applicability of the model is verified by comparison with the experimental results. As a result, the effects of modeling and the mechanism of crack propagation such as crack initiation, progress of surface crack width, propagation behavior of internal cracks and the effect of internal cracks on surface crack width are clarified.

4.2 Experiment of cracking due to rebar corrosion

4.2.1 Specimen set-up

Single-rebar specimens with the dimensions shown in **Figure 4.1** were tested by means of an electric corrosion test as presented in Chapter 2. After 32 days of curing, the electric corrosion test was conducted.

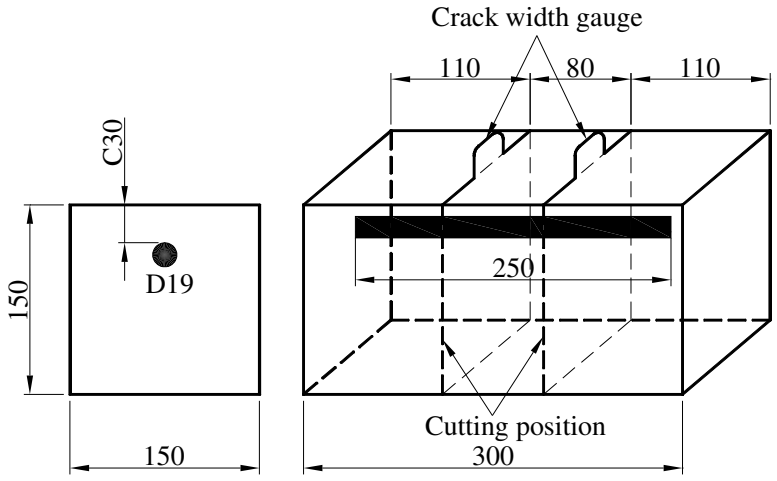

Fig. 1. Specimen dimensions

Figure 4.1. Specimen series 150*150-C30 dimensions

Based on the criterion suggested by Tsutsumi (1996), in the case of this specimen

series, the k value is 4.16 > 3, (k = $(2C+D)/D$ =4.16), so the internal crack patterns would be as shown in **Figure 4.2.**

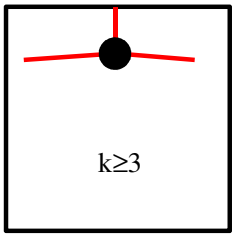

Figure 4.2. Typical internal crack patterns of specimen series 150*150

(proposed by Tsutsumi, 1996)

Prior to the test, the concrete compressive strength and tensile strength were measured to be 18.5 MPa and 1.53 MPa, respectively. During the test, surface crack widths were recorded using crack gauges and logged in computer files as discussed in Chapter 2. The testing time was varied for six specimens to investigate crack patterns, crack width propagation, internal crack propagation against increase of the rebar corrosion amount.

4.2.2 Rebar mass loss and testing time relationship

Figure 4.3 shows a relationship between mass loss W and testing time t for this series. Based on the experimental data, an empirical equation to calculate rebar mass loss was derived as follows:

$$\begin{aligned} W &= 0.235I.t && (I \cdot t < 66\ \mathrm{A \cdot hr}) \\ W &= 0.617I \cdot t - 25.305 && (I \cdot t > 66\ \mathrm{A \cdot hr}) \end{aligned} \qquad (4.1)$$

where W, I and t are rebar mass loss (g), current intensity (A) and testing time (hours) respectively.

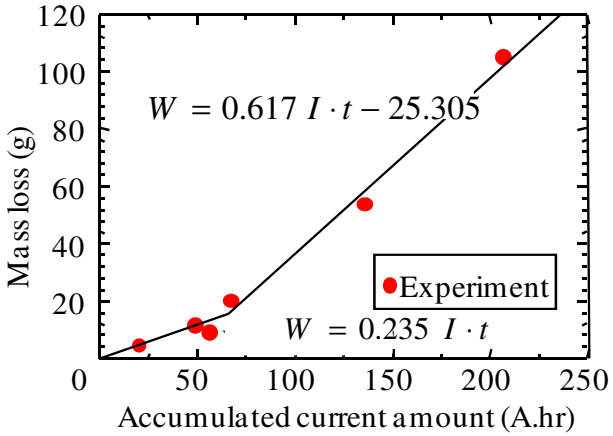

Figure 4.3. Rebar mass loss vs. testing time of specimen series 150*150-C30

Based on the empirical equation, mass loss of rebar can be estimated during the testing time and a relationship between surface crack width measured during the electric corrosion test and rebar mass loss or rebar corrosion amount can be developed as shown in the following section of this chapter.

4.2.3 Surface crack propagation

Based on the empirical Eq. (4.1) and the logged data of surface crack widths during the testing time as shown in **Figure 4.4**, the propagation of surface crack width against corrosion amount was developed, as shown in **Figure 4.5**. The opening of a surface crack initiates after a significant amount of corrosion products is formed. A critical amount of corrosion products is required to build up enough expansion stress and to cause cracking in the surface of a concrete specimen as Oh et al. (2009) discussed. After the crack initiation, the surface crack width rapidly propagates up to a value of about 0.4 mm. After that, the speed of propagation slows with the occurrence of lateral cracks and the effect of the penetration of corrosion products into cracks, which is discussed later

in this study. Then, the speed of propagation increases once again.

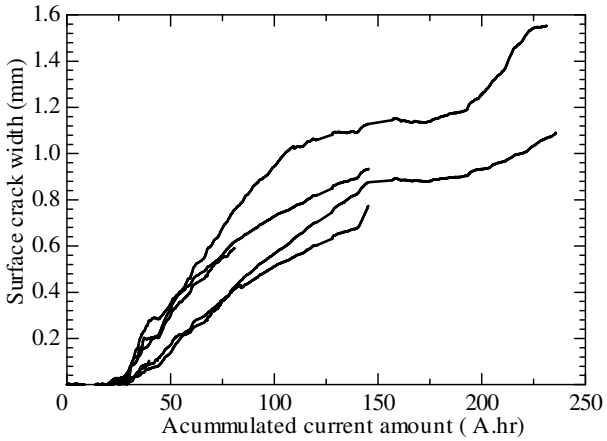

Figure 4.4. Surface crack propagation during test time

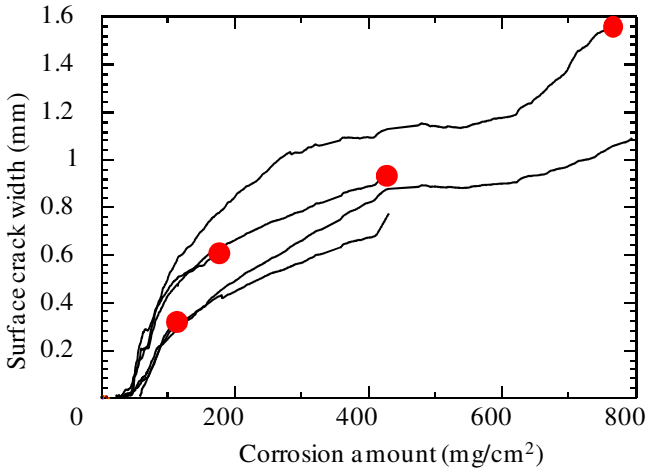

Figure 4.5. Surface crack propagation of series 150*150-C30

4.2.4 Crack patterns

Surface crack pattern at corrosion amount of 450 mg/ cm^2 is shown in **Figure 4.6**. Only single crack is observed along the specimen length which is corresponding to the crack pattern shown in **Figure 4.2**.

Figure 4.6. Surface crack pattern

Figure 4.7 shows internal crack patterns at several corrosion amounts corresponding to the red dots plotted in **Figure 4.5**. The initiation of a visible crack occurs on the surface of the concrete (vertical crack). When the amount of corrosion products increases, the crack propagates to the rebar. After that, lateral cracks appear and their lengths increase along with the increase in surface crack width. The internal crack patterns in the later corrosion stages appear to be agree with the proposal of Tsutsumi (1996)

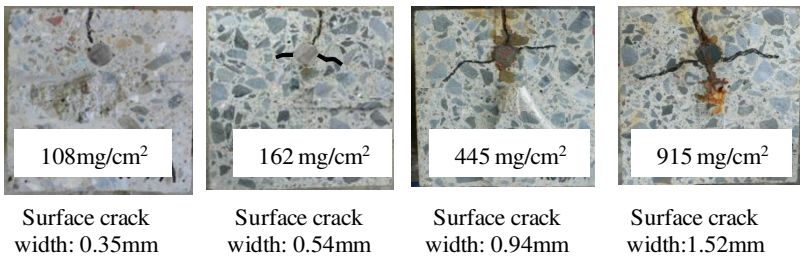

Figure 4.7. Internal crack patterns

4.2.5 Internal crack propagation

Internal vertical crack width is also measured at 5 mm above the rebar and **Figure 4.8** shows the propagation of the vertical crack width against the rebar corrosion amount. As shown in this figure, at the same value of the rebar corrosion amount, the internal crack width just above the rebar is smaller than the surface crack with as shown in **Figure 4.5**. After the crack initiation, the crack width also increases when the corrosion amount increases. However, the propagation slope is much smaller than the one for

surface crack width in **Figure 4.5**.

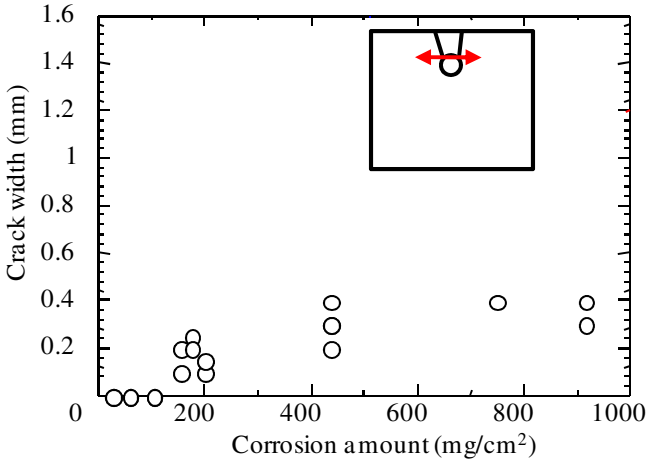

Figure 4.8. Propagation of vertical crack next to the rebar

Figure 4.9 shows the propagation of internal crack length. Internal crack length is horizontally measured from the side of the rebar to the tip of visible cracks as discussed in Chapter 2. The internal crack length increases rapidly to a value of 40 mm after initiation which is at a corrosion amount around 400 mg/cm^2 corresponding to surface crack width value of about 0.4 mm. Then, the crack length seems not to increase although the corrosion amount increases.

Figure 4.10 shows the propagation of internal crack width at several positions from the rebar side (i.e. 10 mm and 40 mm). At 10 mm from the rebar side, the internal crack width gradually increases to a value around 0.6 mm after initiation. The lateral crack width near the rebar becomes larger than the vertical crack width just above the rebar. On the other hand, at the position 40 mm from the rebar side, the propagation of the lateral crack width slows to a value around 0.2 mm. This behavior appears to be simultaneous to the propagation of internal crack length in **Figure 4.9**

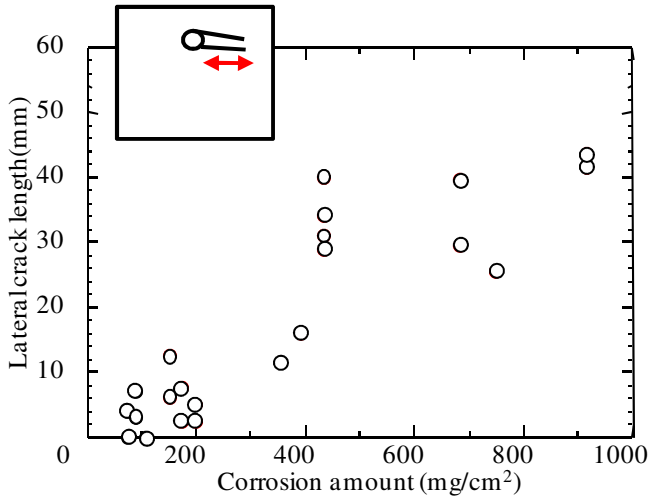

Figure 4.9. Propagation of internal crack length

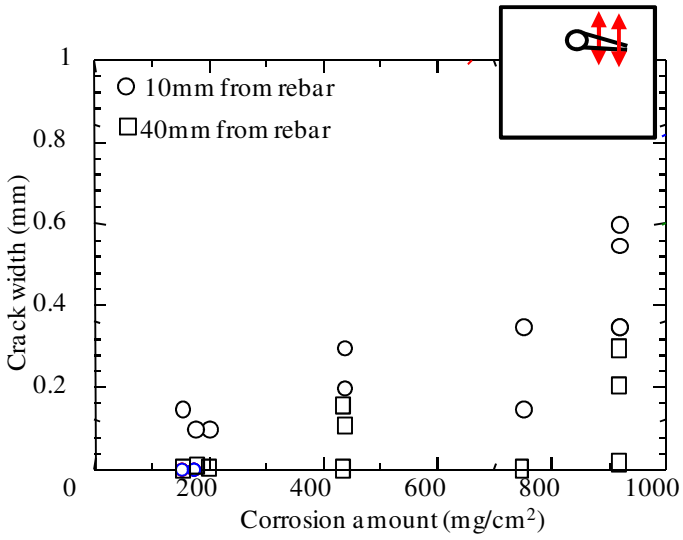

Figure 4.10. Propagation of internal crack width

4.2.6 Surface deformation

As mentioned in Chapter 2, the vertical deformation of specimen surface is measured during the corrosion process using a laser displacement meter having an accuracy of 1μm. The arrangement of the surface deformation measurement is shown in **Figure 4.11**. The length of the specimens used in this measurement is 200mm as explained in

Chapter 2. At the start of the electric corrosion test, the concrete compressive strength was 19.8 MPa. Vertical deformation was measured at points 75 mm and 125 mm from the end of each specimen (the red dashed lines in **Figure 4.11**) which are the same positions of the cut planes after the corrosion test for this specimen series. For each measuring line, the starting point is 10 mm in from the specimen edges and the measurement is 130 mm. The measurement interval was 250 µm (0.25 mm).

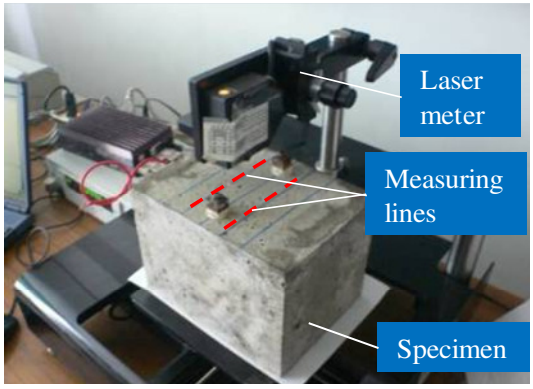

Figure 4.11. Measurement of surface displacement of series 150*150

Figure 4.12 shows the measurement surface deformation of specimens No. 1 and No. 2 at a stage of minor surface crack width evolution (**Figure 4.12a**) and a stage of visible surface crack width evolution (**Figure 4.12b**). After measuring the deformation at visible crack widths, the specimens were cut along the measuring position shown in **Figure 4.11** to enable observation of corresponding internal crack patterns (**Figure 4.12c**). Deformations of the specimen surface are small (approximately 25 µm), corresponding to minor surface crack widths (0.012 mm or 0.054 mm) in which a visible crack is not yet observed. The surface crack deformation shape shows that the specimen surface is bent when rebar corrosion amount is formed within concrete. This

behavior appears to be similar to the observation of Nguyen et al. (2006) by using a CCD camera. With the addition of more rebar corrosion products, the deformation of the surface specimens increases and surface crack width increases accordingly (**Figure 4.12b**). It is interesting that surface deformation reaches a maximum value where the surface crack opening initiates (the dashed lines in **Figure 4.12b**). When lateral cracks initiate and propagate, the distribution area of the surface deformation is closely related to the lateral crack patterns and the lateral crack lengths; see the dashed lines between **Figure 4.12b** and **Figure 4.12c**. For example, when internal cracks propagate diagonally (right side crack in **Figure 4.12c** of specimen No.2), surface deformation area is not increased in this case.

Figure 4.13 shows the relationship between the surface crack width and surface deformation. The surface deformation is measured at the middle of the specimen. The relationship of surface deformation values and the surface crack width seems to be linear. So, in this specimen, when the surface deformation increases, the surface crack width proportionally increases.

From the measurement of the specimen surface deformation, it can be seen that the surface crack opening is corresponding with the surface deformation intensity and the surface deformation area is corresponding to the lateral crack length propagation as limited between the red dash lines in **Figure 4.12**.

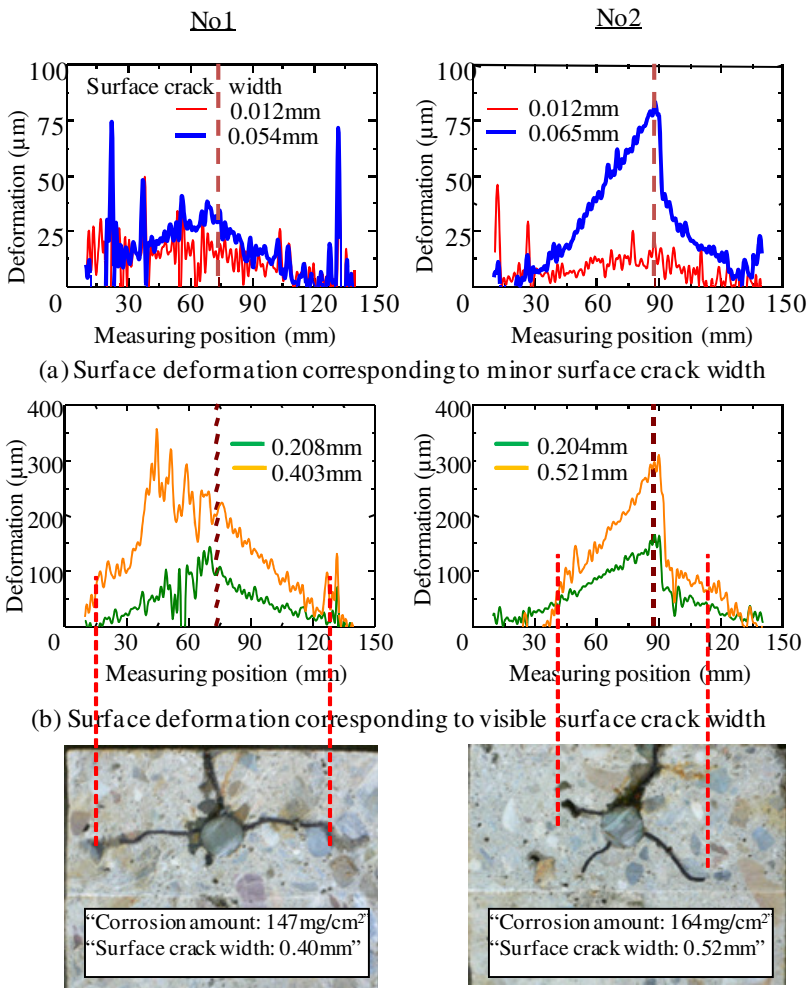

Figure 4.12. Surface deformation

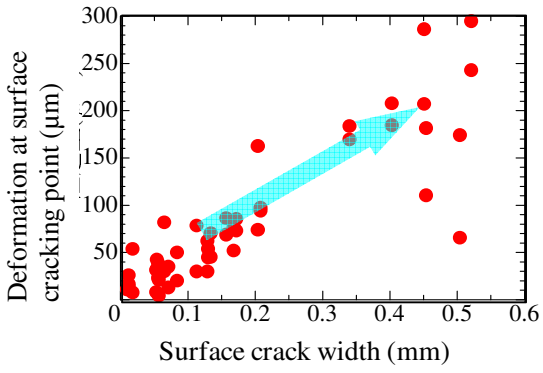

Figure 4.13. Relationship of surface deformation and surface crack width

4.2.7 Observation of rebar corroded sectional patterns

After cutting the specimens, the corroded rebar sections are observed at several rebar corrosion amounts. The actual corroded rebar sections are shown in **Figure 4.14**. The figure shows that the rebar parts facing to the concrete surface are more corroded rather than the other parts of the rebars. It clearly shows that rebar is not uniformly corroded around its section in the experiment. This observation is similar to some experimental results reported in the literature (Yuan et al., 2009).

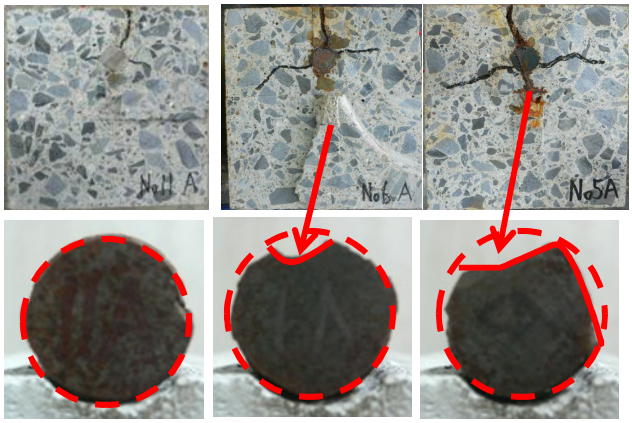

Figure 4.14. Actual corroded rebar sectional patterns

4.3 Analysis of cracking due to rebar corrosion

4.3.1 Modeling of specimen

Figure 4.15 shows the RBSM modeling of the specimen. In the analysis, mesh sizes of the Voronoi particles are 5 mm in the cover area and 25 mm in the other areas as shown in. Another arrangement of the Voronoi particles was tried to confirm the similarity of the analytical results. The specimen is supported by simple supports under the bottom as shown in **Figure 4.15**.

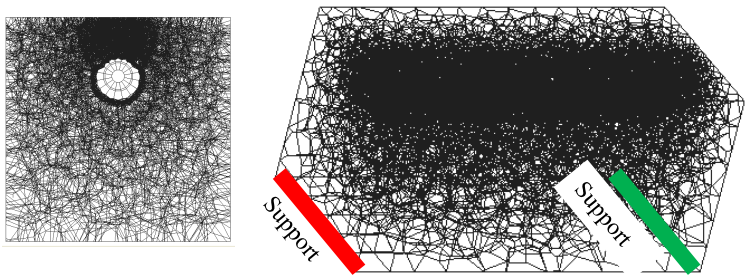

Section 3D view

Figure 4.15. RBSM model of specimen 150*150-C30

It was not easy to measure the properties, such as thickness and linear elastic modulus, of the corrosion products in the experiments. We analyzed specimens with various values for the thickness and the linear elastic modulus of the corrosion products layer. As a result, in the RBSM analytical model, an initial thickness (H) of 1.0 mm which is kept to be constant in the analysis, as explained in Chapter 3 and an elastic modulus (E_r) of 500 MPa simulate reasonable cracking behavior in terms of crack patterns and surface crack width propagation in comparison with the experimental results. The recommended elastic modulus of the corrosion products layer is also similar to the results of compression test of corrosion products conducted by Ouglova et al (2006). The initial thickness (H) of 1 mm appears to be suitable for numerical modeling of the corrosion products layer in the three-phase corrosion material as discussed in Chapter 3. The elastic modulus (E_r) of the corrosion products influences the initiation of the crack initiation as discussed in the later part in this chapter.

In terms of the rebar sectional corrosion pattern, the local corrosion QUARTER model will be applied and compared with the HALF model. This is an assumption in the analysis because it is not enough data to confirm an actual rebar corroded patterns in the test. However, it is definitely, uniform corrosion pattern around the rebar section should

not be used in the analysis as discussed above.

The local penetration effect, which was described in Chapter 3, is also considered in the analysis.

4.3.2 Surface crack propagation

The analytical surface crack width propagation is compared with the experimental results as shown in **Figure 4.16**. The analytical results agree with the experimental results; not only in terms of crack width values, but also propagation tendency. That is, the surface crack width initiates at a corrosion amount of around 40 mg/cm^2 of rebar and it propagates rapidly to a value of around 0.4 mm, then the crack width continues to increase but the speed of propagation reduces.

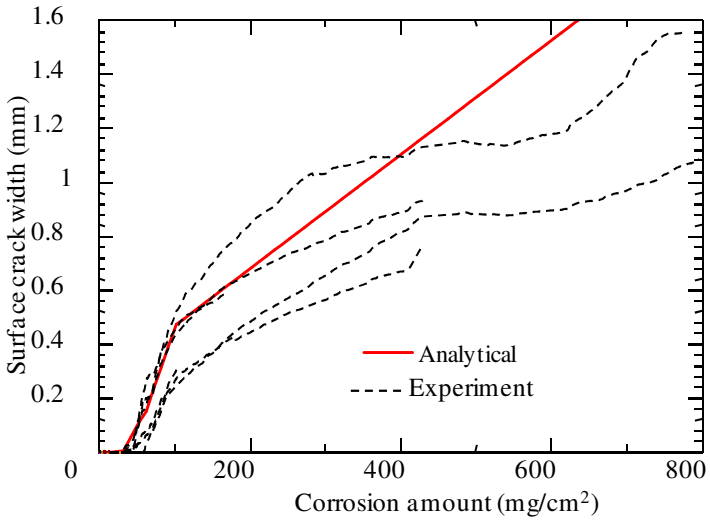

Figure 4.16. Analytical surface crack propagation

4.3.3 Crack patterns

Three- dimensional deformations of a specimen at several rebar corrosion amounts

are shown in **Figure 4.17**. The surface crack pattern can be observed from the deformation, where Voronoi particles are separated. This demonstrates the merit of the RBSM model. The surface crack patterns appear to be agreed with the experimental crack pattern shown in **Figure 4.6**, i.e. surface crack along the specimen length.

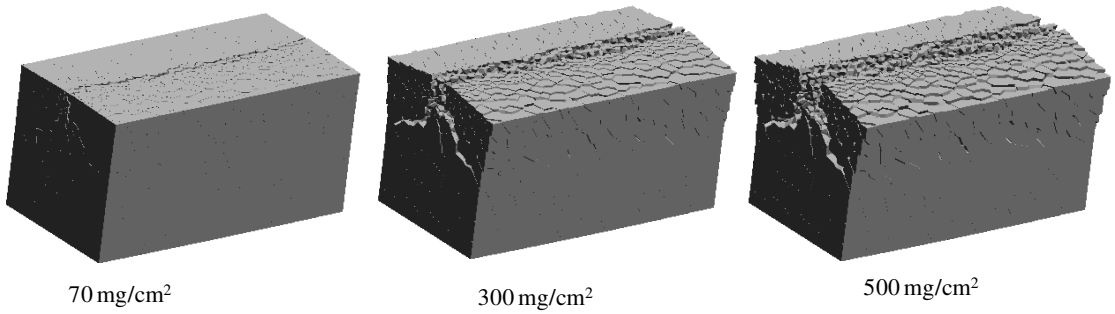

Figure 4.17. 3D-deformation (magnification = 25)

In order to show internal crack patterns , crack width are represented using the indication of crack width value as shown in **Figure 4.18**. Visible cracks are assumed to be wider than w_1, corresponding to ε_{tu} in the concrete tension response in Chapter 3 (where stress transfer is lost), and shown in the red colour range. Green colour range and yellow colour range show minor cracks having crack width smaller than 0.03 mm and smaller than 0.17 mm respectively. Internal crack patterns at several rebar corrosion amounts are shown in **Figure 4.19**. For clarity, only visible cracks (red colour range) are displayed in the sections. The analytical internal crack patterns appear similar with the test results in **Figure 4.7**. That is, visible cracks initiate from the surface and propagate to the rebar. With a further amount of corrosion products, lateral cracks initiate and propagate toward the specimen sides.

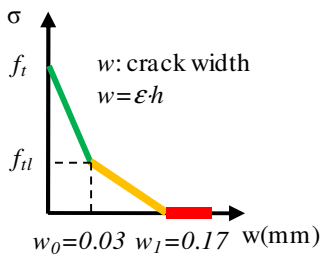

Figure 4.18. Indication of crack with value

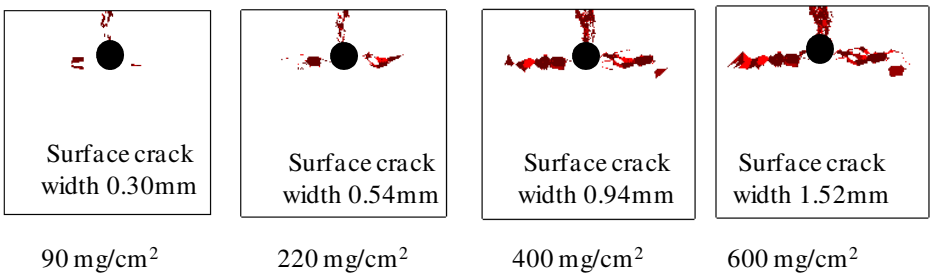

Figure 4.19. Analytical internal crack patterns

4.3.4 Internal crack propagation

It is necessary to simulate internal crack propagation to predict internal cracking behavior from surface cracks. The analytical results of propagations of vertical crack width near the rebar and lateral crack width and length are compared with the experimental results. **Figure 4.20** shows the propagation of near rebar vertical cracks from the analytical results. The analytical result appears agreement with the experimental results. That is, after crack initiation, crack width also increases when the corrosion amount increases.

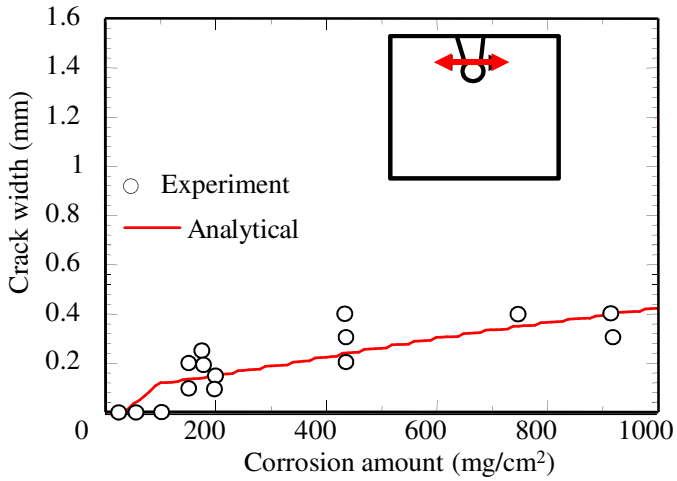

Figure 4.20. Analytical propagation of near rebar vertical crack

Figure 4.21 shows the propagation of internal crack length based on the analytical results. The analytical results simulate well behavior such as, rapid increase in lateral crack length before a corrosion amount of 400 mg/cm^2 and then the lateral crack length appears to be convergence although rebar corrosion amount increases.

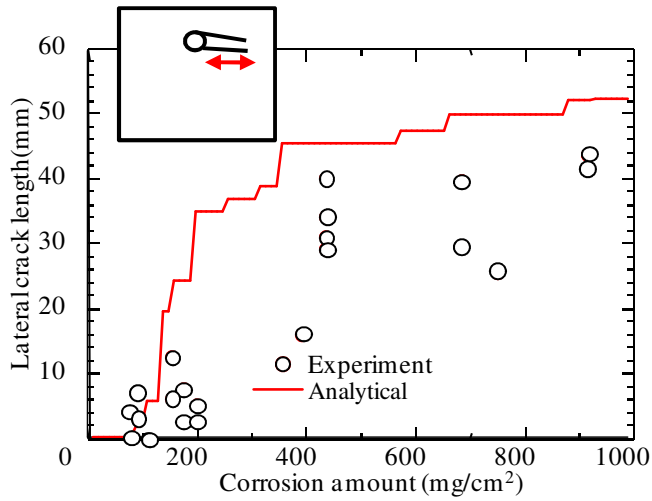

Figure 4.21. Analytical propagation of internal cracks

Figure 4.22 shows the propagation of internal crack width at several positions from the rebar side (i.e. 10 mm and 40 mm) based on the analytical results. The analysis reasonably simulates crack width propagation as well as crack length. That is, rebar closer crack width (at 10mm) faster propagates than the one farer from the rebar side (at 40 mm) at the same level of rebar corrosion.

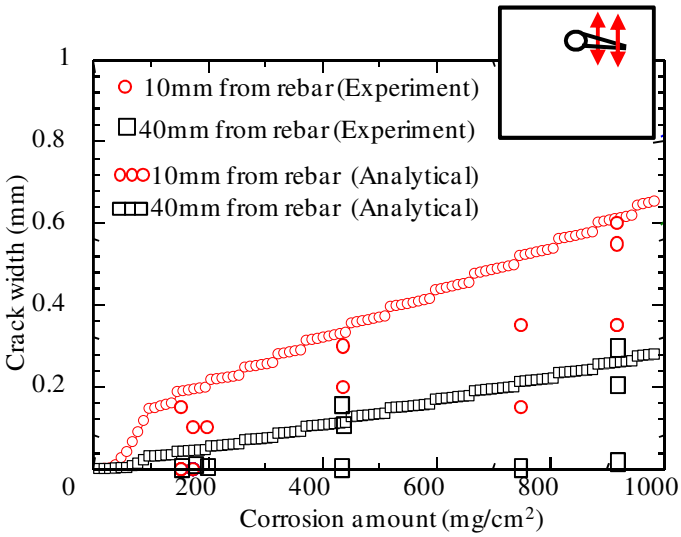

Figure 4.22. Analytical propagation of internal crack width

4.3.5 Surface deformation

Figure 4.23 shows the analytical surface deformation compared with the experimental results. The analytical values agree reasonably well with the test values such as deformation area, deformation shape and deformation value. The maximum analytical deformation area is about 40 mm - 50 mm from the middle point of the specimen surface which is relevant to the maximum lateral crack length shown in **Figure 4.21**.

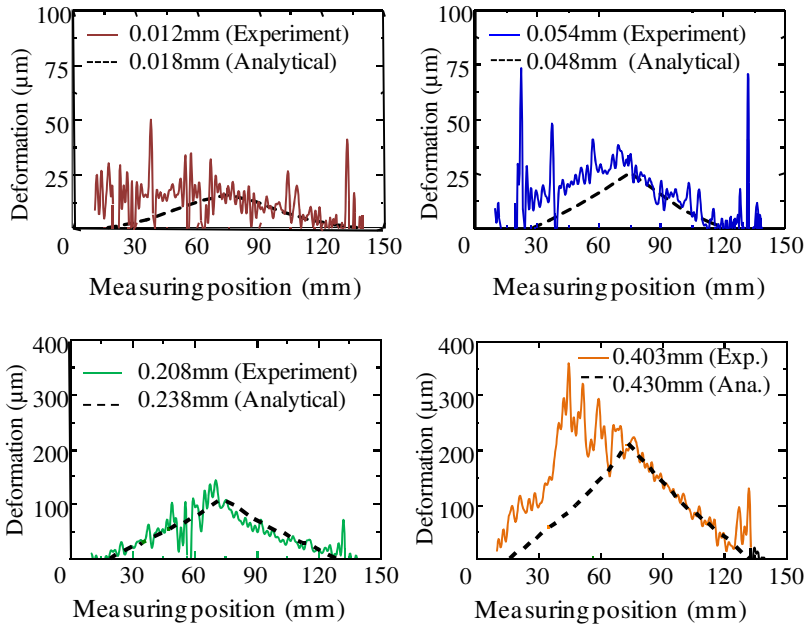

Figure 4.23. Analytical surface deformation

Figure 4.24 shows the propagation of vertical surface deformation at the cracking position (i.e. 75 mm from the specimen edge) against surface crack width (analytical results against experimental results). The propagation appears in a linear relationship and the analytical results agree with the experimental results.

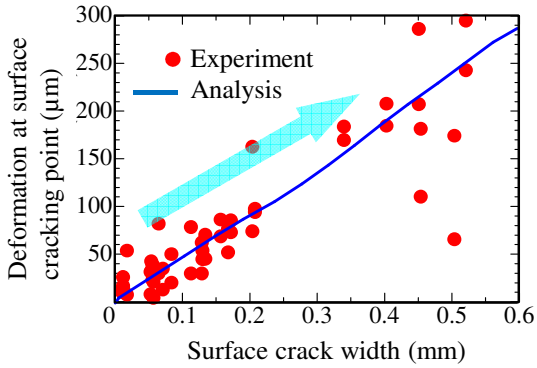

Figure 4.24. Analytical surface deformation and surface crack width relationship

4.4 Effects on the crack propagation

The analytical model is applied with some changes in order to evaluate effects of the corrosion products elastic modulus, sectional rebar corrosion pattern and penetration of corrosion products into cracks.

4.4.1 Effect of stiffness of corrosion products

The analytical mode is re-applied with a new value for the corrosion products elastic modulus E_r=100 MPa. The analytical surface crack width propagation is compared with the one for E_r=500 MPa presented in Section 4.3.2. At the same corrosion amount, with a higher value for the elastic modulus of, E_r=500 MPa, the corrosion expansion pressure induced by corrosion products is larger than the one in the case of E_r = 100 MPa. In **Figure 4.25**, the propagation in the case of E_r = 100 MPa is similar to the one of E_r = 500 MPa but the initiation of crack occurs at a higher corrosion amount value of about 100 mg/cm^2. In comparison with the experimental results, the value of E_r=500 MPa can result a better crack initiation. The value E_r=500 MPa is also similar a test result reported in the literature Ouglova et al (2006). So, the elastic modulus parameter of the corrosion products layer directly affects the surface crack initiation.

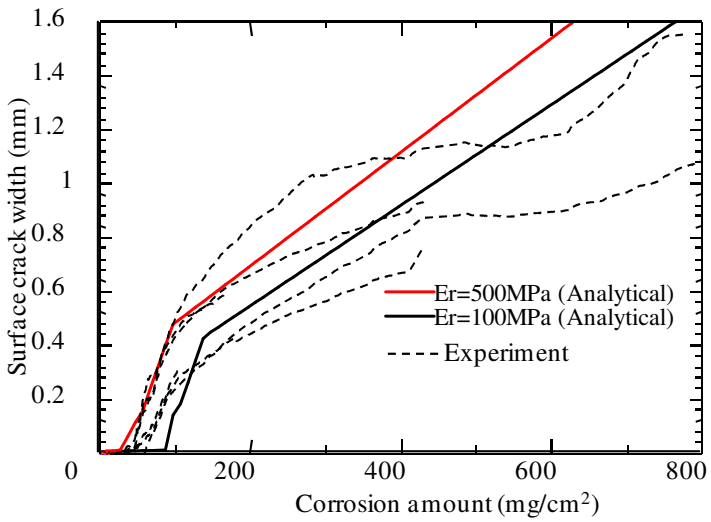

Figure 4.25. Effect of E_r on surface crack width propagation

4.4.2 Effect of local corrosion

The local corrosion HALF model and the uniform corrosion model are applied and compared with the local QUARTER model of rebar sectional corrosion pattern. The local corrosion is modeled based on the assumptions mentioned in Chapter 3. Regarding the internal crack patterns, the behaviors of the local corrosion (QUARTER or HALF) and the uniform model are different as shown in **Figure 4.26**. That is, at the early stage of corrosion, at the same value of the surface crack width (i.e. 0.54 mm), the local corrosion models induce internal cracks earlier than the ones induced by the uniform corrosion model. At the later stage of corrosion, there are inside cracks propagating from the rebar conforming to the behavior of uniform corrosion which is typically different from the crack patterns induced by the local corrosion models. That is because when uniform corrosion is assumed, corrosion expansion pressure acts in all direction around the rebar. Then, the expansion pressure under the rebar causes an inside crack. The crack patterns corresponding to the uniform corrosion case are different from the

experimental crack patterns shown in **Figure 4.7**. On the other hand, the crack patterns of the QUARTER model and the HALF model are similar to the test results. The local corrosion model of the rebar can, therefore, better simulate crack patterns in comparison with the experimental results. So, the local corrosion model is necessary to be used in the analysis.

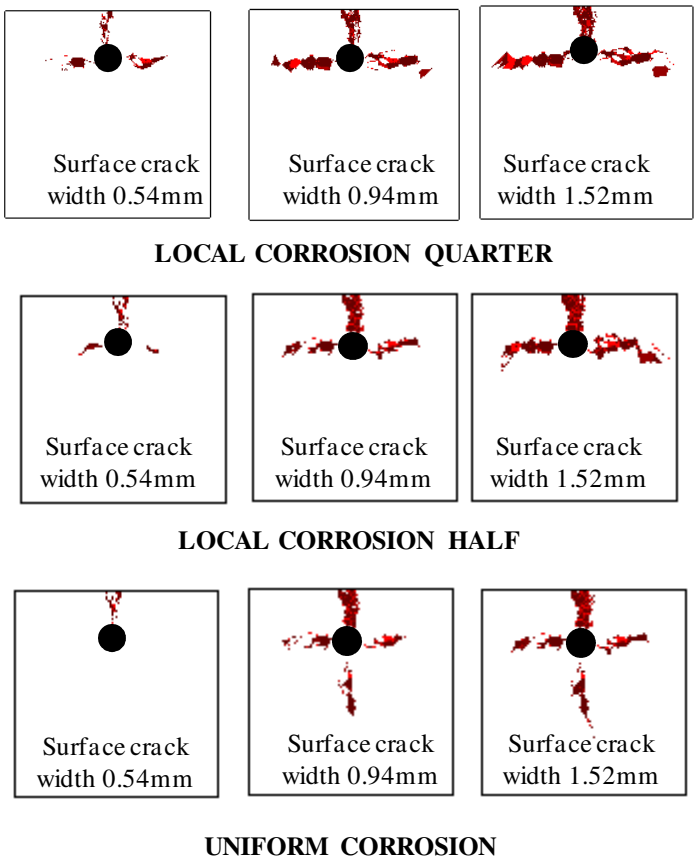

Figure 4.26. Effect of local corrosion model on internal crack patterns

In this specimen series, due to the narrow width of specimen, the difference of internal crack patterns in the case of different local corrosion model is not significant. However, in the case of wider specimens, such as 400 mm width and 600 mm width,

there is a significant difference between the local corrosion models as shown in **Figure 4.27** for a 400 mm wide specimen at corrosion rebar 500 mg/cm^2. In this case, the local QUARTER model results a better internal crack pattern in comparison with the test results which will be presented in Chapter 6. Again, the local corrosion model is an assumption in this study and it will require further investigation in future to determine which corrosion model should be used in the analysis.

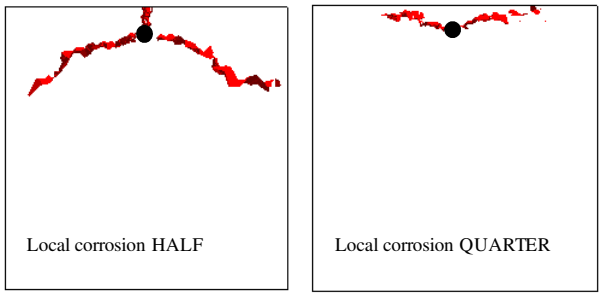

Figure 4.27. Effect of local corrosion model in a 400 mm wide specimen

Figure 4.28 shows the surface crack width propagation for each local corrosion model and the uniform corrosion model. In this comparison, the penetration effect of corrosion products after cracking is not taken into account. The penetration effect will be discussed in the later part of this chapter. The surface crack propagation is similar for each local corrosion model. However, the surface crack width induced by the local corrosion model is a bit larger than the one induced by the uniform corrosion model. This can be explained that in the local corrosion model only internal expansion pressure is distributed in the concrete cover toward to the surface of the specimen which will cause more surface deformation and therefore, more crack opening on the surface.

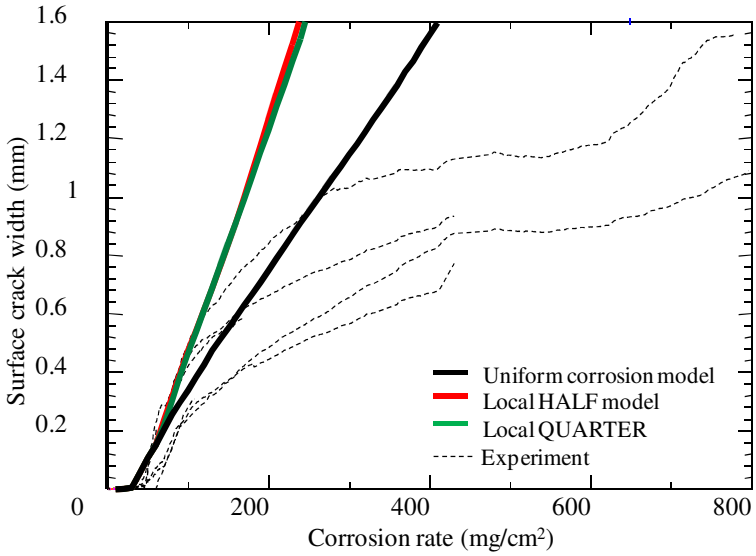

Figure 4.28. Effect of local corrosion model on surface crack propagation

4.4.3 Effect of penetration of corrosion products into cracks

In order to evaluate the effect of penetration of corrosion products into cracks, the analysis is conducted again for several cases; without the penetration effect and with the penetration effect but the threshold value for the crack width, which corrosion products can penetrate in cracks, is changed to 0.2 mm.

Figure 4.29 shows analytical surface crack width propagations in comparison with the experimental results. Without the penetration effect, the internal expansion pressure is highest and it causes the biggest crack width at the same corrosion amount value. Also, the surface crack width proportionally increases with the corrosion amount. In this case, the crack width values appear to be overestimated against the experimental results especially in the later stage of the corrosion process.

When penetration is taken into account, and with an assumed crack width threshold of 0.1 mm, the propagation speed of the surface crack width is reduced at the point corresponding to a surface crack width value of about 0.40 mm. At this point, the

internal crack is bigger than the threshold value, so corrosion products penetrate into the cracks and induce a reduction in the internal corrosion expansion pressure. Therefore, the penetration behavior is important to accurately simulate an evaluation of cracking with propagation. With threshold of 0.2 mm, the changing point of propagation corresponds to a crack width of 0.8 mm because there is small amount of fewer corrosion products penetrating into the cracks in this case. The tendency of crack width propagation after the changing point is similar to the case of a threshold of 0.1 mm.

Figure 4.30 shows the propagation of lateral crack length without penetration effect, and with a penetration effect with thresholds of 0.1 mm and 0.2 mm. In the case of penetration with different threshold values, the propagation in the early stage after cracking is clearly different but in the later stage with very large amounts of corrosion, the lateral crack length appears to convergence to a value of about 50 mm for both threshold values. Therefore, the penetration of corrosion products into cracks not only affects the surface crack width propagation, but also internal crack propagation.

As shown in **Figure 4.29**, a corrosion model that takes into consideration the penetration effect at a threshold of 0.1 mm simulates crack width propagation most closely to the experimental results. The threshold value greatly affects surface crack width propagation. In the experiments, corrosion products may not fully penetrate into cracks and the speed of penetration depends on crack width and the properties of corrosion products. In the analysis, we have assumed the fastest and most penetration, which induces the largest reduction in corrosion expansion. The above assumptions are simple cases for the analysis in this study and it will definitely require further work to simulate this effect. More experiments are needed to validate the simulations.

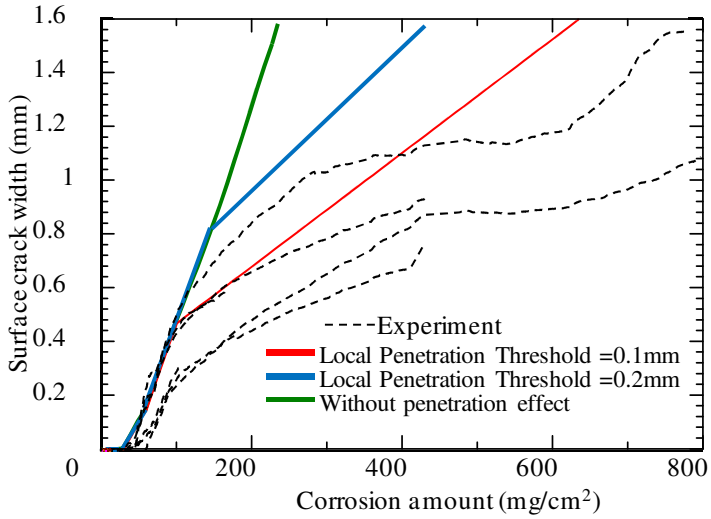

Figure 4.29. Effect of crack width threshold on surface crack propagation

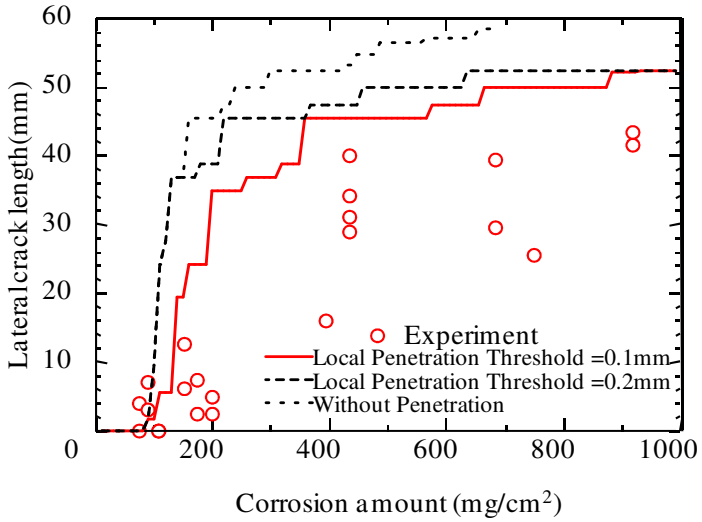

Figure 4.30. Effect of crack width threshold on internal crack propagation

4.5 Crack propagation mechanism

4.5.1 Crack initiation

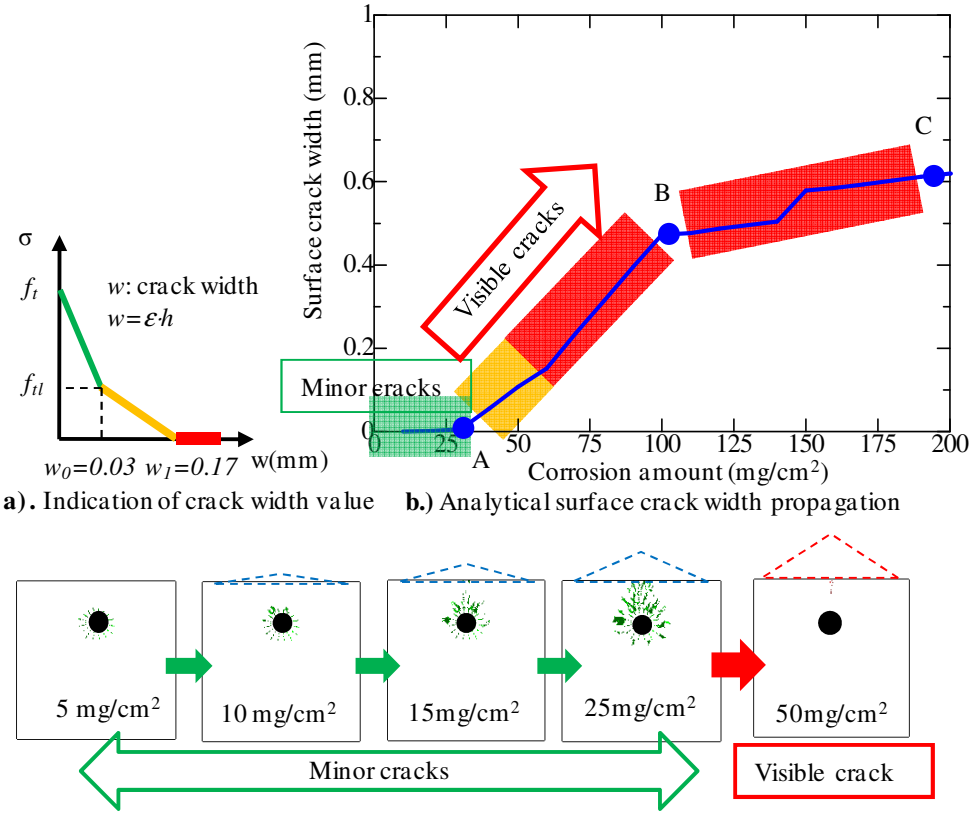

a). Indication of crack width value **b.)** Analytical surface crack width propagation

c.) Crack pattern development with surface deformation

Figure 4.31. Initiation of minor crack and visible crack (analytical)

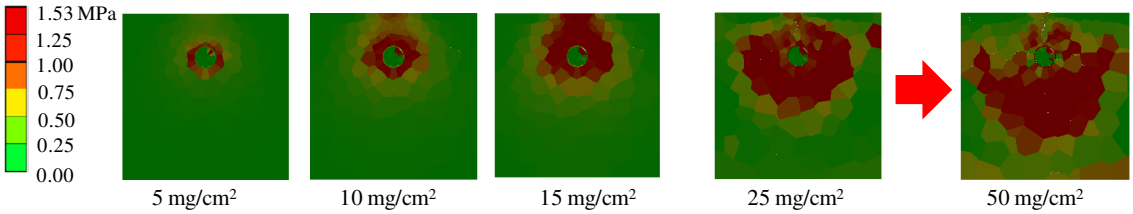

Figure 4.32. Principal stress distribution in the stage of crack initiation

Figure 4.31 shows the initiation of minor cracks and visible cracks based on the analytical results. **Figure 4.31a** shows crack width values corresponding to the colours

(green, yellow and red) shown in analytical crack patterns as mentioned above. **Figure 4.31b** shows regions of minor cracks and visible cracks with the surface crack width propagation. **Figure 4.31c** shows crack propagation from minor cracks to visible crack. Based on the analytical crack pattern and analytical surface deformation (**Figure 4.31c**), the initiation of cracks can be understood. That is, minor cracks initiate around rebar at rebar corrosion amount about 10 mm/ cm^2 when the tensile stress just exceeds the concrete tensile strength (green color). With a further amount of corrosion products forming on rebar, minor cracks propagate from the rebar and surface deformation occurs due to expansion pressure, at rebar corrosion amount about 15 mg/ cm^2. Then, minor cracks initiates on the surface, surface deformation is further increased and minor cracks propagate from both sides, i.e. rebar and surface, and accumulate in the concrete cover thickness when rebar corrosion amount is about 25 mg/cm^2. When the corrosion amount increases to a particular value about 50 mg/cm^2, cracks becomes visible on the surface (red crack pattern) corresponding to the bending effect of the surface.

Figure 4.32 shows principal stress distribution of the specimen corresponding to the stage of crack initiation. It shows that in early stage, tension stress of concrete exceeds the tensile strength around the rebar (at 5 mg/ cm^2) and then on the surface of the specimen (10 mg/ cm^2). When the rebar corrosion amount is 15 mg/cm^2, concrete cover exceeds the tensile strength and then the crack occurs on the surface of the specimen and the stress is released where cracks initiated (25 mg/cm^2 and 50 mg/cm^2).

4.5.2 Crack propagation (visible cracks)

In order to investigate crack development, propagation of cracks at several rebar corrosion amounts are shown with the corresponding surface deformation in **Figure**

4.33. After the crack initiation on the surface, the increase of surface deformation induces increase of the surface crack width (**Figure 4.33a**). Then, with the further amount of rebar corrosion, visible internal cracks initiate and propagate corresponding with increase of surface deformation width (**Figure 4.33b**). At this stage, internal cracks initiate, propagate and cause the deformation area shown in **Figure 4.33b** wider than the one in **Figure 4.33c.** In the later stage of rebar corrosion, the surface deformation further increases corresponding with the increase of the surface crack opening and the internal cracks further propagate corresponding with the increase of the surface deformation width (**Figure 4.33c** and **Figure 4.33d**).

Figure 4.34 shows principal stress distribution of the specimen in the stage of crack propagation. In this stage internal cracks initiate and propagate so the stress are almost released inside the specimen.

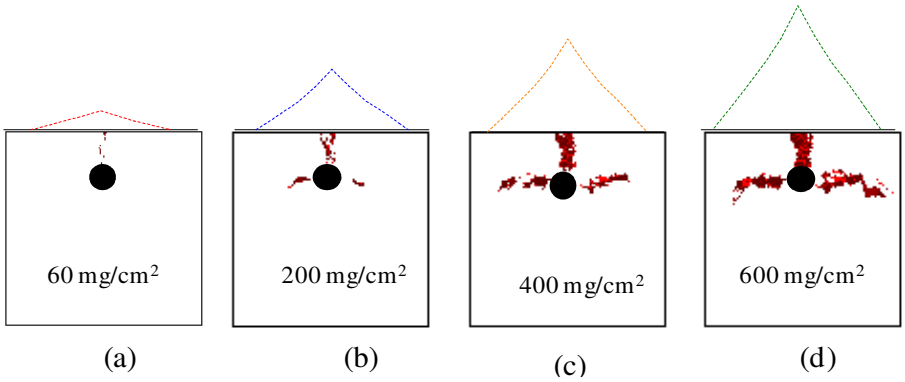

Figure 4.33. Crack propagation with surface deformation (analytical)

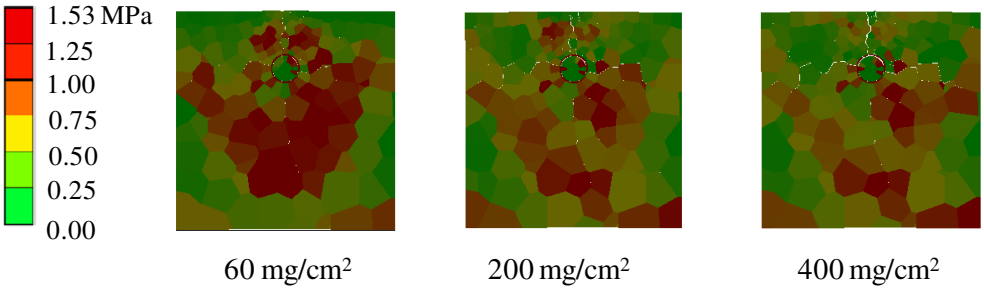

Figure 4.34. Principal stress distribution in the stage of crack propagation

4.5.3 Cracking mechanism

Based on the analytical results shown in **Figure 4.31** and **Figure 4.33**, a mechanism of surface visible crack width propagation with internal crack propagation can be proposed as follows:

a) When rebar corrodes, minor cracks are formed around the rebar when the tensile stress in concrete exceeds the concrete tensile strength. With an increase in the amount of corrosion products, a visible crack is initiated from the concrete surface due to the bending of the surface (**Figure 4.35a**) and it propagates to the rebar. In this stage, the surface crack width rapidly increases corresponding to stages A, B in **Figure 4.31b** due to stress release for the brittle behavior after cracking.

b) Then, internal cracks initiate (**Figure 4.35b**) and then increase in their widths and lengths simultaneously (**Figure 4.35c**). Corrosion products penetrate into cracks at this stage and reduce the speed of surface crack width propagation in comparison with the previous stages (stages B, C in **Figure 4.31b**).

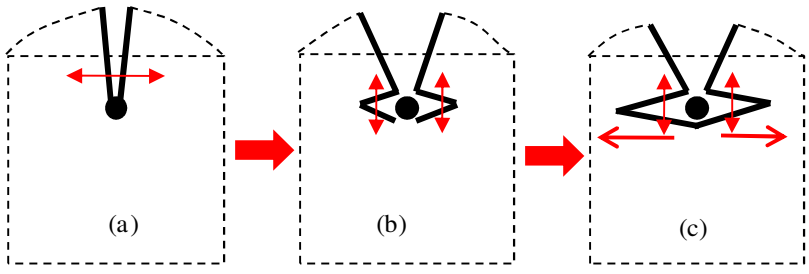

Figure 4.35. Series 150*150-C30 cracking mechanism

4.6 Summary

This chapter investigates crack propagation of the specimen series 150*150-C30 experimentally and analytically. Several corrosion conditions such as local corrosion and penetration of corrosion into cracks as well as properties of corrosion products are evaluated to clarify a cracking mechanism of this type of specimen. The following summary and conclusions were derived in this chapter.

(1) The proposed three-phase material corrosion-expansion model was appropriate to simulate corrosion- induced expansion pressure since properties of corrosion products could be assumed directly in the model. The values of the thickness and linear elastic modulus of corrosion products as of 1mm and 500MPa respectively were recommended for the RBSM analytical model.

(2) The local corrosion model after concrete cracking was necessary to considered in the analysis rather than the uniform corrosion model since it strongly influenced the internal crack patterns.

(3) The penetration of corrosion products into cracks should be considered in the corrosion induced cracking analysis because it quantitatively influenced the crack propagation. The penetration threshold value is a sensitive parameter in the model and it would require further experiments to evaluate.

(4) The proposed analytical model using 3D-RBSM was able to simulate efficiently the local corrosion and the penetration of corrosion products into cracks since crack widths and crack volumes could be obtained directly during the analysis.

(5) When rebar corroded, visible surface cracks initiated from the specimen surface and then propagated to the rebar. After that, the internal cracks initiated and

propagated with the increase of the surface crack widths. This mechanism was confirmed by the experimental results and the analytical results.

(6) A surface deformation measurement was evaluated using a laser displacement meter. The mechanism of the relationship between surface deformation, surface crack propagation, and internal crack propagation was confirmed. That is, the surface crack width is dependent on the surface deformation value and the lateral crack length is related to the surface deformation area. Therefore, in order to evaluate the surface crack propagation, the internal crack propagation should be precisely evaluated in the analysis.

(7) The results of the analytical model were verified qualitatively and quantitatively against the experimental results and they showed generally reasonable agreement, not only in the values but also in the propagation tendency.

5. EFFECTS OF CONCRETE COVER THICKNESS AND REBAR DIAMETER

5.1 Introduction

Concrete cover thickness and rebar diameter as well as ratio of cover thickness to rebar diameter were known as the fundamental factors affecting the cracking behavior due to rebar corrosion. Several researchers studied on effects of these factors and their studies were reported in the literature (Tsutsumi et al., 1996 and Alonso et al., 1998).

Tsutsumi et al. (1996) proposed a criterion of the effect of concrete cover thickness to rebar diameter ratio on the internal crack pattern of a single rebar specimen as shown in **Figure 5.1**. The criterion was that if k value was less than 3, cracks propagated diagonally to concrete surface and caused spalling of concrete cover. If k was larger than 3, cracks developed in the shortest path to the concrete surface, i.e. single surface crack appeared in the concrete cover and concrete surface. The criterion was governed by the elastic theory. The experiment was also carried out to verify the criterion but crack patterns around the threshold value of $k = 3$ were not known. Moreover, effect of k

on the crack propagation was not reported.

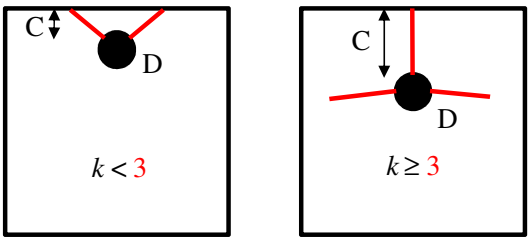

$$k = \frac{2 \cdot C + D}{D}$$

Figure 5.1. Tsutsumi's criterion for crack pattern

Alonso et al. (1998) conducted an experiment on testing specimen series with various rebar diameters and various cover thicknesses and they found that larger C/D ratios delayed surface crack initiation. However, effect of the C/D ratio on internal crack propagation was not known.

In this chapter, two specimen types which are the same cover thickness C = 30 mm having various rebar diameters and the same rebar diameter D19 and various concrete cover thickness are tested by using electric means to investigate the effect of variation of the rebar diameter and cover thickness on the crack propagation. These specimens are simulated to investigate the effect of rebar diameter and cover thickness analytically. Based on the experimental results and analytical results, the effect of rebar diameter or ratio of concrete cover to rebar diameter can be discussed.

Then, in order to investigate effect of variation of the internal expansion area on the cracking behaviour, a parameter study is conducted on specimens with a rectangle-shaped “rebar”. Based on the analytical results, effects of the variation of the internal expansion area are clarified.

5.2 Effect of rebar diameter on the cracking behavior

5.2.1 Specimen set-up and test results

Two specimen series are tested by using the electric corrosion test. Series 150*150-D10 includes specimens with D10 rebar and series 150*150-D25 is with D25 rebar. The concrete cover thickness is constant in this study. **Figure 5.2** shows specimen setting dimensions for these series**.** The concrete composition is the same as the one introduced in Chapter 2. In terms of Tsutsumi's criterion, k = 7 for Series **150*150-D10** and k = 3.4 for Series **150*150-D25,** so both cases may have crack patterns with a single crack propagating to the surface as shown in **Figure 5.1**. In terms of C/D ratios, the C/D ratios are 3 and 1.2 for these specimens accordingly.

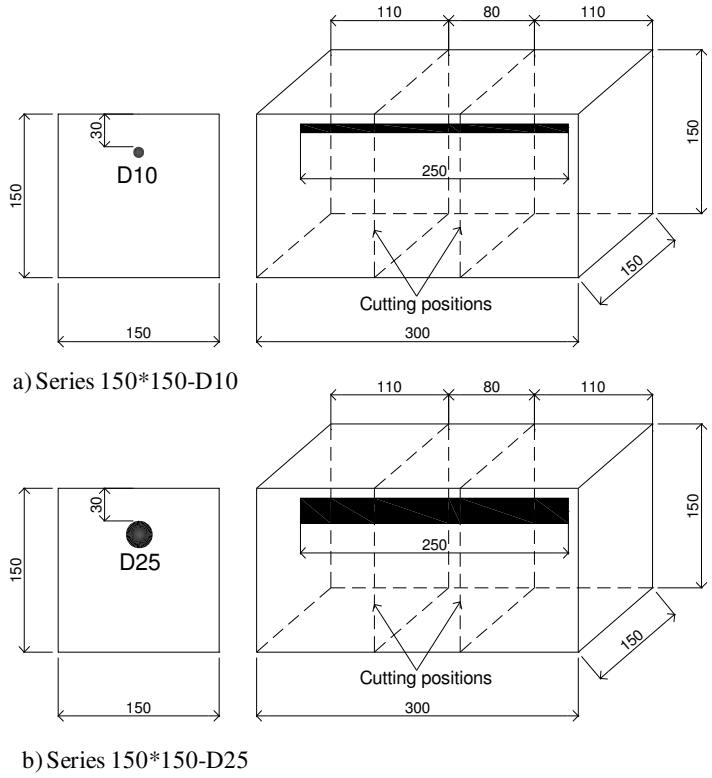

Figure 5.2. Set-up of specimens with different rebar diameters

Figure 5.3 shows propagation of surface crack observed in the electric test for specimens with D25 rebar and D10 rebar. It is clearly understood that the bigger rebar diameter induces larger surface crack values than the ones induced by the smaller rebar diameter in both intensity and tendency. This may be due to the larger internal expansion pressure area inside the concrete.

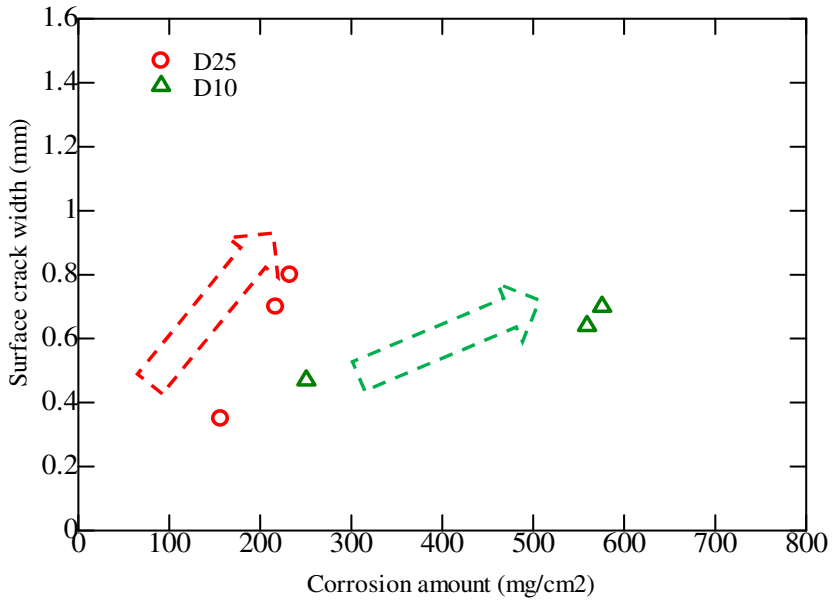

Figure 5.3. Surface crack propagation (different rebar diameters)

Figure 5.4 and **Figure 5.5** shows surface crack patterns and internal crack patterns of the D10 specimens and D25 specimens respectively. The surface crack pattern appears similar in each case. That is single crack propagating along the specimen case. This crack patterns are compatible with the Tsutsumi's proposal. The internal crack patterns show that internal cracks already propagated when the rebar corrosion amount is more than 200 mg/cm^2. And the internal crack patterns also appear to be compatible with the proposal of Tsutsumi in the case of k>3. It is also seen that corrosion products

immigrated into cracks in most of the cases.

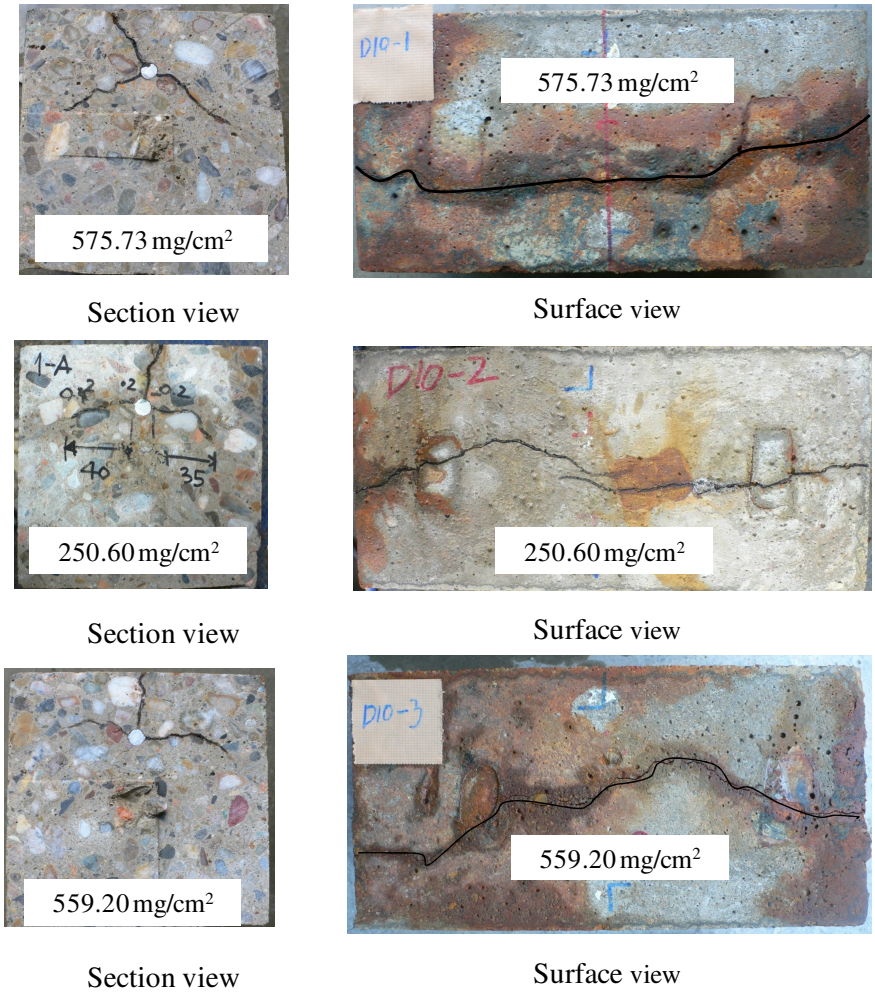

Figure 5.4. Crack patterns of 150*150-D10 specimens

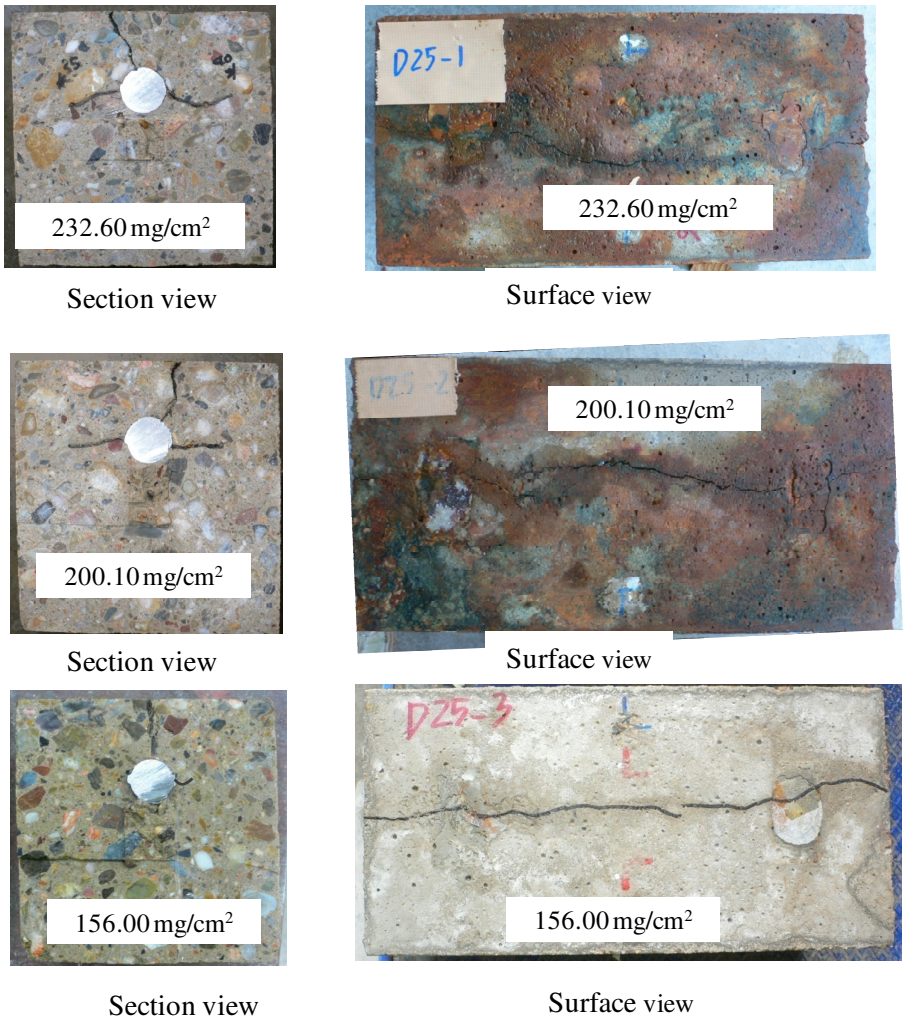

Figure 5.5. Crack patterns of 150*150-D25 specimens

Figure 5.6 shows internal crack length propagation of the various rebar diameter cases. Due to the different rebar diameters, the crack length is measured from the rebar center to the visible crack tips for easy comparison. The internal cracks initiated when rebar corrosion amount is about 200 mg/ cm^2 and then speedily propagate to a value of about 50-60 mm length.

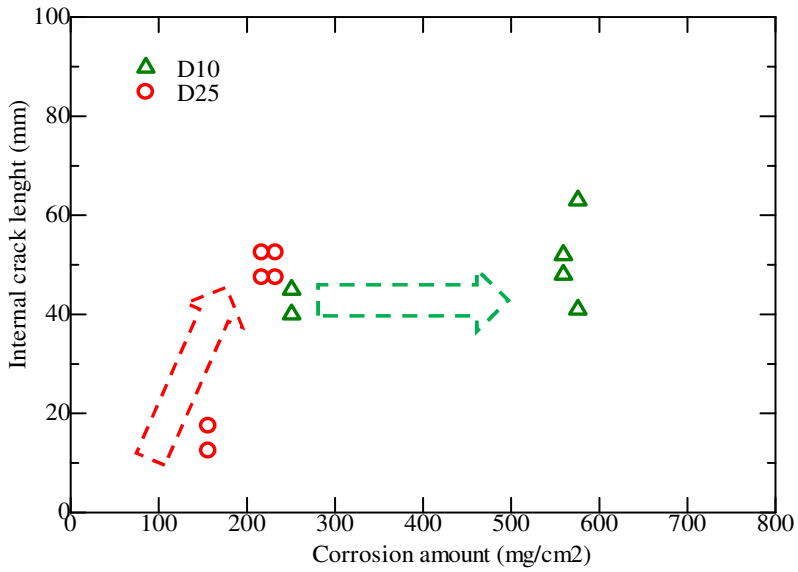

Figure 5.6. Internal crack length propagation (different rebar diameters)

Figure 5.7 shows a relationship between propagation of internal crack and surface crack for various rebar diameter cases. It shows that after initiation, internal cracks tend to slightly increase or not to increase when the surface crack develops. It may be due to the limit of the specimen size, i.e. 150 mm.

After cutting the specimens, the corroded rebar sections are observed at several rebar corrosion amounts. The actual corroded rebar sections are shown in **Figure 5.8**. The figure shows that the rebar parts facing to the concrete surface are more corroded rather than the other parts. It is also clearly shown that rebar is not uniformly corroded around its section.

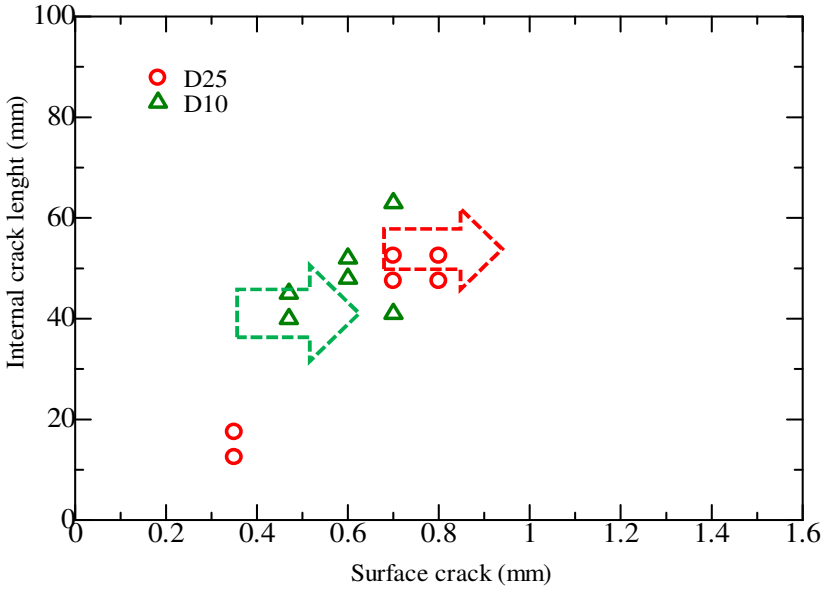

Figure 5.7. Surface crack and internal crack relationship (different rebar diameters)

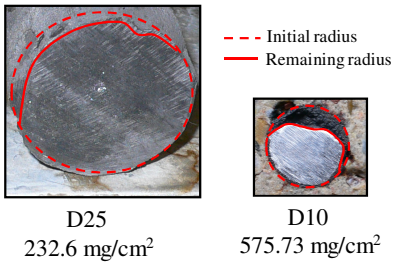

Figure 5.8. Corroded rebar sectional patterns (different rebar diameter)

5.2.2 Numerical evaluation of effect of rebar diameter

In the modeling, cover thickness is modeled with 5 mm meshes and the others are modeled with 15-25 mm meshes. The local corrosion QUARTER model is assumed in the analysis and the penetration of corrosion products into cracks is also taken into account as observed in the experiment.

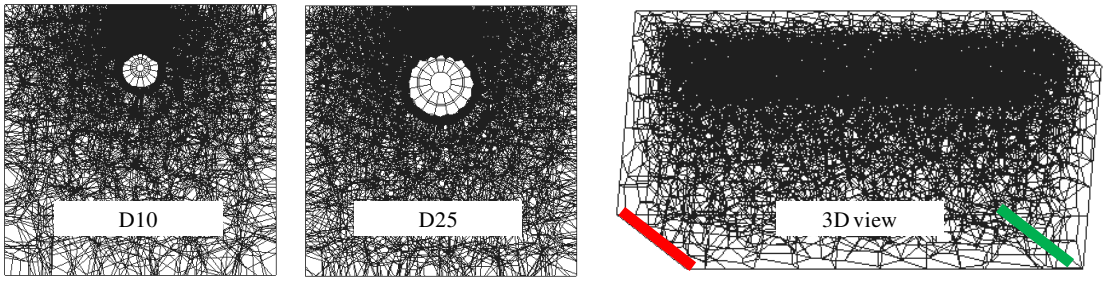

Figure 5.9. RBSM modeling of different rebar diameter specimens

Figure 5.10 shows surface crack propagation obtained from the analysis. The results show that D10 specimen (*C/D* = 3) delayed the initiation of the surface crack in comparison with D25 specimen. After the initiation, the surface crack width propagates and then the speed of propagation reduces due to the penetration of corrosion products into cracks. After the initiation of the crack, the crack propagation slope of specimen D25 also higher than the one of specimen D10 because the D25 rebar diameter induces larger internal expansion than the one induced by D10 rebar. So, this tendency appears to be agreement with the test results.

Figure 5.11 shows deformation of the specimens at several rebar corrosion amounts. Surface crack patterns can be observed from the deformation by the separation of the particles. The crack patterns look similar to the test results, in which cracks propagate along the specimen lengths. It can be seen that at the same value of rebar corrosion amount, D25 specimens results wide surface crack opening due to the larger internal expansion in comparison with D10 specimens.

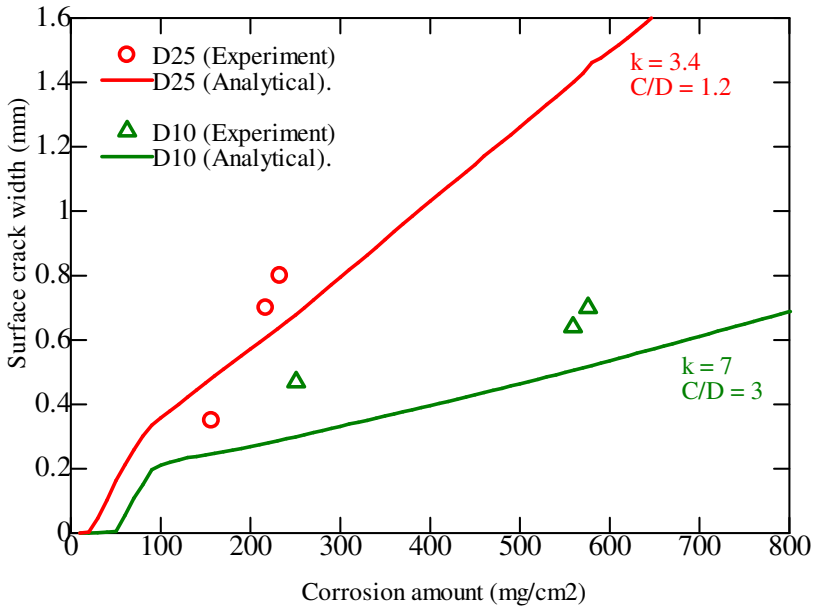

Figure 5.10. Analytical surface crack propagation (different rebar diameters)

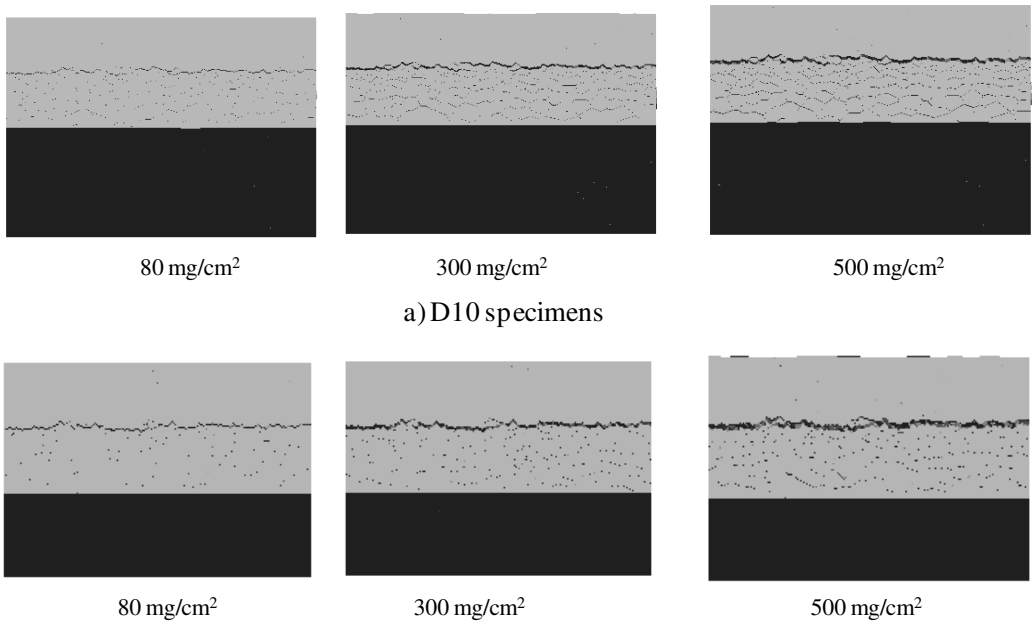

Figure 5.11. Specimen deformation (different D)

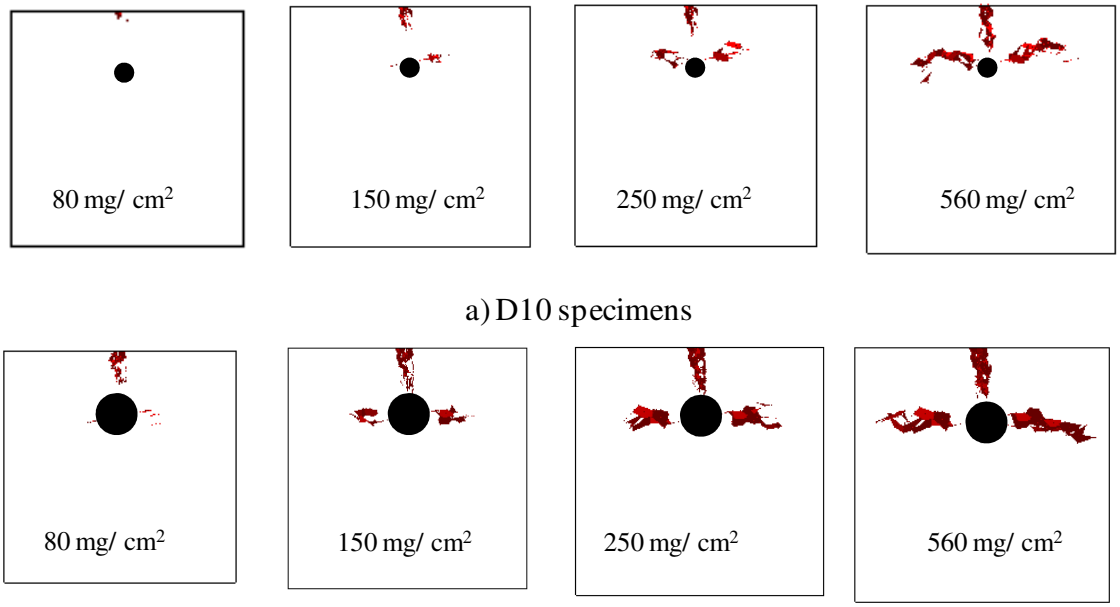

Figure 5.12. Analytical internal crack patterns (different rebar diameters)

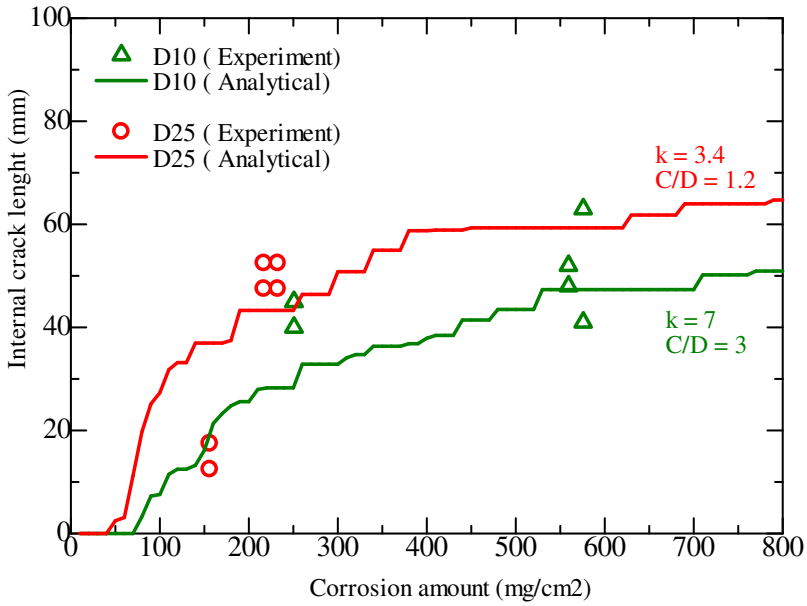

Figure 5.13. Analytical internal crack propagation (different rebar diameters)

Based on the experimental result and analytical results, it can be seen that the bigger

rebar diameter (smaller k values or C/D ratios) induces earlier initiation of surface crack and internal cracks and in the later stage of rebar corrosion, the bigger rebar diameter also induces larger crack width and length.

5.3 Effects of cover thickness and k value

5.3.1 Specimen set-up and test results

Specimens series having the same rebar D19 and various cover thicknesses including the series 150*150-C7.5, 150*150-C15 and 150*150-C45 are tested by using the electric means. **Figure 5.14** and **Table 5.1** show setting dimensions of these specimen series. The concept of these specimens is to investigate the effect of cover thickness and k value on the crack pattern and crack propagation. This also enables observation of crack patterns around the threshold of k = 3.

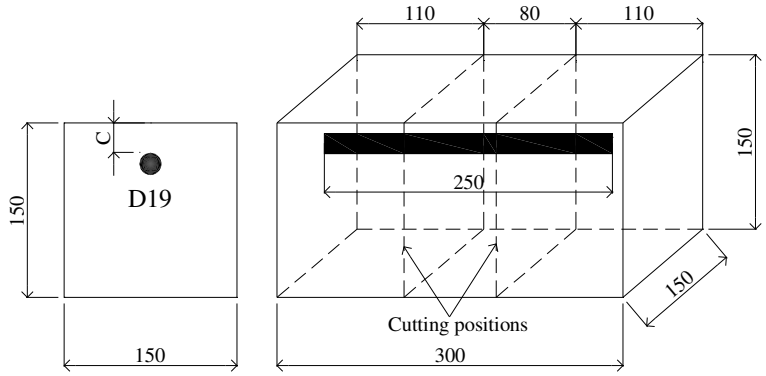

Figure 5.14. Specimen 150*150 with various concrete covers

Table 5.1. Specimens 150*150 with various cover thicknesses

Series	C(mm)	D(mm)	k
150*150-C7.5	7.5	19	**1.79**
150*150-C15	15	19	**2.58**
150*150-C45	45	19	**5.74**

Figure 5.15 shows experimental internal crack patterns at several rebar corrosion amounts for each case of k value. The experiment shows that with k =1.79, cracks diagonally propagated toward the specimen surface, which is similar to the Tsutsumi's conclusion. In the case of k = 2.58, single surface crack is also formed and crack propagates in the shortest path to the specimen surface. If k = 5.74, it is clearly shown that only single crack propagates in the concrete cover as per the Tsutsumi's criterion.

The corroded rebar sectional patterns were also observed for each case of k value as shown in Figure 5.16. Local corrosion on the rebar section was also observed in most of the case. It is noted that Tustsumi used the uniform corrosion model around the rebar section to analyze crack patterns in his study.

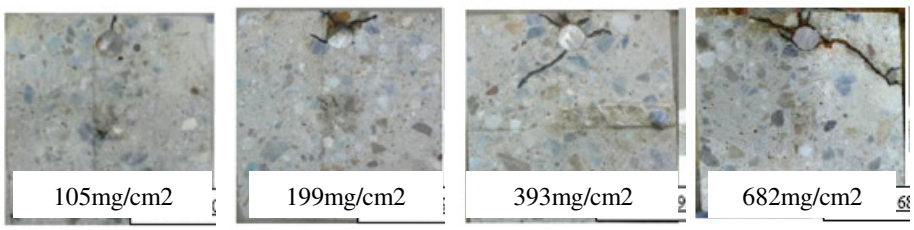

a) C= 7.5; k =1.79

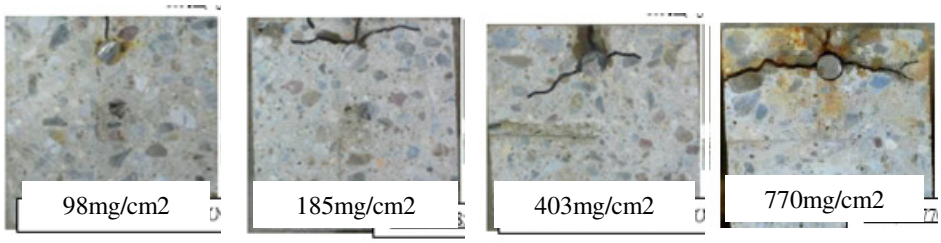

b) C= 15; k =2.58

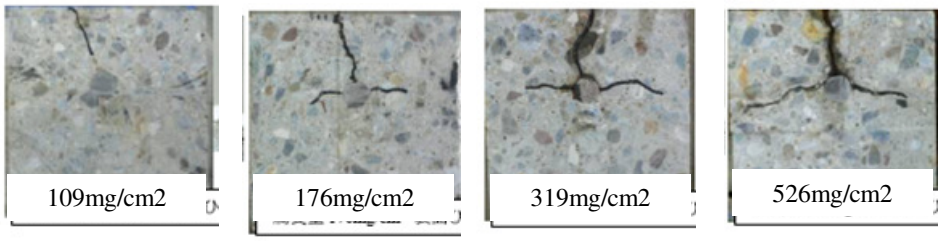

c) C= 45; k =5.74

Figure 5.15. Internal crack patterns with various k values

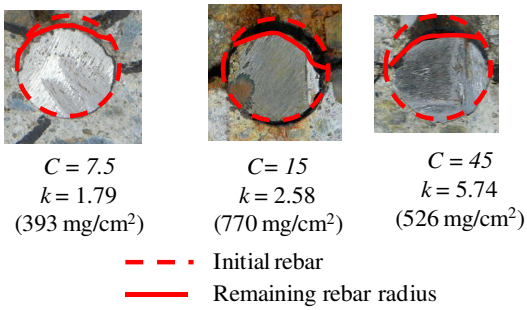

Figure 5.16. Corroded rebar sectional patterns

5.3.2 Numerical evaluation of effect of cover thickness and k value

The specimens are simulated by the proposed RBSM analytical method. The specimen mesh sizes are 5 mm in the concrete cover and 15-20 mm in other parts as shown in **Figure 5.17**. The QUARTER local corrosion is also assumed in the analysis as per the corroded rebar sectional patterns.

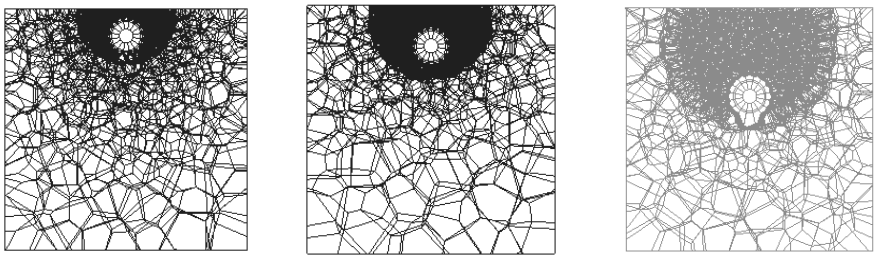

Figure 5.17. Meshing of specimens with various cover thicknesses

Figure 5.18 presents analytical crack patterns at several corrosion amounts for each case of k value. In the case of k = 1.79, cracks diagonally propagated toward the specimen surface, which is similar to the Tsutsumi's criterion. In the case of k = 2.58, single surface crack is formed and crack propagates in the shortest path to the specimen

surface simultaneously with internal cracks which are diagonal cracks. If k = 5.74, it is clearly shown that single crack propagates in the concrete cover, which is also similar to the Tsutsumi's criterion, and the inclined slope of internal cracks area significantly reduced. Based on the experimental and analytical results, it seems that the criterion proposed by Tsutsumi is overestimated in the appearance condition of a single crack in the concrete cover. That is, a single crack may appear in the concrete cover even k value less than 3, for example k is about 2.5.

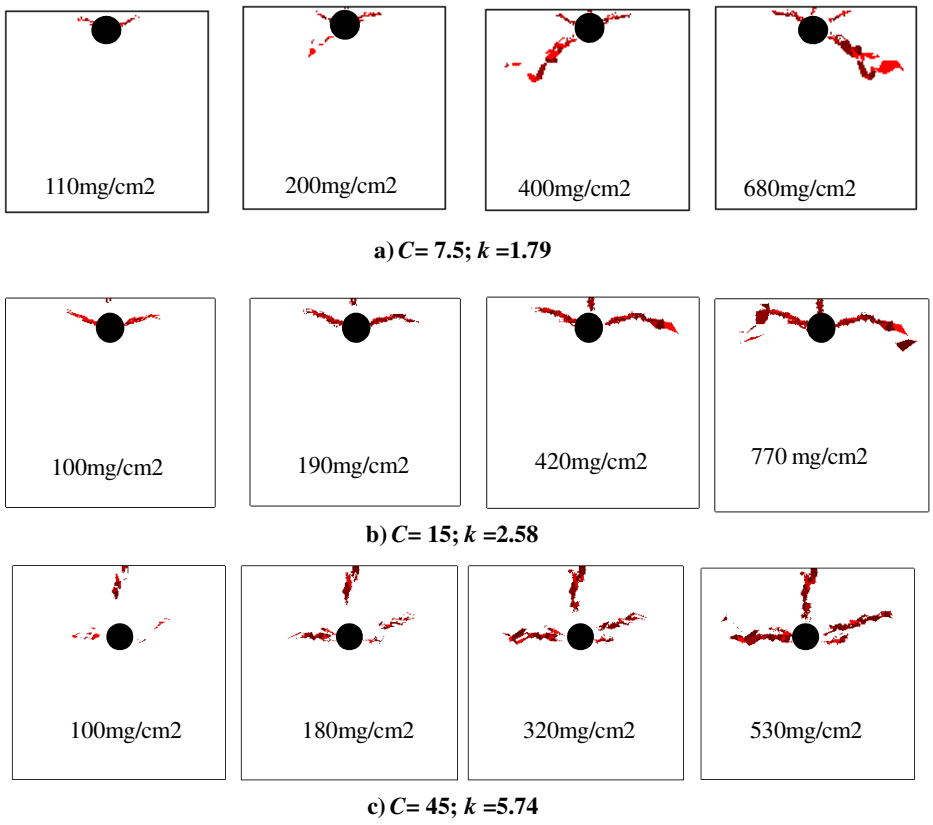

Figure 5.18. Analytical crack patterns with various k values

Figure 5.19 shows propagation of internal cracks and deformation of the specimen having k =1.79 against increases of the rebar corrosion amount. In this specimen type, minor cracks initiate from the rebar and early accumulate in the concrete cover due to

the small concrete cover. With the further amount of rebar corrosion, internal cracks become larger and diagonally propagate to the specimen surface which cause deformation of a part of the concrete cover as shown at the rebar corrosion amount 50 mg/cm^2 . The inside crack appears when the rebar corrosion amount is larger than 170 mg/cm^2 may be due to the displacement of the right-hand side part of the concrete cover when the internal cracks reaching the specimen surface. It is noted that in the test, the inside crack also appeared in this type of specimen.

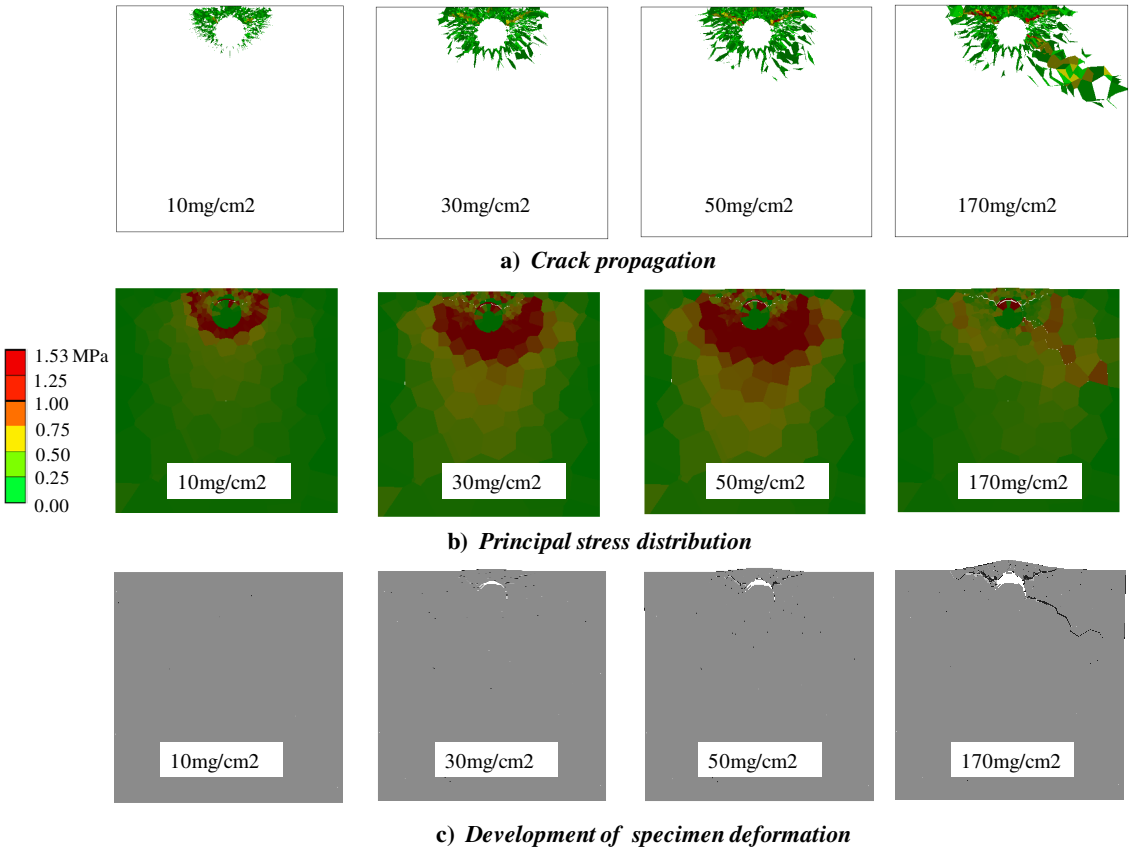

Figure 5.19. Cracking mechanism of a specimen having $k < 3$

In order to verify the criterion more closely around the threshold $k = 3$, the following specimens with various concrete cover thicknesses and rebar diameter D30 are also

simulated. The reason of choosing D30 is to have large concrete cover thickness, so that surface cracks can be easier to observe with more elements in the cover thickness, but the *k* value is still kept less than 3 as shown in **Table 5.2**.

Table 5.2. Specimens 150*150-D30 with various cover thicknesses

C(mm)	D(mm)	*k*
15	30	**2.00**
25	30	**2.67**

Figure 5.20 shows internal crack patterns of these specimens with various *k* values. Again, the analytical results show that a single crack is also formed and propagate in the concrete cover in the case of $k = 2$ or 2.67. And the inclined slopes of the internal cracks are also different in these cases, that is, in the case of $C = 15$ mm, internal crack slopes appear higher than the ones of the case $C = 25$ mm. It is necessary to need more data including experiment and analysis to govern a criterion but with the analysis conducted in this chapter, it roughly appears that when *k* is about 2-2.5, single crack may also appear in the concrete cover. Moreover, *k* value also affects the slope of internal cracks. Basically, smaller *k* values induce more inclined internal cracks toward the specimen surface.

In terms of surface crack propagation, **Figure 5.21** showed analytical crack propagation of the above specimens having various k values or C/D ratios. It seems that *k* values or C/D ratios do not relate to the tendency of surface crack propagation. It is necessary to determine which factors are related to the crack propagation in the future work.

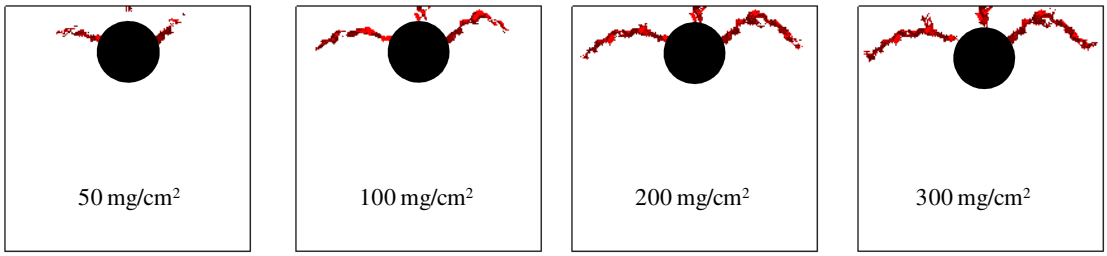

b) D30, C = 15, k = *2.00*

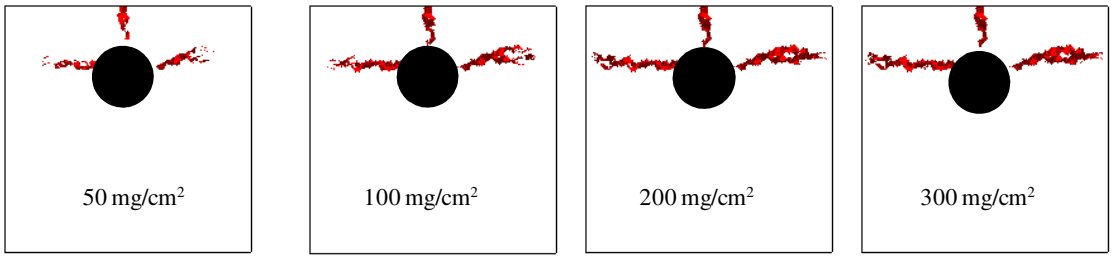

b) D30, C = 25, k = *2.67*

Figure 5.20. Analytical crack patterns (D30 and various *k)*

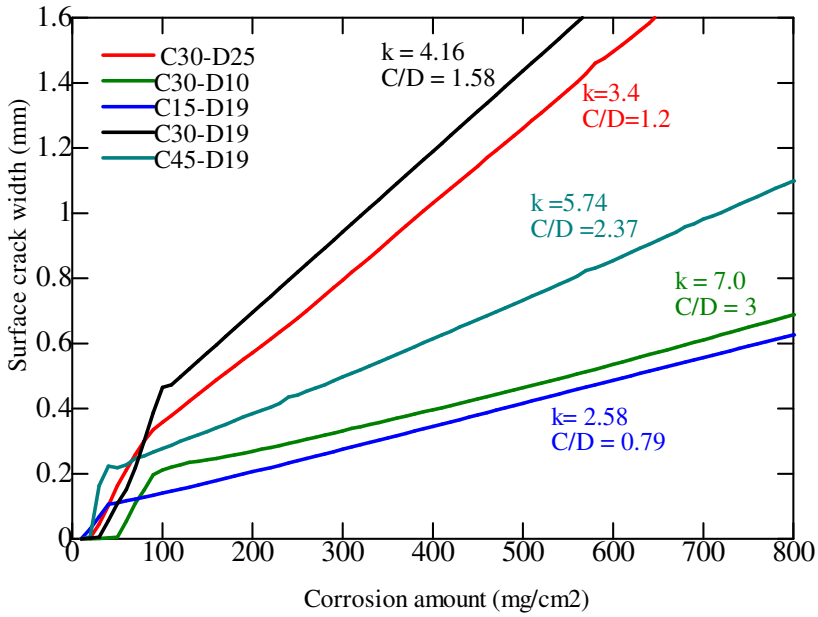

Figure 5.21. Surface crack propagation with various *k* values or C/D ratios

5.4 Effect of variation of internal expansion area

5.4.1 Specimen concept

In order to investigate effect of variation of internal expansion area, a specimen series with a fictitious "rectangle" rebar is simulated. **Figure 5.22** shows dimensions and analytical modeling of the specimens. The concept of this analysis is to investigate effect of variation of the internal expansion area. The specimen size is 150*150 and the concrete cover thickness is kept constantly as 30 mm. **Case 1** includes specimens with varied height rectangle rebars and **Case 2** includes varied width rectangle rebars. In order to investigate effects of only the internal expansion area, the expansion applied uniformly on four sides of the rectangle rebars and the penetration effect of corrosion products into cracks is not taken into account in the analysis.

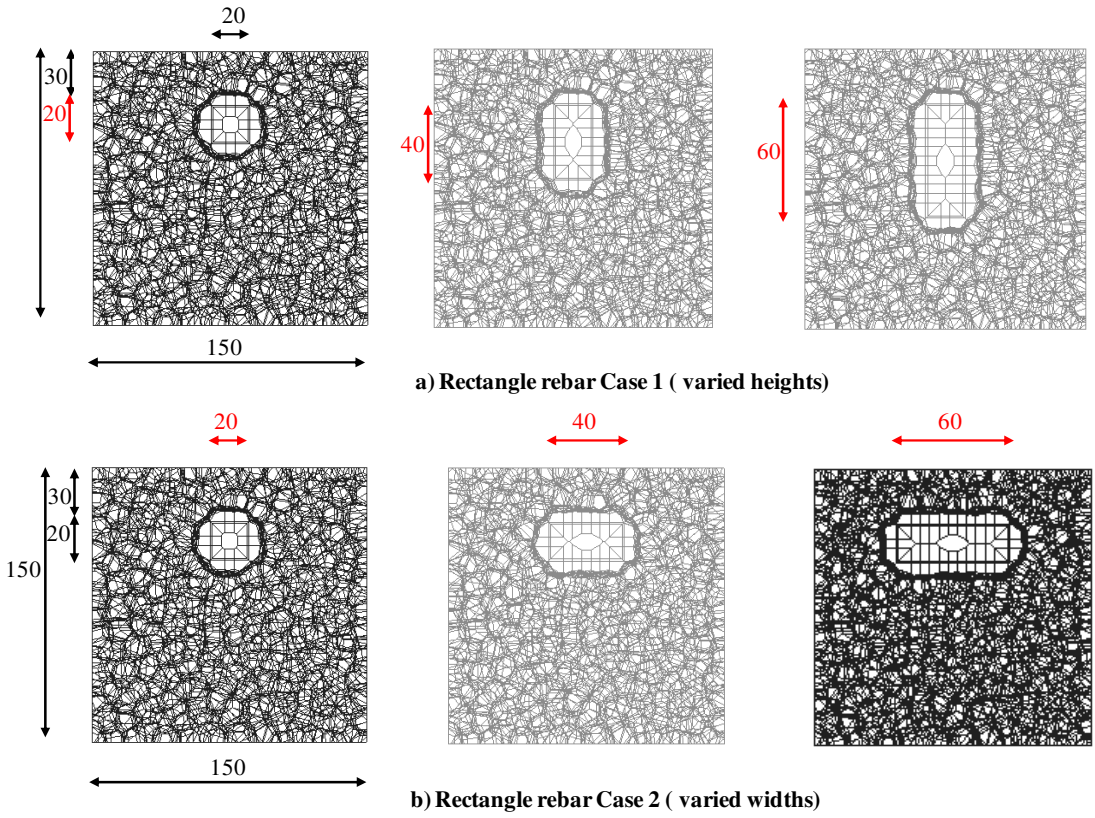

Figure 5.22. Modeling of rectangle rebar specimens

5.4.2 Effect of height of internal expansion area

Figure 5.23 shows surface crack propagation of the specimens with varied height rebar. The surface crack initiates after rebar corrosion amount about 40mm/cm^2 and then rapidly propagates with the increase of the rebar corrosion amount. This behavior is similar with the one induced by the circular rebar as previously discussed. There is no difference on the surface crack propagations between cases of various height of the rebar. So, variation of the height of internal expansion, which is not facing to the concrete cover, does not have influence on the surface cracking. **Figure 5.24** shows propagation of internal crack length for the specimens in **Case 1**. Again, the behavior is similar to the circular rebar. That is, internal cracks initiate after the rebar corrosion amount about 60 mm/cm^2 (later than the surface crack initiation) and then rapidly propagate, in the later stage of rebar corrosion, internal crack lengths also tend to converge to a particular value of about 60 mm. In terms of effect of various heights, there is also no influence due to the variation of rebar height on the internal crack propagation. **Figure 5.25** shows deformation of the specimens at several corrosion amounts. From the deformation, internal crack patterns can be understood and they appear that variation of the height of internal expansion does not have influence on the crack patterns as well.

So, the analytical results show that the variation of internal expansion area height, which is not facing to the concrete cover, does not have influence on the crack propagation of the specimens. This is because the internal expansion induces on the concrete cover is the same for each specimen in this case.

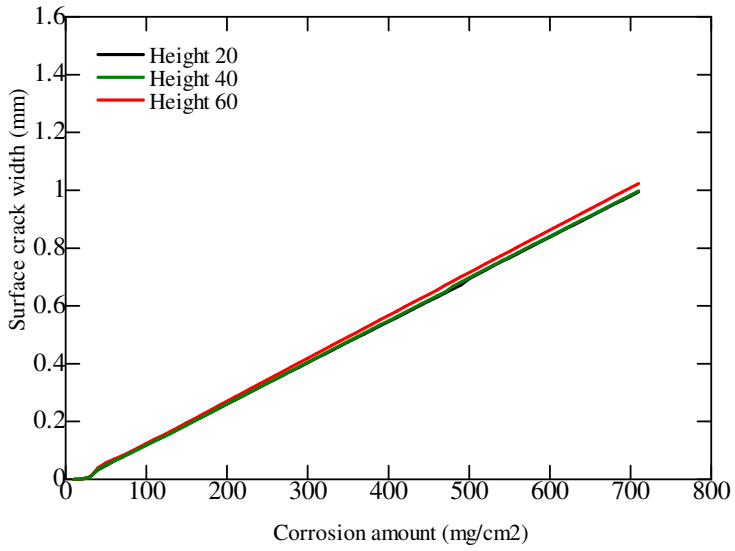

Figure 5.23. Surface crack propagation (various height of internal expansion)

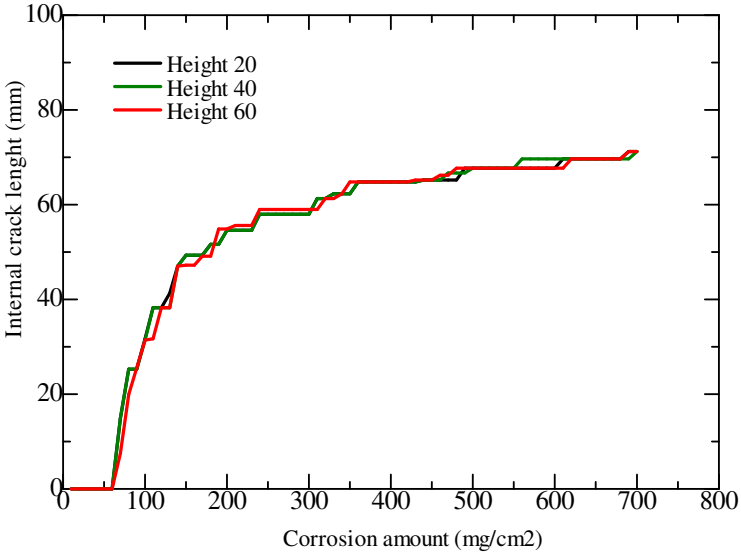

Figure 5.24. Internal crack propagation (various height of internal expansion)

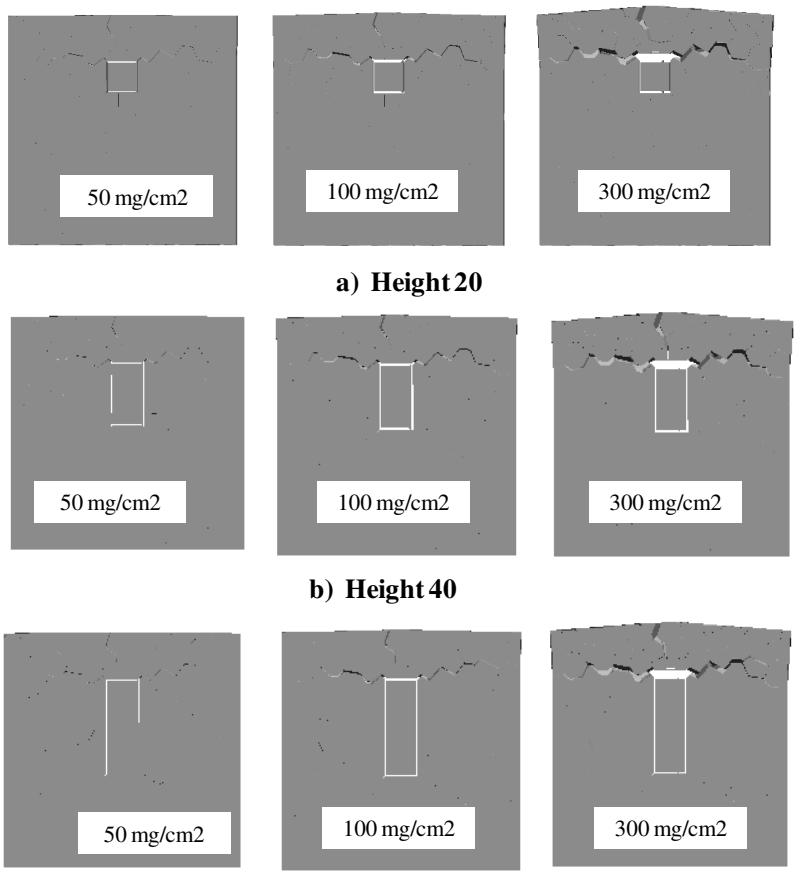

Figure 5.25. Specimen deformation (various height of internal expansion)

5.4.3 Effect of width of internal expansion area

Figure 5.26 shows surface crack propagation of the specimens with varied width rebars. The surface crack initiates after rebar corrosion amount about 40mm/cm^2 and then rapidly propagates with the increase of the rebar corrosion amount. This behavior is similar with the one induced by the circular rebar as previously discussed. It shows that the wider internal expansion area results a larger surface crack width at the same value of rebar corrosion amount.

Figure 5.27 shows propagation of internal crack length for the specimens with varied width rebars. The crack length is measured from the specimen center to visible crack

tips in the analysis for easy comparison. Again, the behavior is similar to the circular rebar. That is, internal cracks initiate after the rebar corrosion amount about 60 mm/cm^2 (later than the surface crack initiation) and then rapidly propagate, in the later stage of rebar corrosion, internal crack lengths also tend to converge to a particular value of about 60 mm. In terms of effect of various widths, the wider area seems to induce longer cracks but the difference is not significant. This may be due to the limit of specimen boundary in this case. **Figure 5.28** shows deformation of the specimens, in which crack patterns can be also understood. It also shows similarity for crack patterns of each specimen.

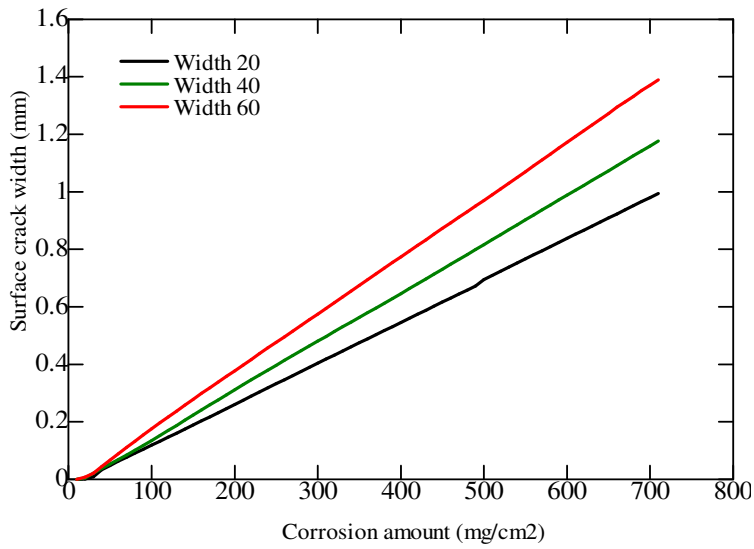

Figure 5.26. Surface crack width propagation (various width of internal expansion)

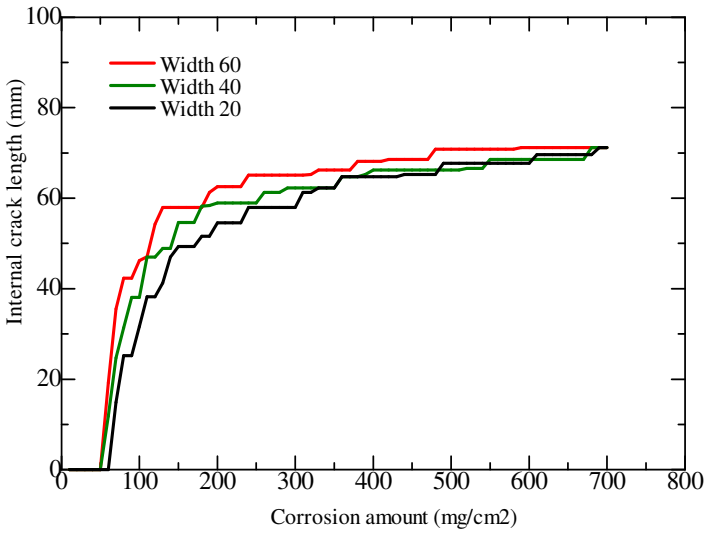

Figure 5.27. Internal crack propagation (various width of internal expansion)

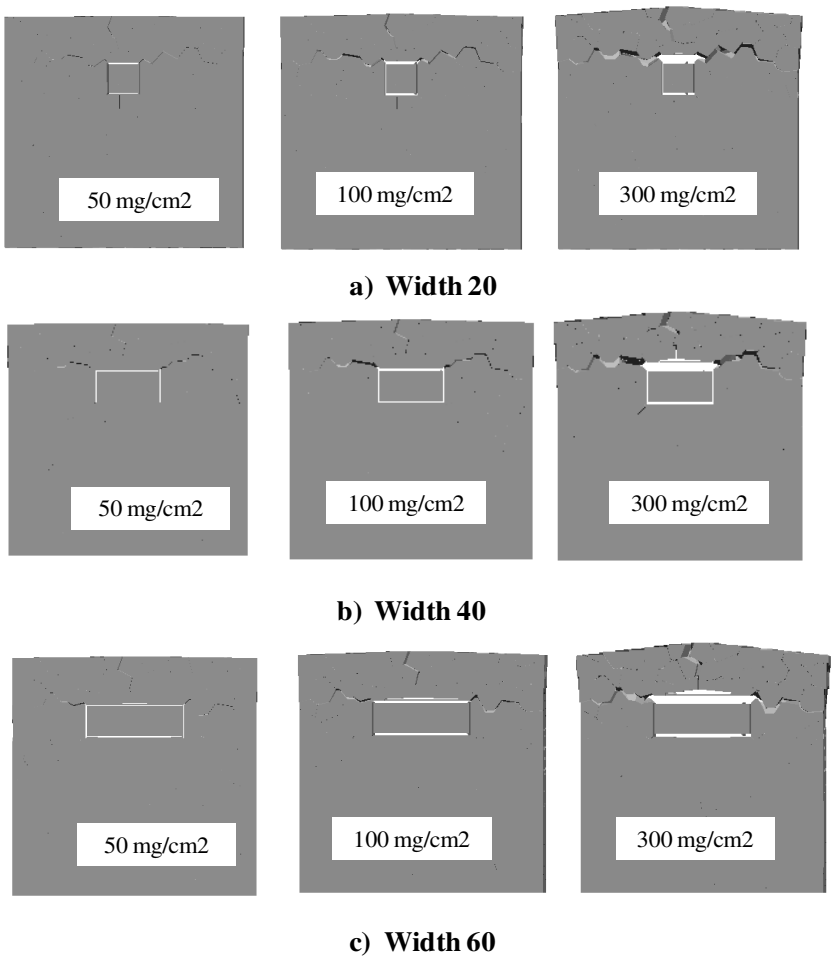

Figure 5.28. Specimen deformation (various width of internal expansion)

So, the analytical results show that only variation of the internal expansion area width, which is facing to the concrete cover, has influence on the crack propagation although the internal expansion is applied on four side of the rectangle rebars. This is because due to the confinement of the concrete around the rectangle rebars, only concrete cover (having the smallest thickness) is deformed due to the internal expansion.

In the case of the circular rebar case, as discussed in Chapter 4, the corrosion pattern on the rebar section (uniform or local) had influence on the cracking behavior. That is because in the local corrosion cases, the internal expansion area facing to the concrete cover is basically larger than the one in the uniform case as mentioned in Chapter 3. So, together with the results in the case of "rectangle" rebars, it can be concluded that only the variation of the internal expansion area facing to the concrete cover has influence on the cracking behavior.

5.5 Summary

This chapter investigated effects of fundamental factors which are cover thickness and rebar diameter, k value and C/D ratio. The following conclusions are derived in this chapter:

(1) The variation of rebar diameter significantly affects on the initiation of surface crack and internal cracks and the crack propagation after the initiation.

(2) k value significantly affects the crack pattern of the single-rebar specimen as reported by Tsutsumi (1996). And, if k =2-2.5, single crack also appears and develops in the concrete cover.

(3) The variation of the width of internal expansion area has influence on the crack propagation. However, the variation of the height of the internal expansion area

does not affect the cracking behaviour.

(4) In the future work, it is necessary to determine which parameter is related to the crack propagation since k value or C/D ratio does not have clear relationship to the crack propagation.

6. EFFECTS OF SPECIMEN BOUNDARY

6.1 Introduction

There have been some studies on effects of concrete cover thickness, ratio of concrete cover and rebar diameter, and other factors such as concrete strength (Alonso ,1993) to the cracking behavior of concrete due to rebar corrosion. However, effects of specimen sizes or structure sizes on the corrosion induced cracking have not been reported in the literature. In Chapter 4, it was clarified that the surface crack initiation, surface crack propagation and the internal crack propagation were relating to deformation of specimen surfaces such as deformation value and deformation area. So, the specimen sizes may have influences in corrosion induced crack propagation in single rebar specimens, since the specimen size is related to boundary condition of the deformation. In this chapter, single rebar specimens with varied specimen sizes are tested and their cracking behaviors are investigated. Specimens have the same value of concrete cover as the series 150*150-C30 investigated in Chapter 4, i.e. 30mm,. Moreover, their crack propagation is also investigated analytically.

In the experiment, internal crack propagation such as internal crack patterns, internal crack lengths and surface crack widths are observed at several rebar radius losses for each type of specimen during the corrosion test.

On the other hand, the specimens are simulated using the proposed RBSM analysis model and the analytical results are verified against the test results. Moreover, an analytical study on effect of variation of the specimen boundary is conducted to indentify which dimension is sensitive to the crack propagation. In the parameter study, some specimens are simulated with two cases of the boundary's variation. Firstly, the height of specimen is fixed, only the width of specimen is varied to see effects of the specimen width. Secondly, both of width and height of specimen are varied. Based on the parameter study, effects of specimen boundary are determined and clarified, and, a cracking mechanism of large width specimen is proposed.

6.2 Experiment of specimen with various sizes

6.2.1 Specimen set-up

Figure 6.1 shows a general setting of specimen series conducted in this chapter. The specimens have the same concrete cover thickness C = 30 mm. **Table 6.1** shows details of each specimen series, in which series 150*150-C30 was investigated in Chapter 4 and it is used in this chapter for comparison . **Table 6.1** shows the mixture proportions of the concrete used to cast the specimens in this chapter. The specimens are cured until 28 days and then they are tested using electric means as described in Chapter 2. Concrete compressive strength of each specimen series, which was determined before starting the electric corrosion test, is shown in **Table 6.1.** During the test, surface crack widths were recorded using crack gauges and logged in computer files as described in

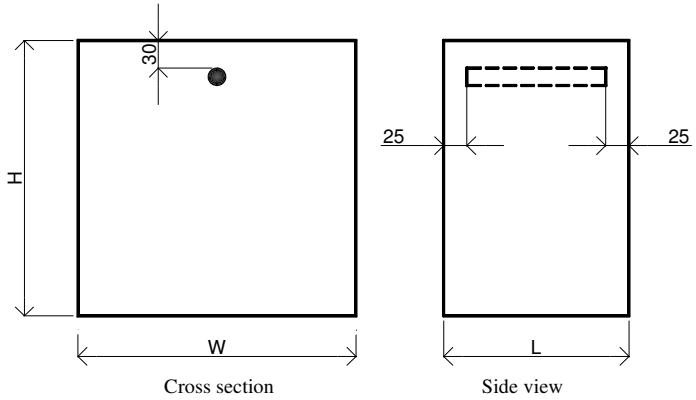

Figure 6.1. Specimen set-up (various sizes)

Table 6.1. Specimen series details (*Unit in mm*)

Series	W	H	L	D	f'_c, MPa
150*150-C30	150	150	300	19	18.5
300*150-C30	300	150	200	19	28.0
250*250-C30	250	250	200	19	25.0
400*400-C30	400	400	200	19	28.0
600*400-C30	600	400	300	19	26.5

Table 6.2. Mixture proportions of concrete

W/C (%)	s/a (%)	Unit content (kg/m^3)				
		Water	Cement	Sand	Aggregate	AE (liter/m^3)
56.5	44.0	166	294	779	990	1.18

Notes:
W/C is the water/cement weight ratio
s/a is the river sand/total aggregate volume ratio
AE is a water reducing agent admixture

6.2.2 Surface crack propagation

Figure 6.2 shows surface crack width propagation against increase of rebar corrosion amount for the above specimen series. Surface cracks initiate after particular values of rebar corrosion amounts and then the surface cracks rapidly propagate and the increasing slopes tend to reduce in the later stages of rebar corrosion due to the penetration of corrosion products in to cracks as clarified in Chapter 4. The experiment shows that the small width specimens result larger crack in comparison with the large width specimens at the same level of rebar corrosion amount. This behavior may be due to the effect of specimen size because at the same level of rebar corrosion amount, the internal expansion pressure would be the same value. The surface crack width propagation of specimen series 600*400-C30 appears abnormally due to the special situation of surface crack patterns and rebar corrosion which will be discussed in Chapter 8.

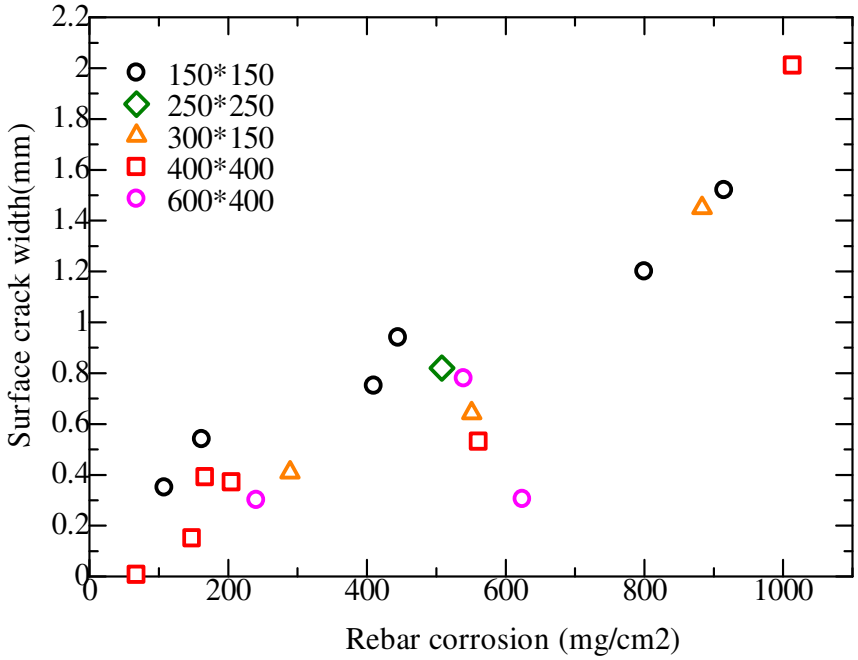

Figure 6.2. Surface crack width propagation (various specimen sizes)

6.2.3 Crack patterns

Figure 6.3 shows surface crack patterns of the specimens at various rebar corrosion amounts. Basically, single surface crack appears along the specimen in most of the cases of varied size specimens, which appears to be similar to the ones of the series 150*150-C30 discussed in Chapter 4. The surface crack patterns of series 600*400-C30 will discussed in Chapter 8.

Figure 6.4 shows internal crack patterns of the various specimen series at several rebar corrosion amount. Based on the experimental results, it can be observed that internal cracks initiate from the rebar and then propagate toward the concrete surface. In most of the specimens, internal cracks propagate toward the surface in inclined directions. The maximum crack length seems not to be inherent with the specimen width and crack lengths appear to converge to a maximum value of about 90 mm in these specimen series.

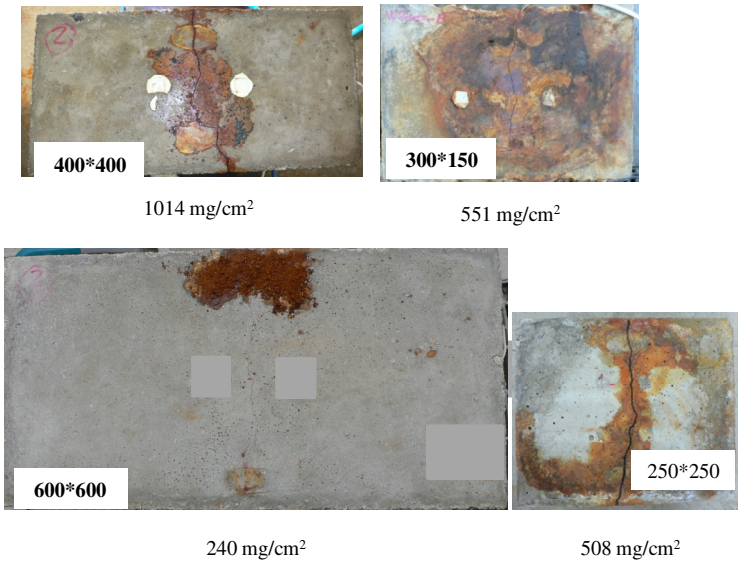

Figure 6.3. Surface crack patterns (various sizes)

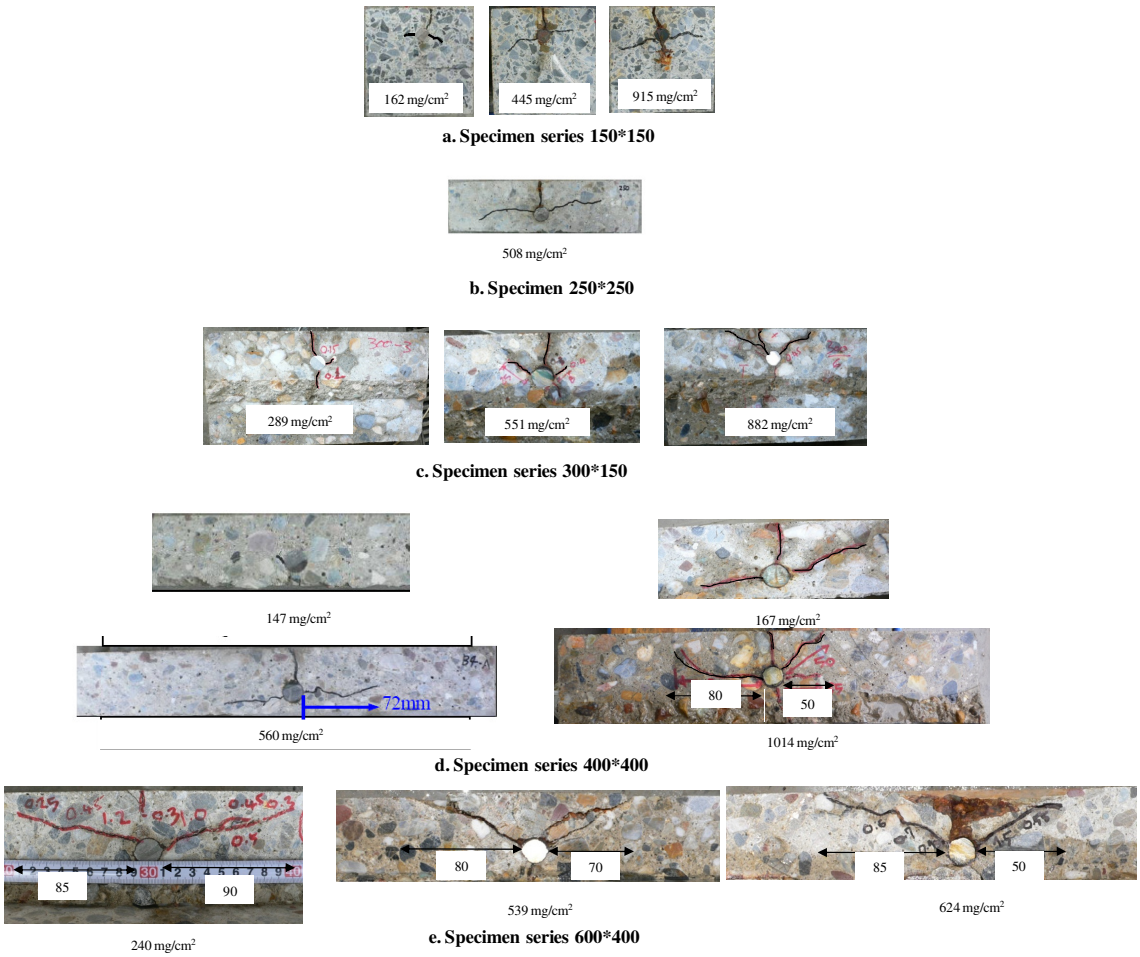

Figure 6.4. Internal crack patterns (various specimen sizes)

Comparison between surface cracks and internal cracks, there is a difference in the crack dominance between the specimens with small widths (series 150*150-C30, 250*250-C30 and 300*150-C30) and the specimens with large width (series 600*400-C30). That is, in the small width ones, surface cracks significantly appeared on crack patterns in comparison with internal cracks (**Figure 6.4a**, **Figure 6.4b**, **Figure 6.4c**) but in the large width specimens, the surface cracks are minor in comparison with the internal cracks. This may be explained that the large width specimens tend to restrain the surface vertical deformation (with larger volumes of concrete cover) than the small width specimens so their surface cracks are minor corresponding to the less deformation of the specimen surface as discussed in Chapter 4. This behavior will be further investigated again in the analytical part of this chapter.

The inclined cracks shown in the internal crack patterns potentially cause de-lamination phenomenon in the concrete cover of some specimens as shown in **Figure 6.5**. The de-lamination phenomenon is necessary to be considered in the maintenance process of concrete structure because only surface cracks are easy to monitor in a period basis. Internal cracks are not easy to monitor so de-lamination phenomenon may suddenly occur on concrete cover.

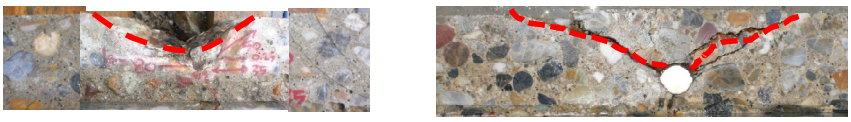

a. Specimen 400*400 b. Specimen 600*400

Figure 6.5. Potential de-lamination

6.2.4 Internal crack propagation

Propagation of internal crack lengths, which were measured from rebar sides to crack

tips, against increase of rebar corrosion amounts are shown in **Figure 6.6**. Internal crack lengths initiate when rebar corrosion amount is around the value of 100 mg/cm^2. Then, crack lengths rapidly increase with increases of rebar corrosion amount. At the same level of rebar corrosion amount, internal crack lengths in the larger width specimens are longer than then the ones in the smaller width specimens. As shown in the figure, the specimen series 600*400-C30 resulted the longest internal crack length with the maximum length about 90 mm and the series 150*150-C30 resulted the shortest length with the maximum about 40 mm. It seems that the internal crack lengths are related to the specimen sizes and this feature will be clarified in the analytical part in this chapter. However, the internal crack lengths seem not to increase inherently with the increase of the specimen width and they appear to convergence to a maximum value of around 90 mm although corrosion amount is largely increased.

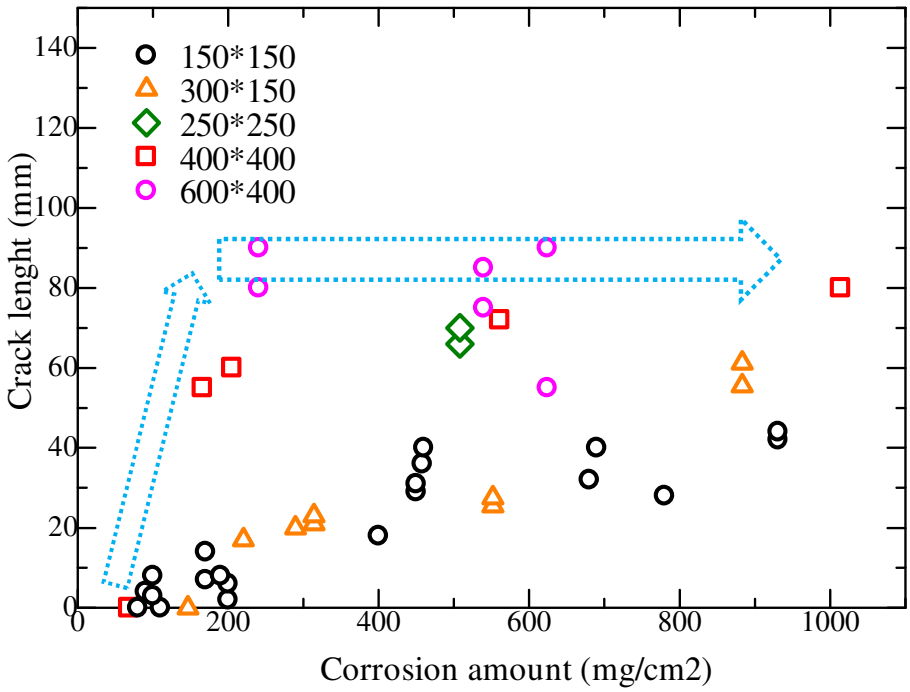

Figure 6.6. Propagation of internal crack length (various specimen sizes)

6.2.5 Relationship between surface crack width and internal crack length

Figure 6.7 shows relationships between surface crack with and internal crack length for the various specimen series. It appears that in the large width specimens, internal cracks already developed when surface crack appears while in the small width specimen, internal cracks develop after surface crack reaches a significant value. In the large width specimen, although surface crack increases, the crack length seems not to increase in the large stage of rebar corrosion. The small width specimen shows a linear relationship between increases of surface crack width and internal crack length.

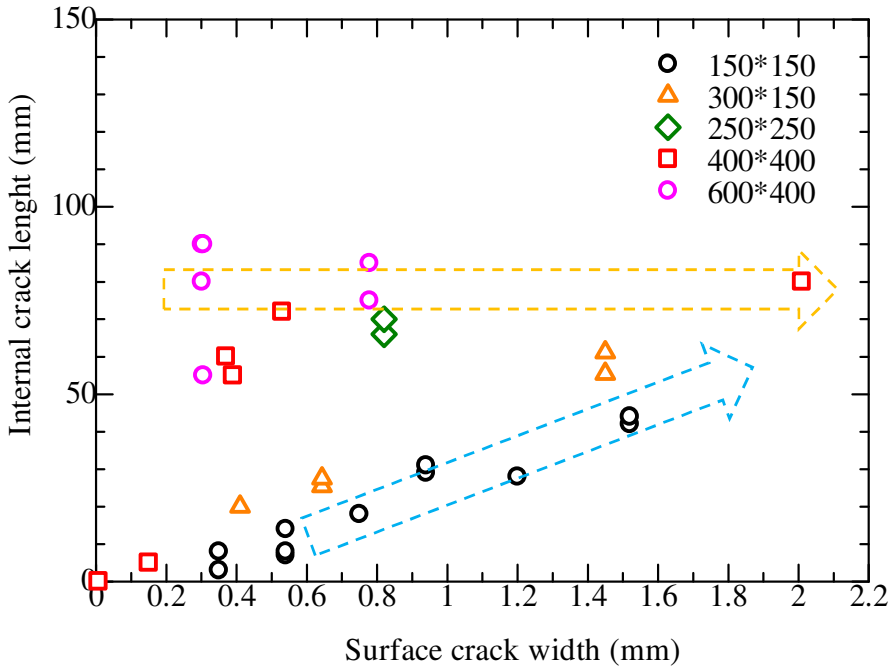

Figure 6.7. Surface crack and internal crack relationship (various specimen sizes)

6.2.6 Rebar corroded sectional pattern

Regarding rebar sectional corroded pattern after the electric corrosion test, in most of the cases having inclined internal cracks, local corrosion pattern is again observed as

shown in **Figure 6.8**.

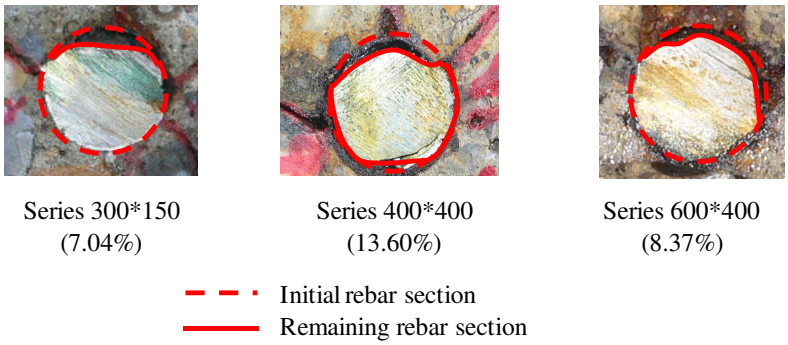

Figure 6.8. Rebar corroded sectional pattern (various specimen sizes)

6.3 Numerical simulation of specimens with various sizes

6.3.1 Modeling of specimens

The mentioned specimen series are simulated using the proposed RBSM model. In the analysis, mesh sizes of the Voronoi particles are arranged 5 mm in the cover thickness and 15-40 mm in the other areas as shown in **Figure 6.9**. Another arrangement of the Voronoi particles was also tried to confirm the similarity of the analytical results.

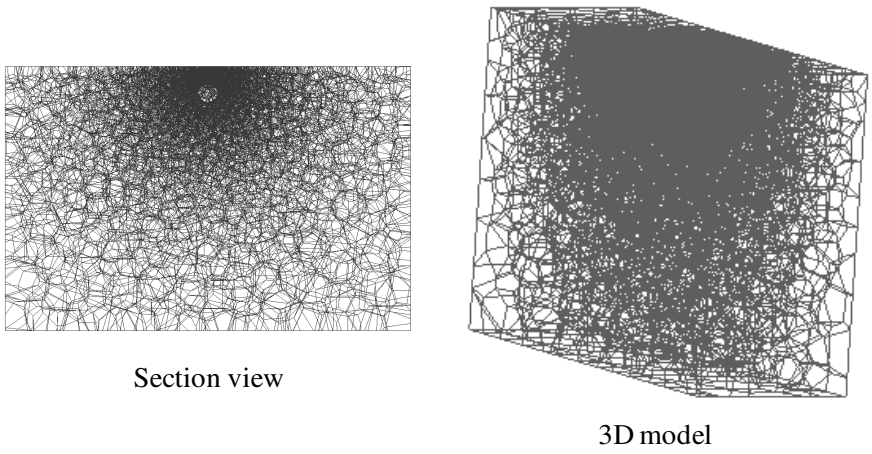

Figure 6.9. RBSM modeling of specimen (various specimen sizes)

From the observation on the remaining rebar section after the test as shown in **Figure 6.8**, the rebar sectional corrosion patterns appear to be close to the assumed QUARTER local corrosion discussed in Chapter 3. So, in the analysis, the local corrosion QUARTER model is assumed. Also, from the observation from the electric corrosion test, corrosion products appeared to penetrate into cracks so this effect is also considered in the analysis.

6.3.2 Surface crack propagation

Figure 6.10 shows analytical surface crack width propagation. In the small width specimens, the surface crack width is larger than the one in the large width specimens at the same level of rebar corrosion amount. The analytical surface cracks in the wider specimen series appear lower than the test results but the tendency of surface crack propagation between the specimens appears similar to the test results. The surface crack propagation seems to be dependent to the specimen sizes.

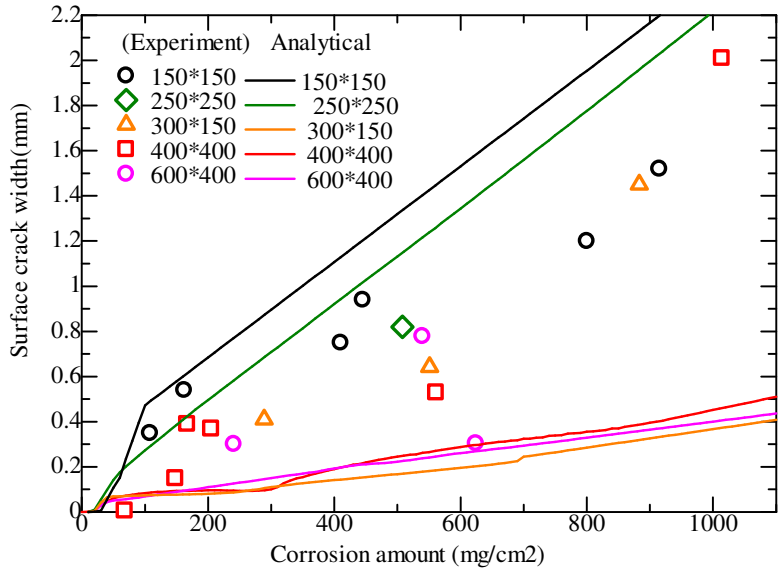

Figure 6.10. Analytical surface crack width (various specimen sizes)

6.3.3 Crack patterns

Figure 6.11 shows deformation of specimens at corrosion amount of 300 mg/cm^2. Surface crack opening can be observed from the deformation by the separation of the particles. The analytical surface cracks of the specimens appear along the rebars. In the large width specimens, the surface crack widths appear smaller than the ones of the small width specimens. The analytical surface crack patterns appear similar to the experimental results shown in **Figure 6.3** and the tendency shown in **Figure 6.2**.

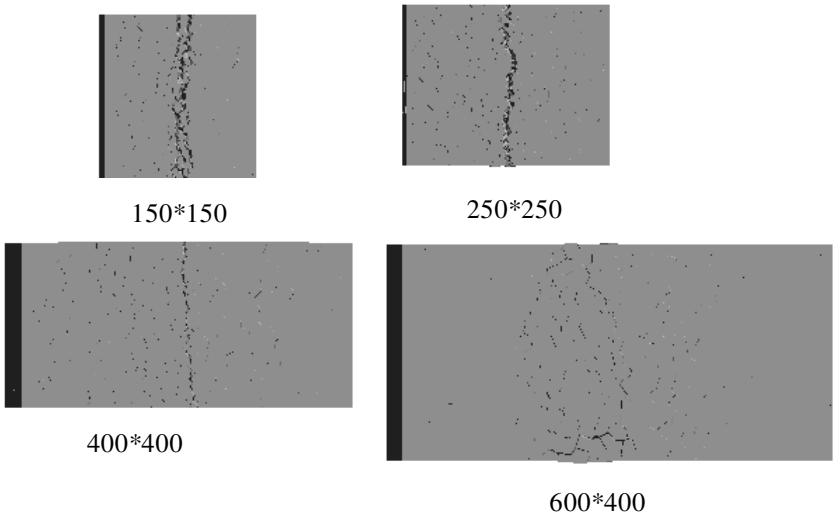

Figure 6.11. Deformation showing surface crack pattern (various specimen sizes)

(Magnification =15)

Figure 6.12 shows internal crack patterns of various specimen series at several rebar corrosion amounts. For clarity, only visible cracks are shown as discussed in Chapter 4. The analytical results show reasonable agreements with the experimental ones shown in **Figure 6.4**. In the case of large width specimens, the analytical shows that the internal cracks are dominant in comparison with the surface cracks. The internal cracks diagonally propagate toward the specimen surface which may cause potential spalling in

the concrete cover thickness.

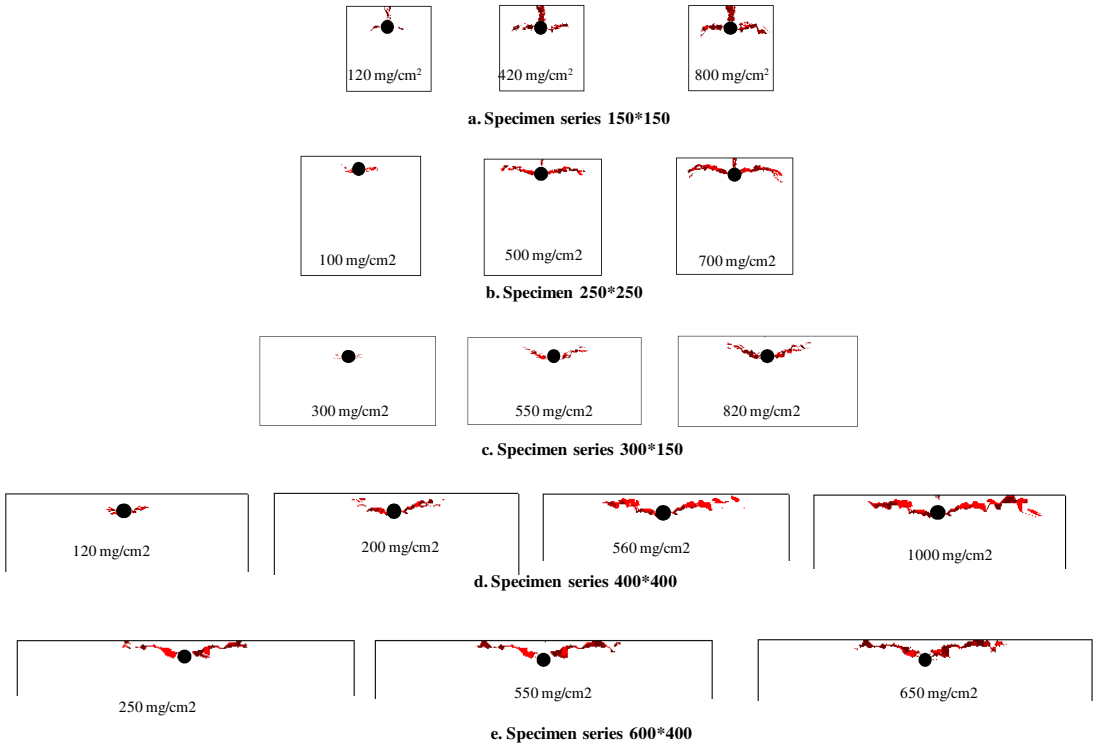

Figure 6.12. Analytical internal crack patterns (various specimen sizes)

6.3.4 Propagation of internal crack length

Figure 6.13 shows analytical internal crack length propagation versus increase of rebar corrosion amount. The analytical results show agreements with the experimental ones, that is, internal cracks initiate when rebar corrosion amount is about 100 mg/cm^2 and then they rapidly increase with the increase of rebar corrosion amount. Basically, at the same value of rebar corrosion amount, wider specimens result longer internal cracks. However, the internal crack lengths appear to converge to a particular value, about 100 mm. The behavior of the internal crack length propagation can be explained that the wider specimens tend to result longer internal cracks due to the wider specimen boundaries and therefore to induce wider surface deformation areas than the narrow

specimens. The convergence of the internal crack length is due to the diagonal cracks propagating toward the specimen surfaces.

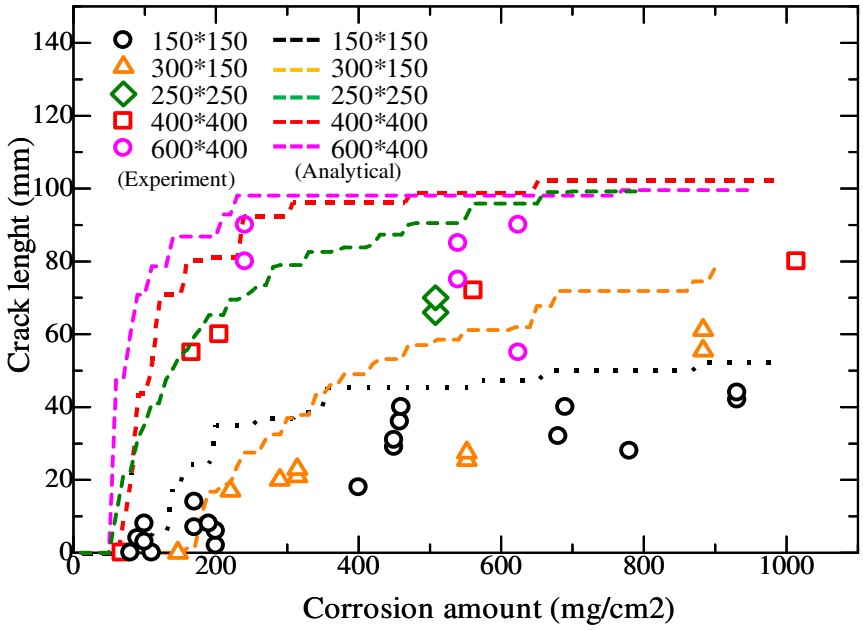

Figure 6.13. Analytical internal crack length propagation (various specimen sizes)

6.4 Cracking behavior of specimens with various sizes

6.4.1 Specimen set-up

Based on the above experimental results and analytical results, it is clearly shown that specimen size or boundary has influence on the cracking behavior of the specimens. In order to investigate effects of the specimen boundary to the crack propagation of the single rebar specimens clearly, the following series of single rebar specimens are simulated and their crack propagation is discussed. The concept of specimen is specimen dimension to be varied in its width and both its width and height.

Series 1 includes specimens with the same height but varied widths. The specimen length is 100 mm and it is set for all specimens in this parameter study. The varied widths are 150 mm, 300 mm, 450 mm and 600 mm respectively as shown in **Figure**

6.14.

Series 2 includes specimens with the varied widths and heights as shown in **Figure 6.15**.

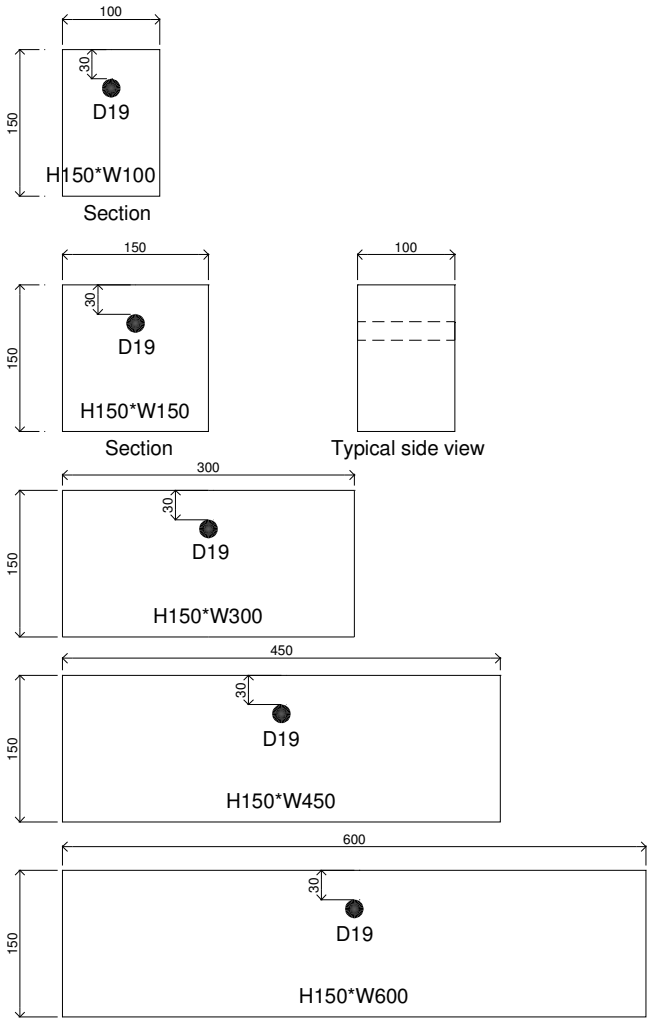

Figure 6.14. Series 1- Varied width specimens

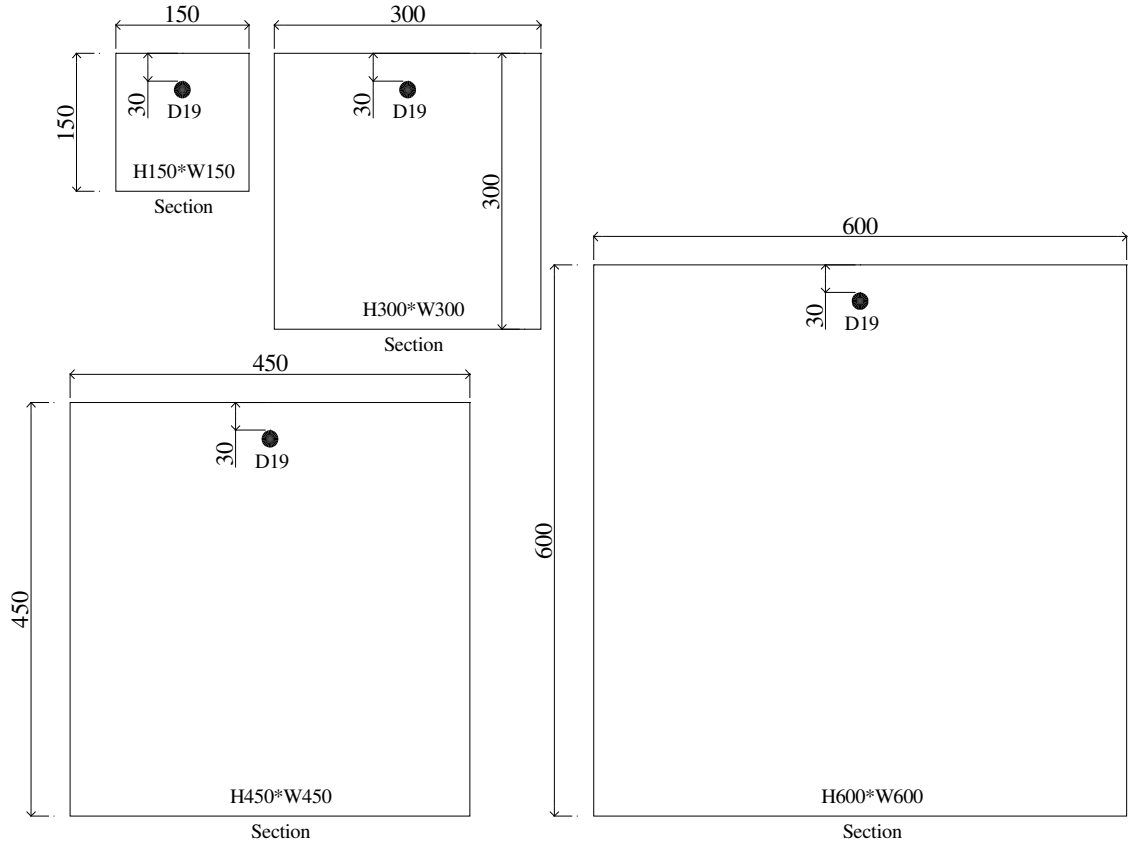

Figure 6.15. Series 2- Varied height and width specimens

In order to observe sectional crack patters from the specimen deformation, the rebar is modeled in the full length of the specimens in this parameter study as shown in the typical side view in **Figure 6.14**. This is slightly different from the tested specimens, in which the rebar is put within the concrete with 25 mm thick concrete cover at the ends of the rebar.

6.4.2 Modeling of specimen

The specimens are modeled with the mesh size 5 mm in the concrete cover and 25-40 mm in the other areas as shown in **Figure 6.16.**

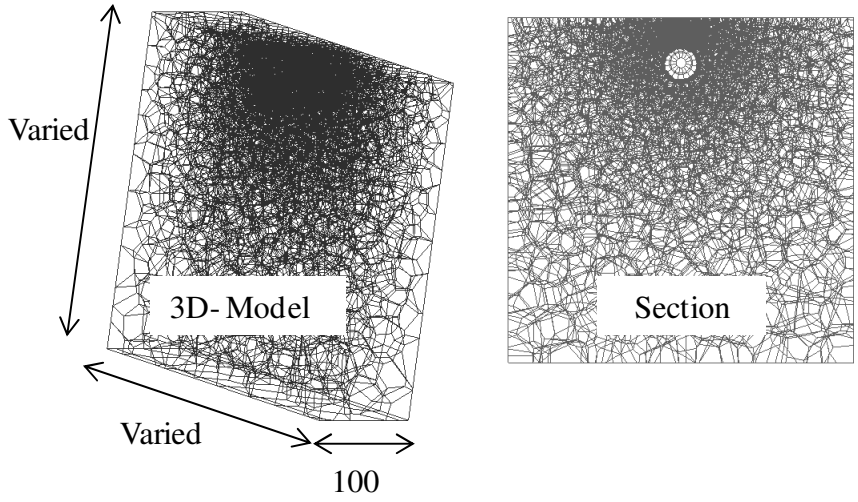

Figure 6.16. Typical RBSM modeling of specimen

The QUARTER local corrosion model is assumed in the analysis. The concrete compressive strength is assumed as 18.5 MPa in this parameter study. The penetration effect of corrosion products into cracks is also assumed in this analysis.

6.4.3 Analytical results of specimens with various widths

Figure 6.17 shows surface crack width propagation of the specimens in Series 1. The surface crack initiation appears the same in all specimens once rebar corrosion amount is about 50 mg/cm^2. **Figure 6.18** shows surface deformation measured during the analysis for the specimens at the rebar corrosion amount 50 mg/ cm^2. **Figure 6.19** shows crack patterns at the rebar corrosion amount 50 mg/cm^2. The color ranges representing crack width value as discussed in Chapter 4. The specimens in this series have the same concrete cover thickness so minor cracks accumulation in concrete cover is similar as shown in **Figure 6.19**. The minor crack accumulation cause the specimen surface deformed as presented in **Figure 6.18**. It can be seen that at this stage, all specimens have the similar surface deformation including the maximum intensity and

the deformation shape. So, the surface crack initiation is the same in all specimens because as discussed in Chapter 4 the surface crack is initiated due to the bending of the specimen surface.

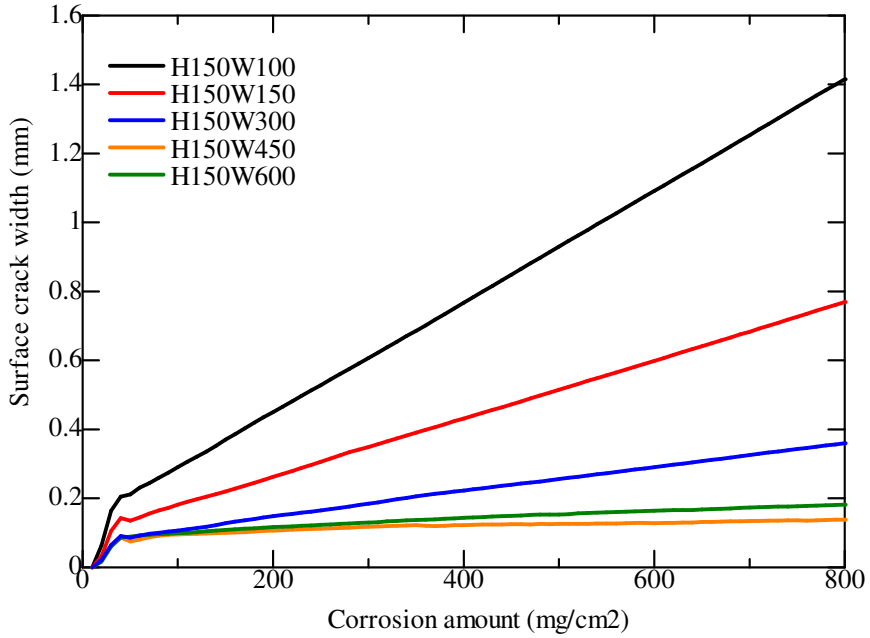

Figure 6.17. Surface crack propagation (varied width specimens)

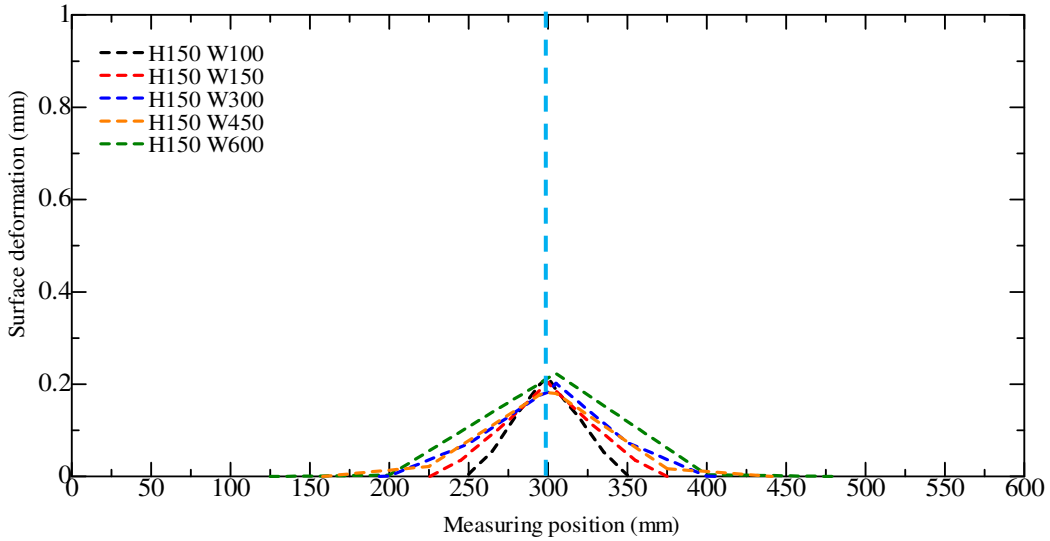

Figure 6.18. Analytical surface deformation at rebar corrosion amount 50mg/cm^2 (varied width specimens)

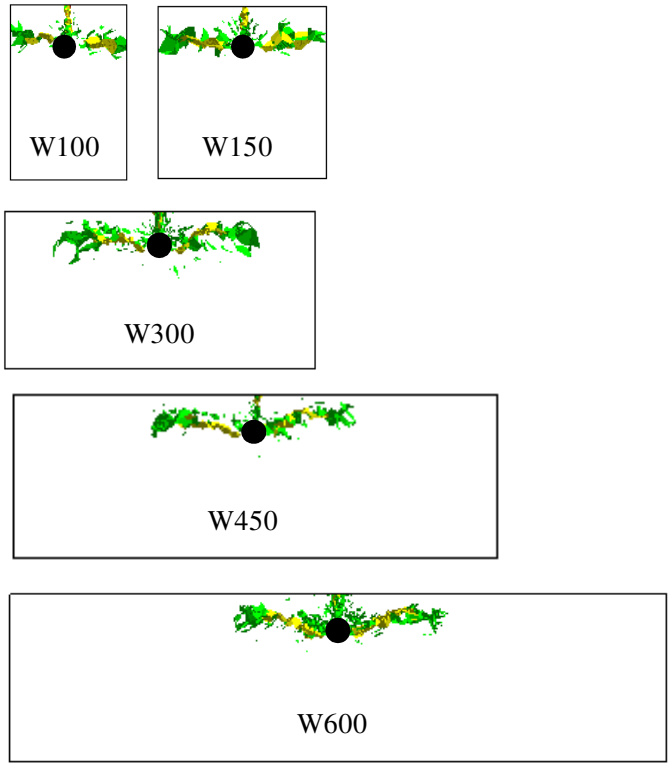

Figure 6.19. Analytical internal crack patterns at rebar corrosion amount 50 mg/cm^2 (varied width specimens)

Figure 6.20 shows surface deformation at rebar corrosion amount 500 mg/cm^2. The dashed lines show limits of specimen boundary for each specimen. It clearly shows that the wide specimens (W300, W450 and W600) result smaller surface deformation rather than the deformation in the narrow specimens (W100 and W150). The slopes of deformation shapes in narrow specimens are larger than the ones of the wide specimens because the deformation region is limited by the specimen boundary. The differences in the surface deformation intensity are because in the wide specimens, large volumes of concrete tend to restrain the deformation of the concrete surface. So, the surface crack opening in the narrow specimens is large than the one in the wide specimens due to the

differences between the slopes of surface deformation as shown in this Figure

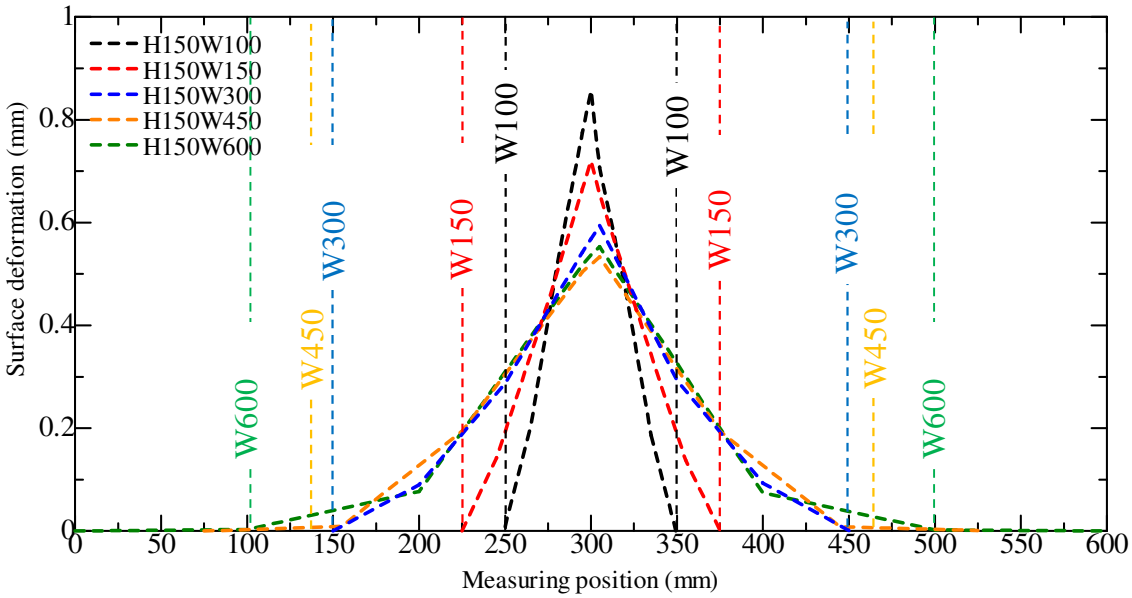

Figure 6.20. Analytical surface deformation at 500 mg/cm^2

(varied width specimens)

The propagation of internal cracks is corresponding to the deformation area of the surface as clarified in Chapter 4. In the narrow specimen, the specimen boundary is limited so the internal crack length propagation is also limited by the specimen boundary. **Figure 6.21** shows internal crack length propagation of the specimens in Series 1. The wide specimen results longer internal cracks due to the wider specimen boundary. So, the surface deformation area of the narrow specimen is smaller than the one induced by the wide specimen as shown in the surface deformation shown in **Figure 6.20**.

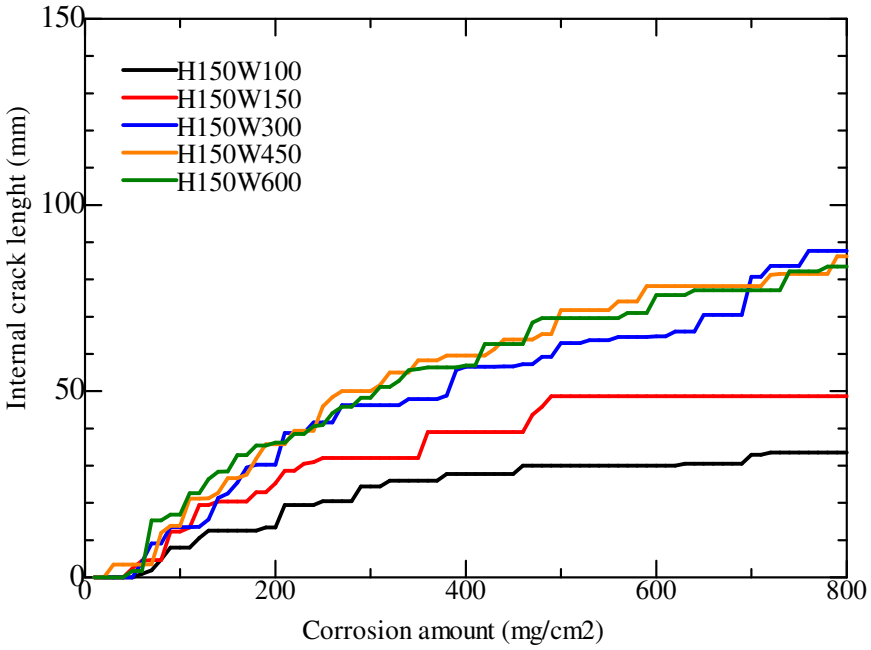

Figure 6.21. Propagation of internal crack (varied width specimens)

Figure 6.22 shows deformation of the specimens at rebar corrosion 500 mg/ cm^2, in which the crack patterns can be also observed.

Figure 6.23 shows relationship between surface crack width and internal crack length for each specimen. It clearly shown that at the same value of surface crack width, the wider specimens have much longer internal cracks. In other word, in the wide specimens, internal crack are dominant than the surface cracks.

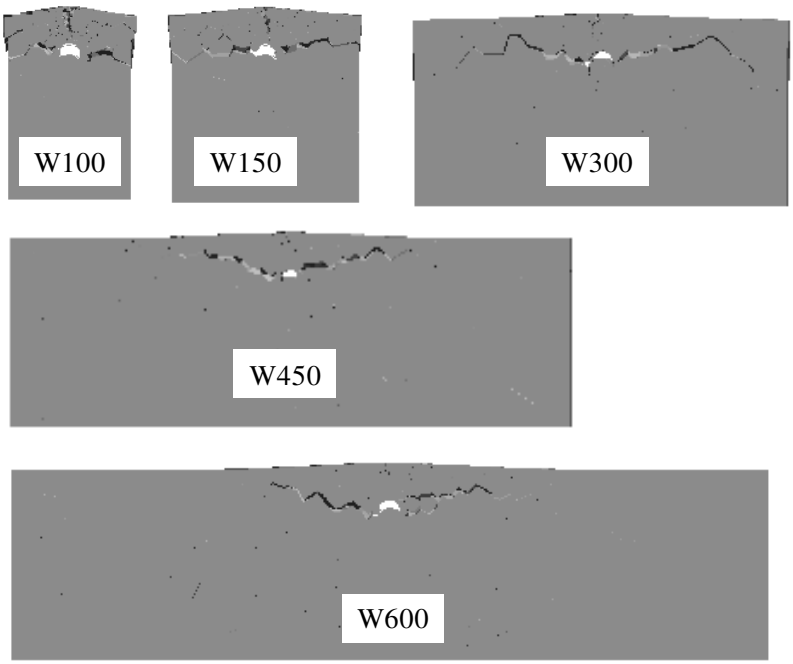

Figure 6.22. Deformation at corrosion rebar 500 mg/cm^2 (varied width specimens)

(magnification=10)

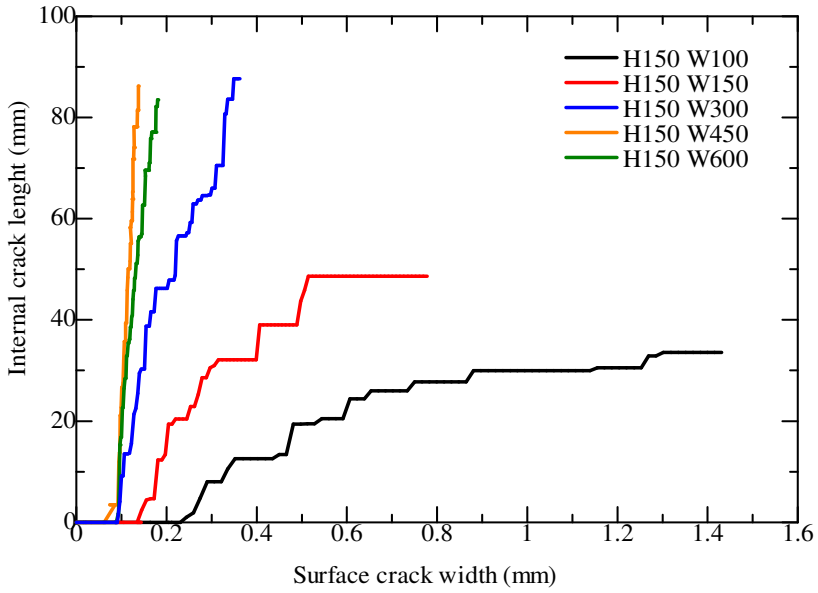

Figure 6.23. Relationship between surface crack and internal crack

(varied width specimens)

Figure 6.24 and **Figure 6.25** shows comparisons of surface deformation and specimen deformation of specimens H150 W150 and H 150 W600 at rebar corrosion amounts 50 mg/cm^2 and 500 mg/ cm^2 in order to understand the cracking mechanism of the wide specimen. In the crack initiation stage, minor cracks accumulate in concrete covers and surface cracks initiate from the specimen surface, which is similar to the narrow specimen. In the propagation stage, with the increase of rebar corrosion amount, due to the large restrain of concrete cover, surface deformation value is slower increasing. This induces slow increase of surface crack opening after the initiation. On the other hand, internal cracks highly propagate due to the wider limit of the specimen boundary. So, the surface deformation area is fast increasing. Therefore, in wide specimens internal cracks are dominant rather than surface cracks. In the later stage of corrosion, internal cracks diagonally propagate toward the surface and the internal crack lengths tend to converge to a particular value.

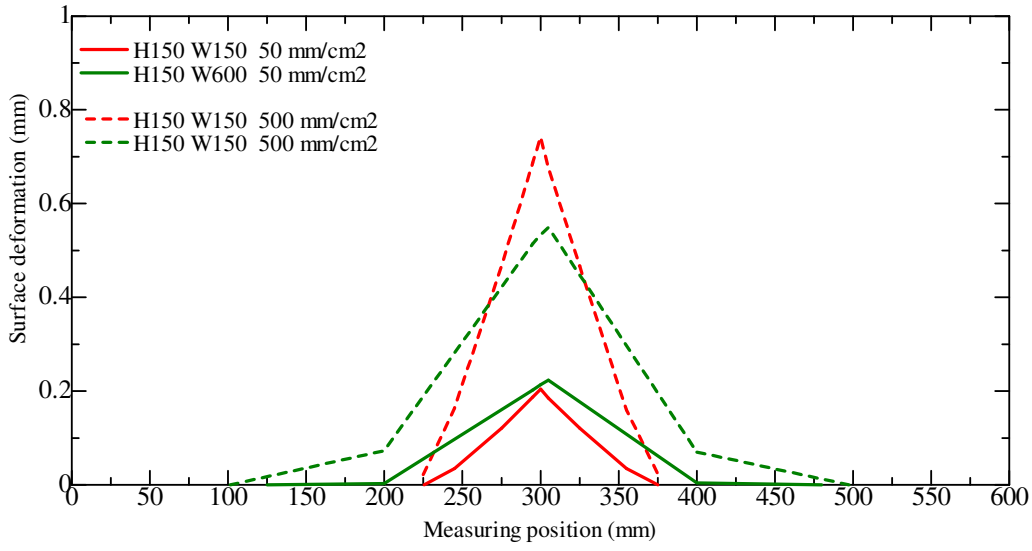

Figure 6.24. Surface deformation comparison

a) Deformation at corrosion amount 50 mg/cm^2

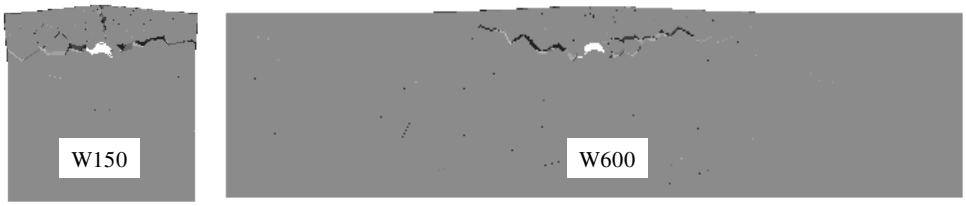

b) Deformation at corrosion amount 500 mg/cm^2

Figure 6.25. Deformation comparison

6.4.4 Analytical results of specimens with various heights and widths

Figure 6.26 and **Figure 6.27** show surface crack propagation, internal crack propagation and specimen deformation respectively for the specimens in Series 2. The cracking behaviors appear to be similar to the ones investigated in Series 1. So, the variation of specimen height does not have too much influence on the cracking behavior.

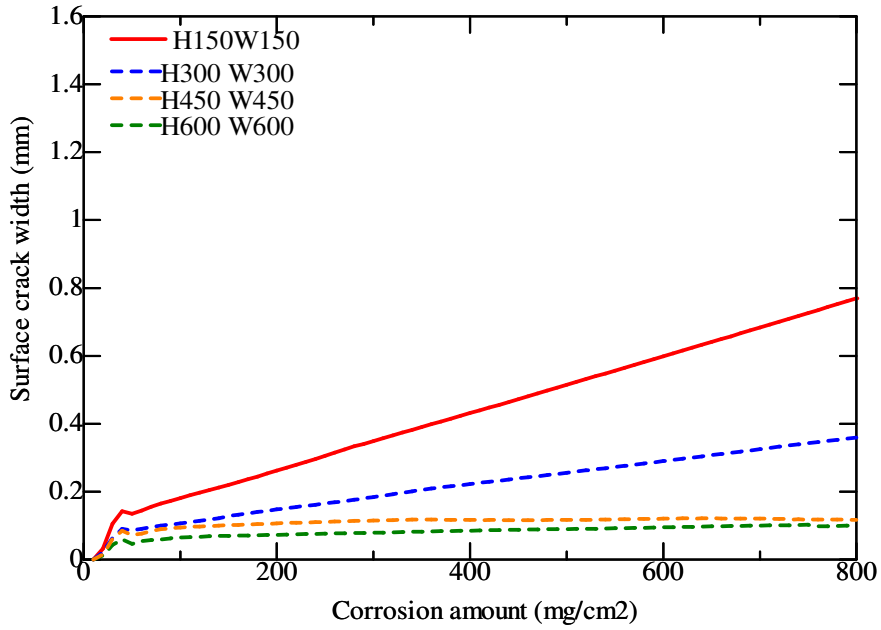

Figure 6.26. Surface crack propagation (varied height and width specimens)

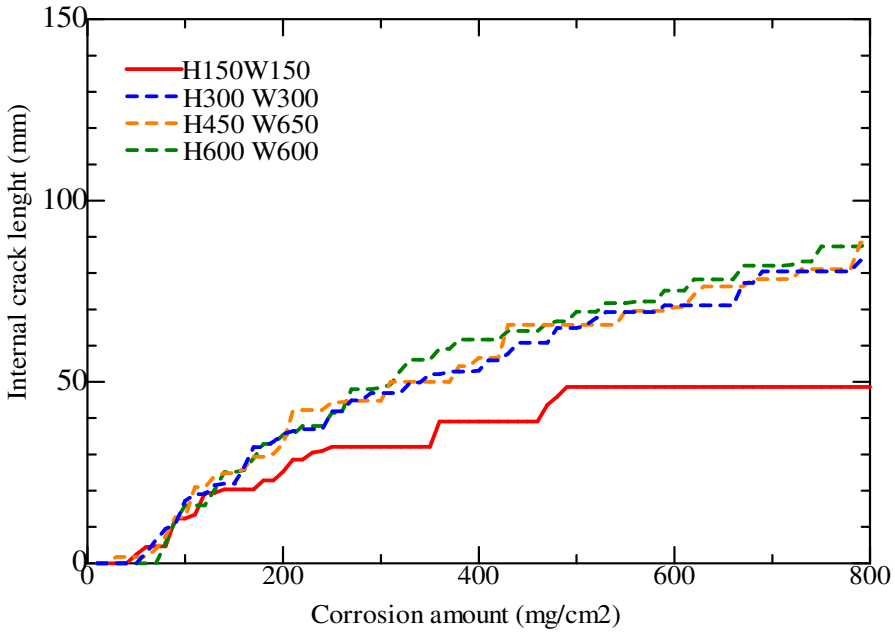

Figure 6.27. Internal crack propagation (varied height and width specimens)

6.5 Summary

This chapter investigated the crack propagation of varied single rebar specimen sizes experimentally and analytically. Moreover, the analytical study was conducted to clarify the effects of specimen boundary on the cracking behavior. The following conclusions are derived in this chapter:

(1) In the wide specimens, internal cracks are dominant in comparison with surface cracks. This behavior may be concerning to slab structures and should be noted in the maintenance process because only surface cracks are monitored periodically.

(2) Internal crack lengths develop rapidly after the initiation and internal crack lengths tend to converge to a particular value in the later stage of the corrosion. The internal cracks tend to propagate toward concrete surface which may cause potential de-lamination area on concrete surface.

(3) Cover thickness is important in crack accumulation and surface crack initiation while other dimensions do not have too much influence at this stage.

(4) Specimen width is important in surface crack width propagation due to its effect on the deformation of specimen surface including the deformation intensity and the deformation slope. Basically, wider specimens restrain surface deformation and so, it results smaller surface cracks.

(5) Specimen width affects the internal crack propagation. Internal crack lengths in the wide specimen are longer than the ones in the narrow specimen due to the wider limit of the specimen boundary.

(6) Variation of specimen height does not affect the crack propagation

7. CRACKING BEHAVIOR DUE TO MULTI-REBAR CORROSION

7.1 Introduction

In the previous chapters, cracking behavior due to single-rebar corrosion has been investigated experimentally and analytically.

In the literature, several researchers carried out experiment of multi-rebar specimens using electric accelerated corrosion tests to evaluate crack propagation such as crack patterns and crack widths due to multi-rebar corrosion (Ahmed et al., 2007, Murakami et al., 2008). The experiment showed that internal cracks joined together between rebars due to the multi rebar arrangement. Crack patterns and internal crack width propagation in the case of multi-rebar corrosion were also simulated (Ahmed et al., 2007). The simulation results showed that internal cracks significantly developed in the case of multi-rebar corrosion. However, a crack propagation mechanism and factors affecting the crack propagation due to multi-rebar corrosion have not been clarified and reported in the literature.

In this chapter, the applicability of the proposed RBSM analytical model was confirmed against the experiments of multi-rebar corrosion specimens carried out by other researchers using electric accelerated corrosion tests. The analytical model shows its applicability to simulate crack propagation of multi-rebar corrosion specimens in terms of crack patterns, surface crack propagation and internal crack propagation. Additionally, an analytical parameter study was carried out for multi-rebar corrosion specimens with varied rebar spacing to investigate effect of rebar spacing on crack patterns, crack propagation, crack joining and surface deformation of concrete cover. As a result, a mechanism of crack propagation in concrete due to multi-rebar corrosion was proposed and compared with the case of single-rebar corrosion analytically.

7.2 Numerical evaluation of cracking due to multi-rebar corrosion

The proposed RBSM analytical method combined with the three-phase material corrosion expansion model presented in Chapter 3 is applied to simulate cracking behavior due to multi-rebar corrosion in this chapter. In the analysis, mesh sizes of the Voronoi particles are 5 mm in the cover thickness and 25-40 mm in the other parts. The local corrosion model on the rebar section is also assumed in the analysis. The analytical results are compared with the test results conducted by other researchers.

7.2.1 Crack pattern and surface crack propagation

The experiment carried out by Murakami et al. (2008) is used to compare with the analytical results in terms of crack patterns and surface crack width propagation. Analyzed specimens include Series S0 having three D16 rebars with the setting dimensions shown in **Figure 7.1**. The external rebars were labeled L, R and the internal

one was labeled M in the specimen.

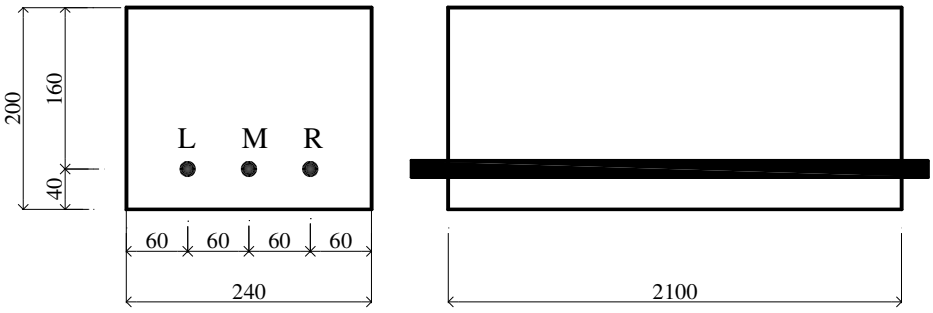

a) Section b) Side view

Figure 7.1. Specimens of Series S0 (Murakami et al., 2008)

Specimens were tested until average rebar corrosion ratios reached 10.2% (S0-10), 18.6% (S0-20) and 26.4% (S0-30). The relationship between the rebar corrosion ratio (Δw) and corrosion amount W_r (mg/cm^2) used in the analysis was described in Chapter 2.

Before starting the electric corrosion test, the concrete compressive strengths were 31.6, 35.5 and 26.2 MPa corresponding to specimens with rebar corrosion ratios of 10.2%, 18.6% and 26.4%. After finishing the electric corrosion test, crack patterns were observed on the bottom surface of specimens and on the ends of specimens. Surface crack width along the external rebars was also measured for each case of rebar corrosion ratio.

3D-RBSM model of the specimen is shown in **Figure 7.2**. Due to the limitation of numerical computation, the specimen's length is modeled as 100 mm in the analysis.

Concrete material properties used in the analysis are f'_c = 31.0 MPa, f_t = 1.92 MPa, E = 26.2 GPa and G_F = 0.04 N/mm.

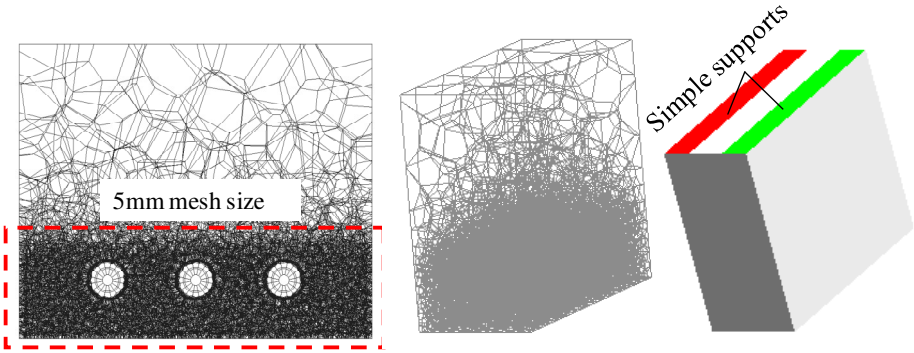

a) Specimen section b) 3D Voronoi particles c) Specimen supports

Figure 7.2. RBSM model of specimen **Series S0**

Figure 7.3 and **Figure 7.4** shows crack patterns on bottom surface and beam ends in the analysis and the experiment respectively. Analytical surface cracks on bottom surface at rebar corrosion ratio 10.2 % (in **Figure 7.3b**) only appear along external rebars along the specimen length which totally agree with the test results shown in **Figure 7.3a**.

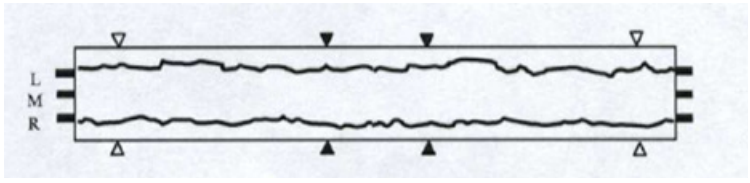

a) Experimental

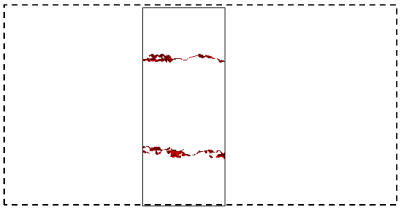

b) Analytical

Figure 7.3. Crack pattern on bottom surface

On the beam ends, analytical cracks are obtained at rebar corrosion ratios as of 10.%,

18.6% and 26.4% as shown in **Figure 7.4b**. There is no crack under M rebar on the concrete cover and cracks between L, R rebars and M rebar are dominant. Internal cracks propagate from the external rebars toward the specimen sides; the internal cracks reach specimen sides when the rebar ratio as 26.4% and they are longer than the ones when the rebar ratio as 18.6%. So, the analytical cracks appear agreement with the experimental ones shown in **Figure 7.4a**.

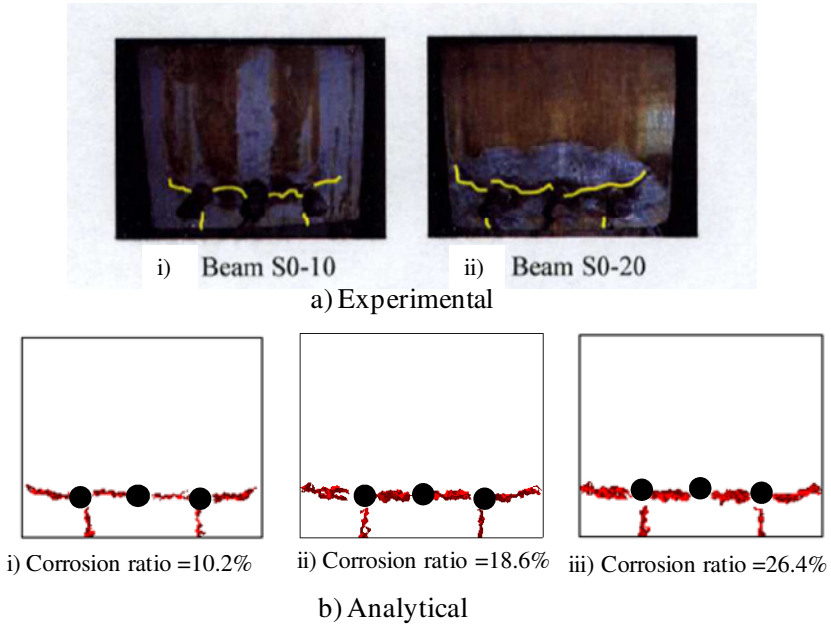

Figure 7.4. Crack patterns on beam end

Surface crack width propagation along L, R rebars is also measured in the analysis. The propagation of surface crack against increase of rebar corrosion ratio is shown in **Figure 7.5**. The analytical crack width propagation also agrees with the experimental results, in which surface crack width initiates after a particular value of rebar corrosion ratio and then rapidly increase corresponding with increase of corrosion ratio.

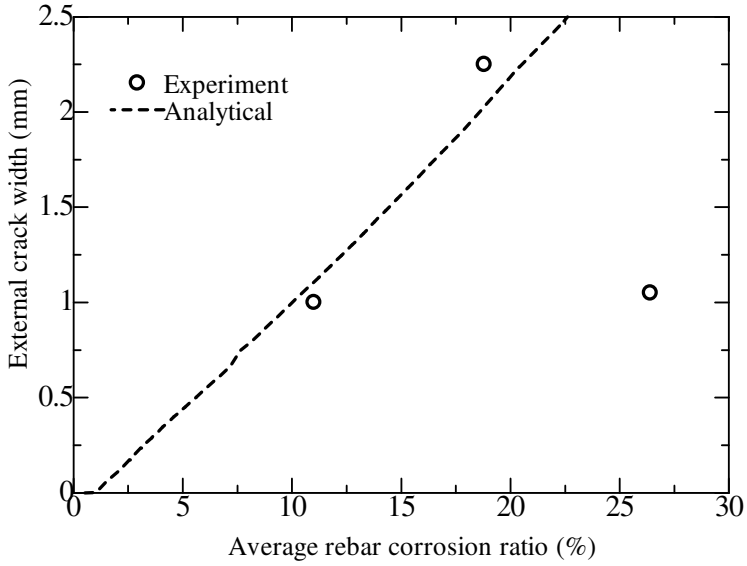

Figure 7.5. Surface crack propagation (along L, R rebar)

7.2.2 Internal crack propagation

The experiment carried out by Admed et al. (2007) is used to compare with the analytical propagation of internal crack in the case of multi-rebar corrosion.

In the experiment, internal strain is measured using a 70 mm long concrete embeddable fiber-optic strain sensor (FOSS) as shown in **Figure 7.6**. With this set-up, the FOSS strain is directly proportional to internal crack width between the external rebar and the middle rebar. In the analysis, the internal crack width can be obtained directly between the pre-input elements. The concrete beam having three D16 rebars was accelerated by an electric corrosion test. The compressive strength of concrete was 40 MPa before the corrosion test.

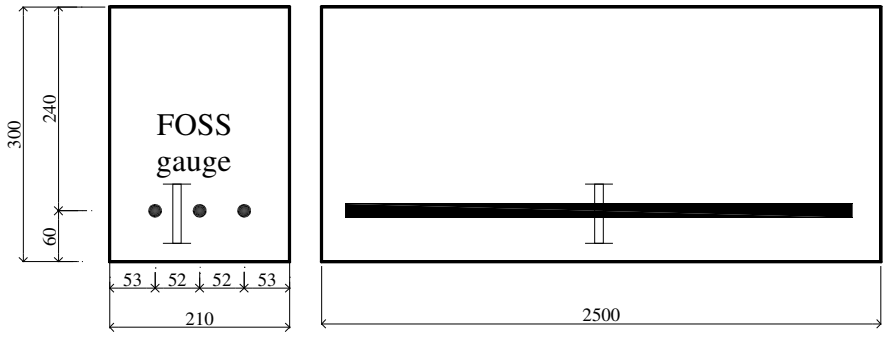

a) Section b) Side view

Figure 7.6. Specimen dimension and FOSS set-up (Admed et al., 2007)

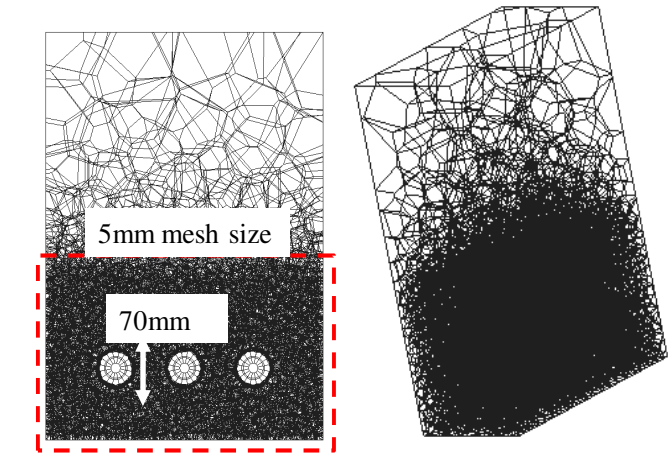

a) Specimen section & internal crack measuring position b) 3D Voronoi particles

Figure 7.7. RBSM modeling of specimen

Figure 7.7 shows 3D-RBSM model of the specimen and a position to measure internal crack. Specimen length is also modeled as 100mm due to the computation limitation. Concrete material properties used in the analysis are f'_c = 40.0 MPa, f_t = 3.35 MPa, E = 32.3 GPa and G_F = 0.07 N/mm.

Figure 7.8 shows analytical strain against the experimental FOSS strain. The analytical strain is obtained by dividing the measured crack width from the analysis for

the distance between the measuring pre-input elements, i.e. 70 mm. The rebar corrosion ratio in this test is smaller than the results of the Murakami test. The analytical strain shows reasonable agreement with the experimental value. That is, internal strain initiates when rebar corrosion ratio reaches a value around 1.5% and then it speedily propagates when the corrosion ratio increases.

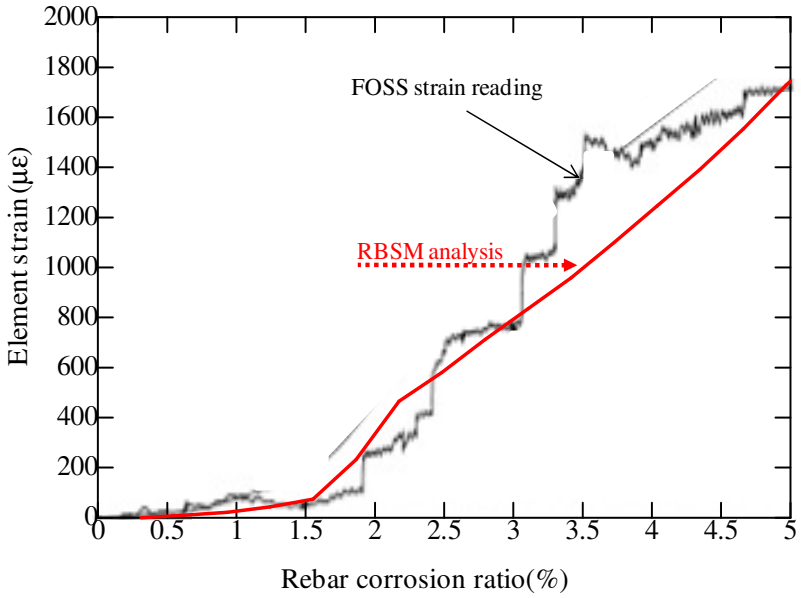

Figure 7.8. Analytical internal strain

The above verifications prove the applicability of the proposed RBSM analytical model in simulation of crack propagation in the case of multi-rebar corrosion specimens in both qualitative amount (crack patterns) and quantitative amount (crack width).

7.3 Numerical evaluation of effect of rebar spacing

In this part, a mechanism of crack propagation due to multi-rebar corrosion is discussed.

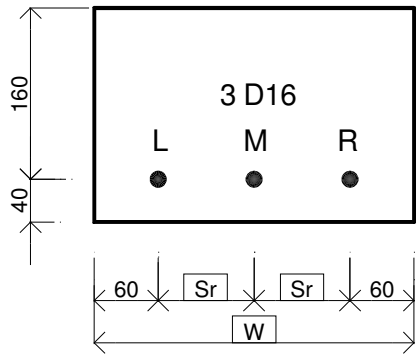

Specimen	Rebar spacing Sr (mm)	Specimen width W(mm)
Sr-40	40	200
Sr-60	60	240
Sr-200	200	520
Single	N/A	240

Figure 7.9. Specimen set-up with varied rebar spacing

In order to investigate effect of rebar spacing on crack patterns in the case of multi-rebar corrosion, the specimen in the Murakami's experiment is simulated again with varied rebar spacing dimensions which are varied from 40 mm to 200 mm as shown in **Figure 7.9**. Other dimensions from rebars to specimen surfaces are kept constant to eliminate other effects caused by these factors as discussed in the previous chapters. Specimen Sr-60 is the same as the specimen Series S0 in the Murakami experiment. Moreover, a specimen with single-rebar arranged in the middle of the specimen and the other dimensions are kept the same with specimen Sr-60 is simulated to compare behavior of the single-rebar specimen with the multi-rebar corrosion specimens.

Figure 7.10 shows bottom surface deformation of the specimens with varied rebar spacing at several rebar corrosion ratios. In the single rebar specimen, the maximum deformation is at the middle of specimen which is coinciding with the rebar position. With the increasing rebar corrosion ratio, deformed area is expanded and the surface deformation is increased. In the multi-rebar corrosion specimens, there are three types of surface deformation shape due to different rebar spacing at rebar corrosion ratio of 1.9%. In specimen Sr-40, the maximum deformation is at the middle of specimen and

then it develops with increase of corrosion ratio which is similar to the single-rebar corrosion specimen. It is noted that the surface deformation width is about 200 mm and it does not increase although the rebar corrosion ratio increases. It is due to the propagation of internal cracks is limited by the specimen width, i.e. 200 mm, in this case. In specimen Sr-60, the surface deformation is in a trapezium shape with the changing slope at the L, R rebar positions. In specimen Sr-200, initially, surface is bent similar to the single-rebar corrosion case at each rebar position. With further increase of rebar corrosion ratio, surface deformation is increased and changed to a trapezium shape with the changing slope at the L,R rebar positions. Then, the surface deformation increases and changes with a slope reduction at M rebar position. Furthermore, the value of deformation in multi-rebar corrosion specimens is larger than the value of the single-rebar corrosion specimen. It is obviously understood that the crack propagation mechanism of the multi-rebar corrosion specimens is different from the one of the single rebar specimen.

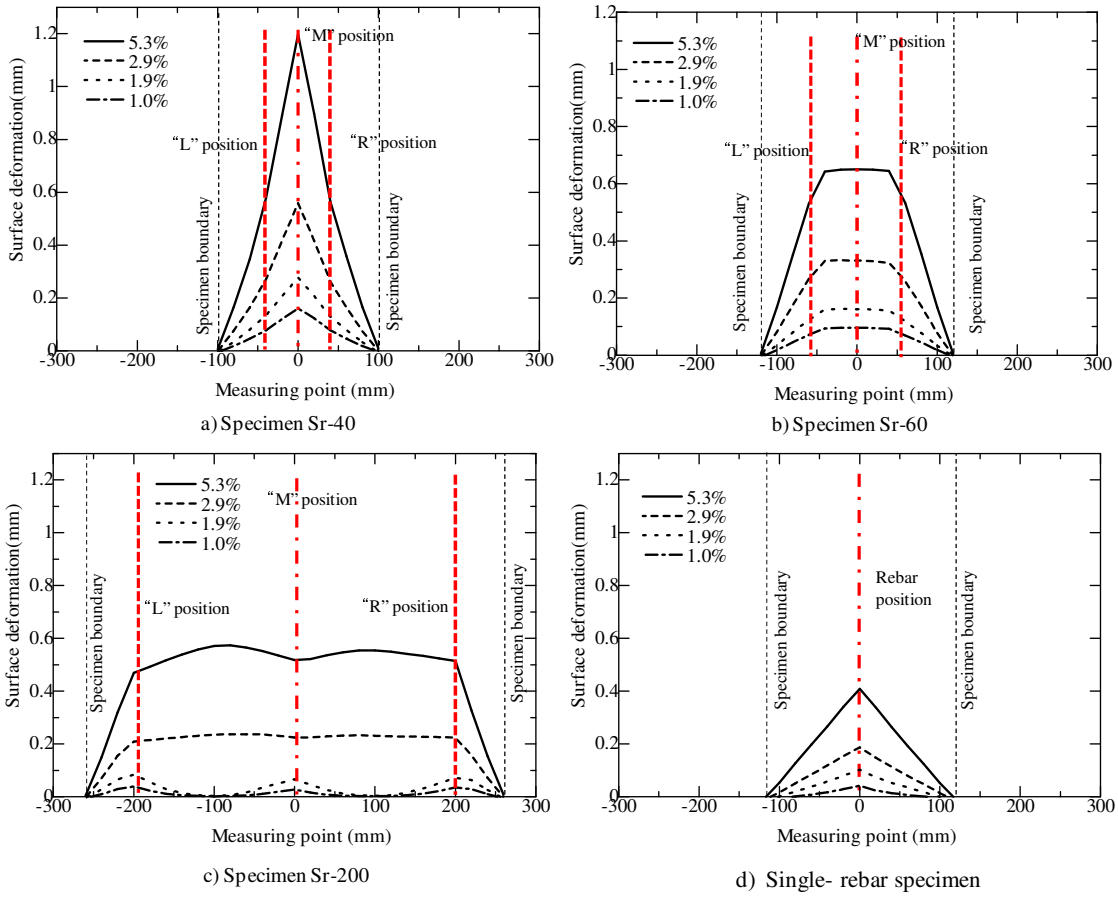

Figure 7.10. Surface deformation development

Figure 7.11 shows propagation of surface crack width measured below L,R rebar (external surface cracks) and M rebar (middle surface crack) against increase of rebar corrosion ratio. In specimen Sr-40, the middle surface crack is dominant corresponding to the surface deformation shape. In specimen Sr-60 and specimen Sr-200, external surface crack is dominant. The middle surface crack of Sr-60 increases then keeps its width unchanged after corrosion rebar ratio of 1.5%. The middle surface crack of Sr-200 rapidly increases after the initiation and then reduces its width at rebar corrosion ratio of 2.5% due to the changing surface deformation at M rebar as shown in **Figure 7.10c**

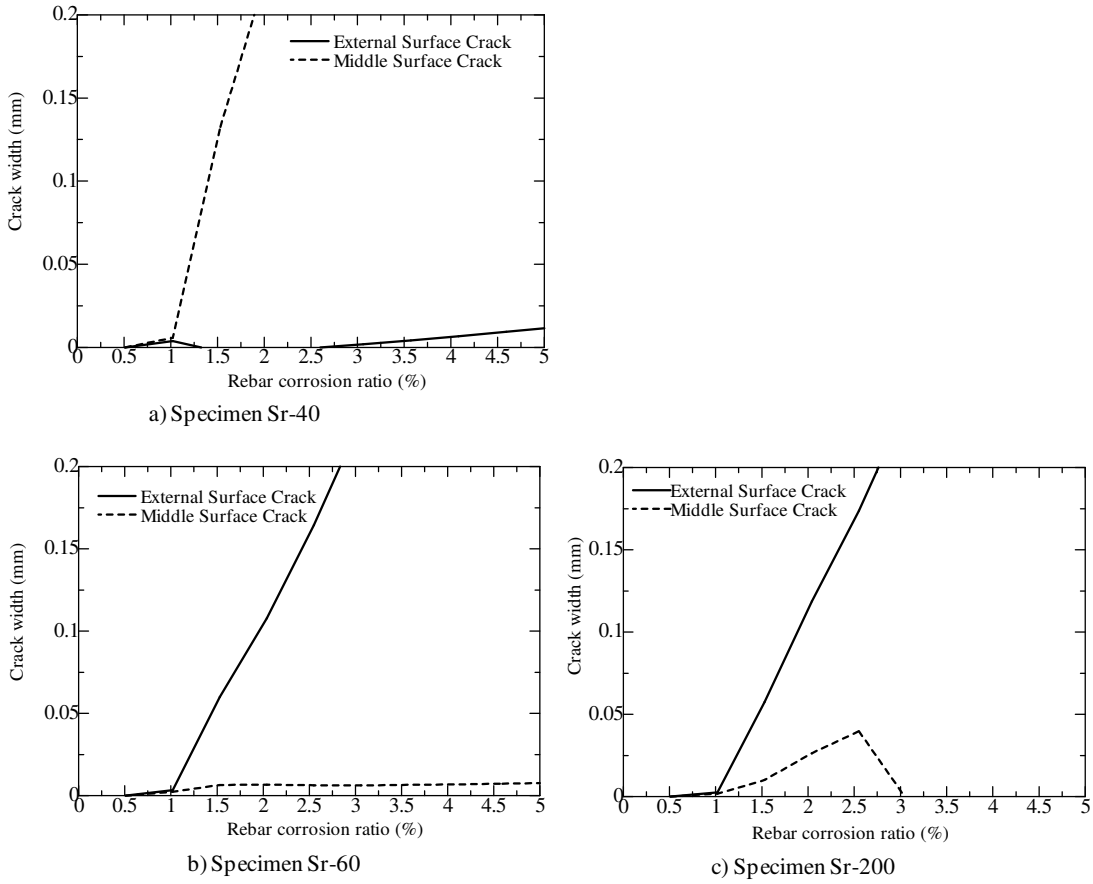

Figure 7.11. Propagation of surface crack width (External and Middle)

The tendency of specimen Sr-40 is different from the one of Sr-60 and Sr-200 because due to the closer rebar spacing, specimen Sr-40 behaves similarly to the single-rebar specimen, in which the maximum surface crack opening is at the specimen centre. This behaviour can be understood from the surface deformation shown in **Figure 7.10a**.

Figure 7.12 shows propagation of surface crack width and internal crack width against increase of rebar corrosion ratio. Surface crack width is measured below L,R rebar of specimen Sr-60 and Sr-200 and below M rebar of Sr-40 and the single-rebar specimen. Internal crack width is measured between L, R rebar and M rebar in the

multi-rebar specimens. In the single-rebar specimen, internal crack width is measured at the position as the same as the one in Sr-60. The diagrams showing crack measuring positions are also added in this figure for clarity. In the single-rebar specimen, surface crack width is larger than internal crack width. On the other hand, in the multi-rebar specimens, internal crack width is basically larger than the surface crack width. In the case of specimen Sr-40, surface crack width and internal crack width are almost the same. In the later stage of specimens Sr-60 and Sr-200, internal crack width is larger than the surface crack width. Surface crack width and internal crack width of specimen Sr-40 are bigger than the ones of specimen Sr-60 and specimen Sr-200. Therefore, the multi-rebar corrosion case should be noted on the propagation of internal cracks because internal cracks are not easy to observe. The significance of the comparison between the surface crack width and the internal crack width is to see the development of inside damage against the outside damage. The internal cracks tend to cause spalling of concrete cover and cannot be monitored easily in a period basis. In the multi-rebar specimens, when surface cracks develop to visible cracks, internal cracks have already been large and they may cause spalling of the concrete cover suddenly.

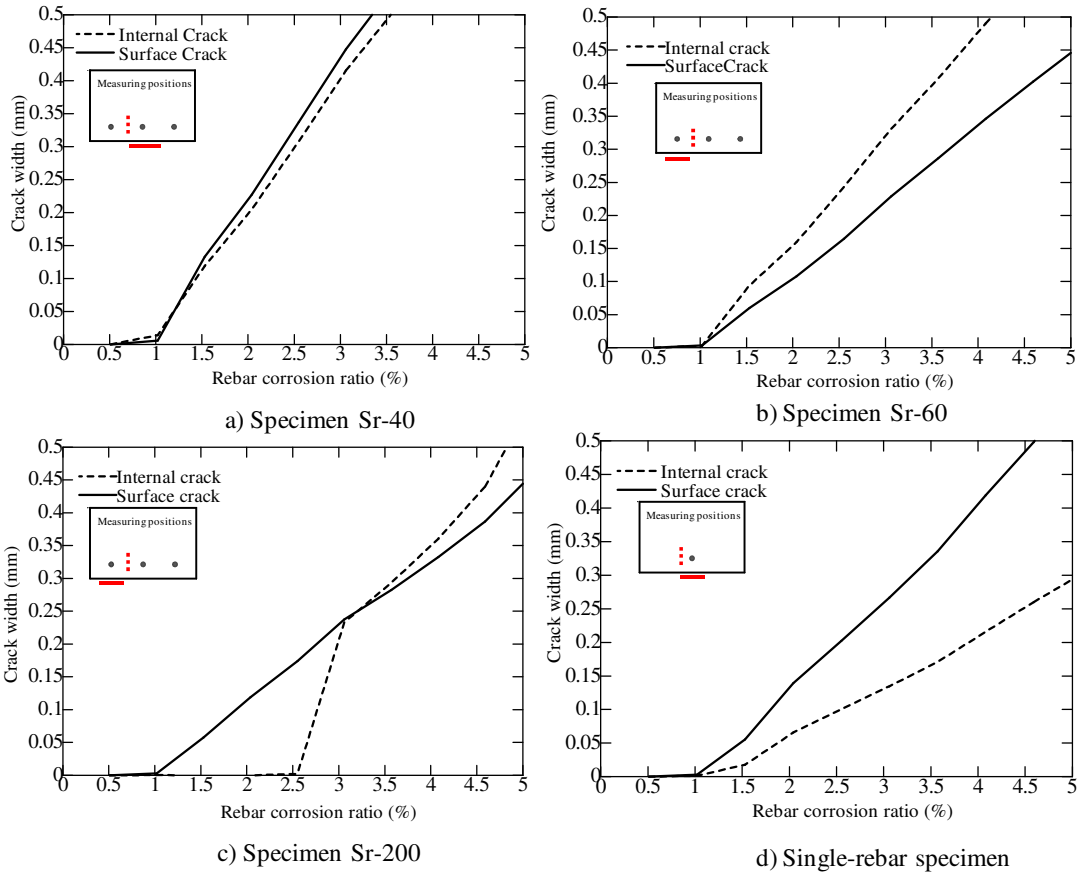

Figure 7.12. Propagation of surface crack and internal crack

Figure 7.13 shows crack development at several rebar corrosion ratios for all specimens. The color ranges (green, yellow and red) represent crack width values, in which the range of red color corresponds to visible cracks (larger than 0.15 mm width), the yellow one corresponds to 0.02 mm - 0.15 mm wide cracks and the green one to minor cracks. For clarity, the specimens are shown upside down with the rebars on the top side. At rebar corrosion ratio about 0.5%, minor cracks occur around rebars. The minor cracks distribution is similar in specimen Sr-60, Sr-200 and the single-rebar specimen. On the other hand, in Sr-40 specimen, minor cracks join between the rebars

and distribute on the surface. The effect of rebar spacing is already observed for narrow rebar spacing case. At rebar corrosion ratio about 1%, internal cracks join together between L, R rebar and M rebar for small rebar spacing specimens (Sr-40, Sr-60). Then, they develop to larger cracks (red color). Surface cracks initiates along L,R rebar in specimen Sr-60 and specimen Sr-200 and along M rebar in specimen Sr-40 corresponding to the bending of surface. This means that internal cracks have already developed when visible surface cracks are observed. In specimen Sr-200, internal cracks become larger after the joining cracks between the rebars at corrosion ratio of 2.5%, the internal cracks are significant dominant in this case rather than surface cracks. In comparison with the single-rebar corrosion, the multi-rebar corrosion causes large internal cracks to be formed earlier, for example, at rebar corrosion ratio of 1.9%, there are significant amount of large cracks (red color) are formed in Sr-40 and Sr-60 rather than the ones of single rebar specimen. This is the effect of multi-rebar arrangement. That is, internal cracks propagate from each rebar to the horizontal direction, internal crack width increases due to the interference of cracks. Therefore, in the single rebar corrosion, the surface crack width is larger than the internal one but in the multi-rebar cases, the internal crack is larger than the surface ones.

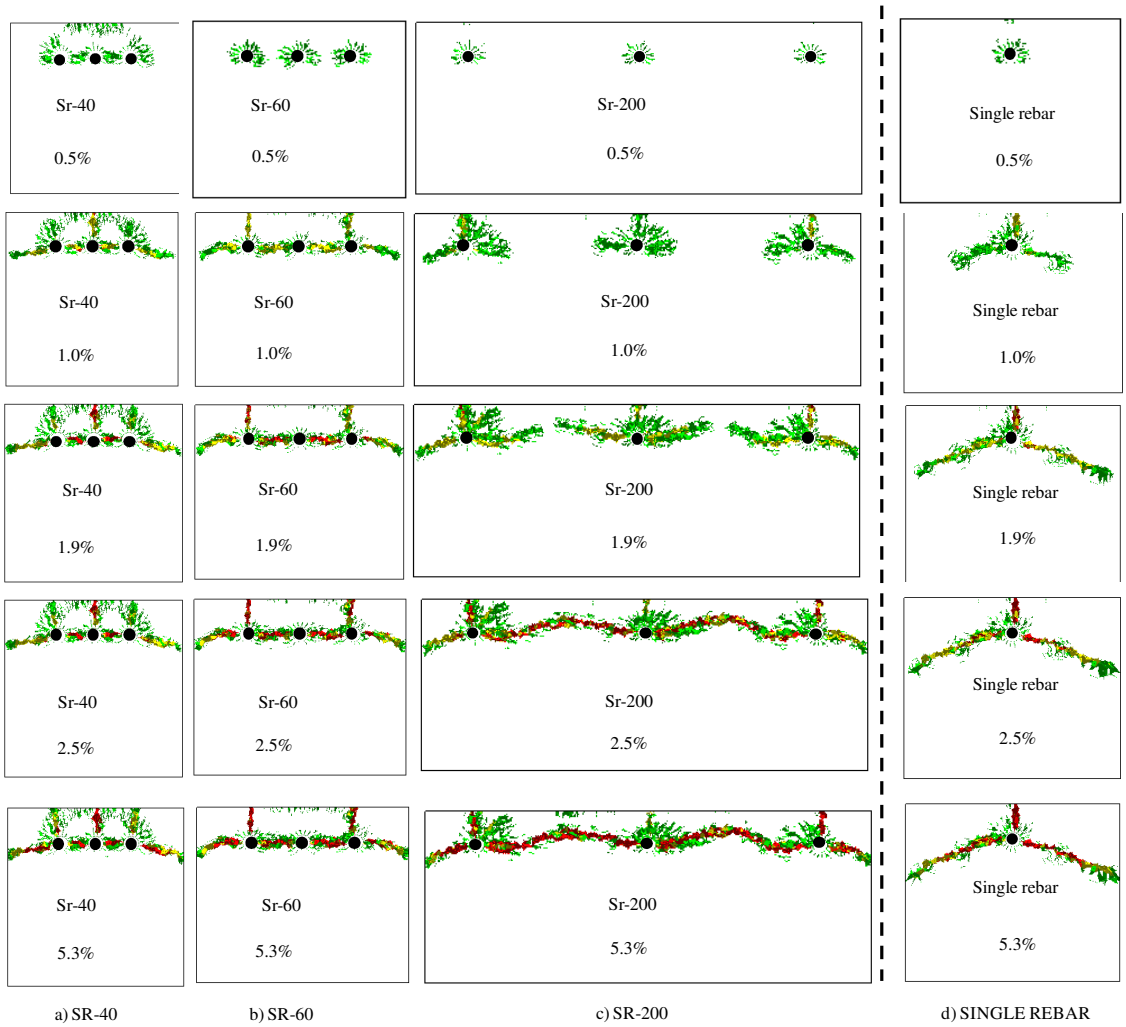

Figure 7.13. Crack development

Deformation of specimens at rebar corrosion ratio 5.3% are shown in **Figure 7.14**. Crack patterns are also understood from the deformation by the separation between rigid bodies in RBSM. Crack patterns on the beam ends are significantly affected by the rebar spacing. Surface cracks appear along M rebar in specimen Sr-40. Cracks also appears along L,R rebars in specimen Sr-40 but they are not dominant as the one along M rebar. In specimen Sr-60, surface cracks appear along L,R rebar. Surface cracks along M rebar do not propagate. In specimen Sr-200, the surface cracks behave similarly with the ones

of specimen Sr-60. In specimens Sr-60 and Sr-200, the middle parts of cover concrete seem to be delaminated due to propagation of internal cracks between rebars and cracks along L, R rebars.

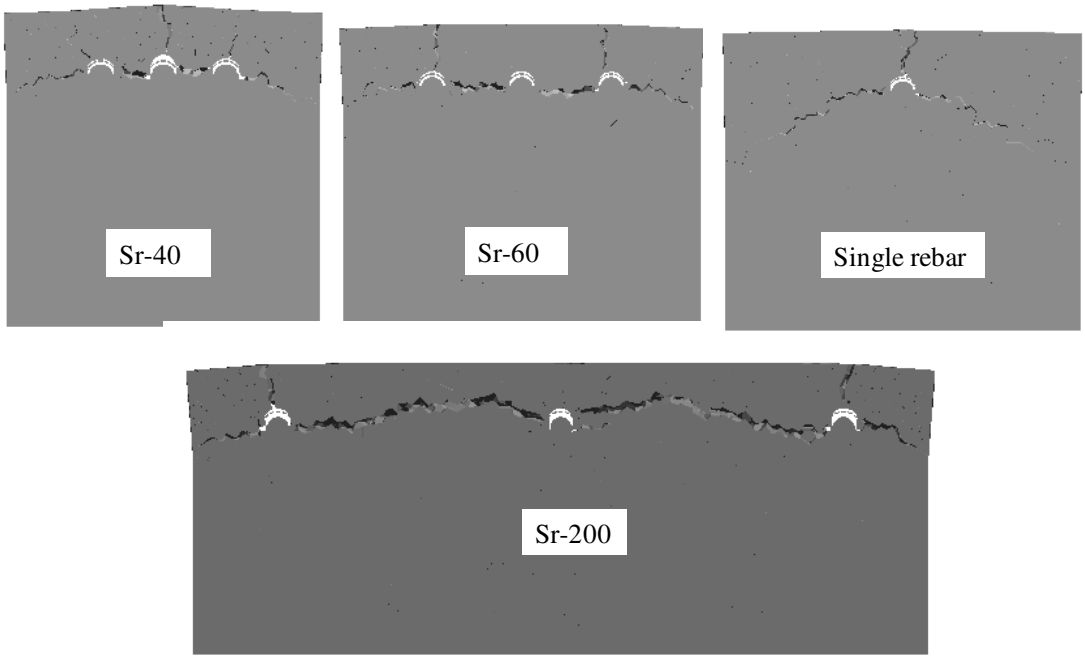

Figure 7.14. Specimen deformation at rebar ratio 5.3%

(magnification= 5)

7.4 Summary

This chapter simulated crack propagation behavior due to multi-rebar corrosion using the proposed RBSM analytical method to investigate the effect of rebar spacing on to crack patterns, and to clarify a cracking mechanism of multi-rebar corrosion specimens. The following conclusions are derived in this chapter.

(1) The applicability of the analytical method in the case of multi-rebar corrosion was confirmed qualitatively and quantitatively by the experimental results in terms of crack patterns, surface crack width propagation and internal crack width

propagation.

(2) In the case of multi rebar-corrosion, internal cracks joined together between the rebars and developed to large cracks in the early stage of the rebar corrosion and earlier than internal cracks in the single-rebar corrosion.

(3) Rebar spacing significantly affects the crack patterns and crack propagation in the case of the multi-rebar corrosion. This parameter, therefore, is an important factor in the evaluation of the cracking due to multi-rebar corrosion.

(4) In the case of multi-rebar corrosion, the dominant and the early development of internal cracks tend to cause sudden de-lamination of the concrete cover although surface cracks may not be observed during the maintenance.

(5) The cracking behavior derived in this study is based on some assumption mentioned in this study such as constant concrete cover parameters. In order to apply the outcome of this study to a general case of structure it is necessary to consider effects of other parameters. The outcome of this study may be useful for the maintenance process of an existing structure. That is, due to the difference of the rebar spacing, the internal damage situation may be different. So, the internal damage cannot adequately evaluate if the investigation is only based on the surface condition as being done in several current maintenance processes.

8. LONGITUDINAL LOCAL CORROSION AND DE-LAMINATION PHENOMENON IN SLAB

8.1 Introduction

In the previous chapters, surface crack propagation and internal crack propagation were discussed in various cases of the rebar corrosion in concrete structure. In the maintenance process, surface cracks caused by corrosion of rebar are able to be monitored by visual inspection or equipments (Bentur, 1997). However, internal cracks cannot be easily monitored. In some cases, internal cracks suddenly induce de-lamination phenomenon on concrete cover although surface cracks have not appeared on the surface of concrete. Propagation of internal cracks, relationship of internal cracks, de-lamination phenomenon of the concrete surface and effects on the surface damage were not clarified in the literature.

In this chapter, propagation of internal cracks, propagation of surface cracks and

de-lamination phenomenon of concrete cover due to longitudinal local corrosion of the rebar with three-dimensional cracking behavior are investigated experimentally and analytically.

In the experiment, longitudinal local corrosion phenomenon of rebar is observed during the electric accelerated corrosion test. The longitudinal local corrosion causes differences on the crack propagation in comparison with the experiments presented in the previous chapters. That is, crack propagation is non-uniform along the specimen length.

In the analysis, specimens are simulated to investigate the three-dimensional behavior of the crack propagation. The analytical results are compared with the experimental results in various conditions of the longitudinal local corrosion of the rebar. Moreover, the proposed RBSM analytical model is applied to simulate de-lamination phenomenon of a real-slab structure which has been recently degraded by the rebar corrosion. The simulation results were compared with the survey data.

Finally, effects of cover thickness and corrosion length of the rebar on internal crack propagation and de-lamination area of concrete slab are investigated analytically. As a result, it is found that once rebar is corroded, concrete cover thickness significantly affects internal crack propagation and de-lamination area on the slab surface. Local corrosion length of the rebar is significantly affects the area of the de-lamination on the slab surface.

8.2 Three-dimensional cracking due to longitudinal local corrosion

8.2.1 Experiment of longitudinal local corrosion

In the experiment of specimen series 600*400-C30 described in Chapter 6, two

specimens showed that their rebars were not uniformly corroded along their lengths. That is, some parts of the rebar are more corroded than the other parts. **Figure 8.1** shows dimensions of this specimen series. These two specimens were cast with the same concrete composition presented in Chapter 6 but the applied corrosion current density was double the value mentioned in Chapter 2, i.e. 1.8 mA/cm^2. The local corrosion along the rebar may be due to the large size of the specimen or the higher corrosion current density which induced a faster speed of corrosion. In this chapter, these specimens are used to investigate crack propagation due to the local corrosion along the rebar. This rebar corrosion situation may be similar to the situation of rebar corrosion occurred in slab structure with the large surface area.

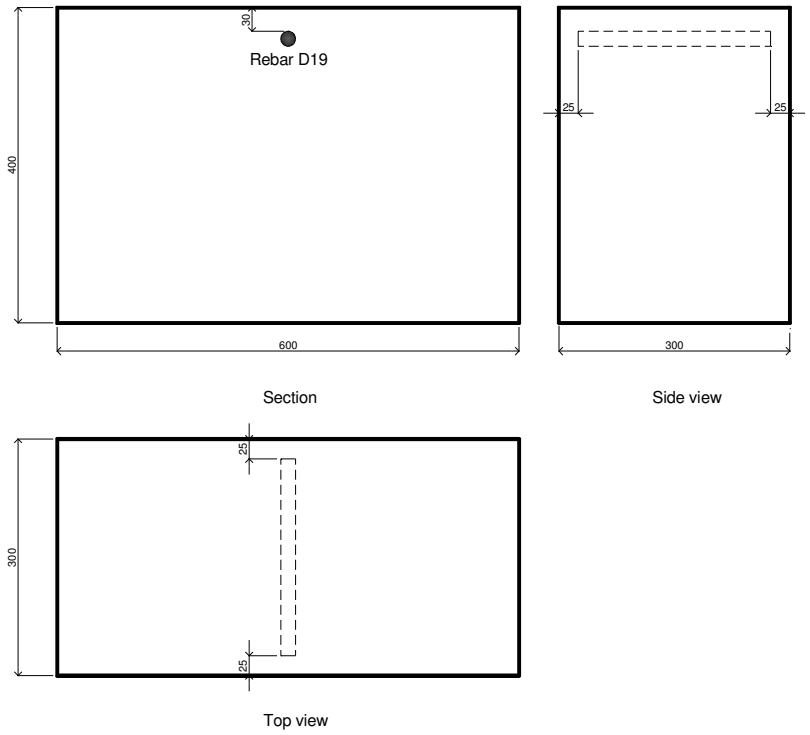

Figure 8.1. Specimen series 600*400-C30 dimension

8.2.2 Experimental crack patterns

Figure 8.2 shows surface crack pattern and internal crack patterns of specimen No. 1. The average corrosion amount of the rebar after the test was 539 mg/cm^2. In this case, surface crack pattern is different from the cases presented in the previous chapters for the single rebar specimens. That is, the surface crack pattern of specimen No. 1 is not uniformly along the specimen length as shown on the top view of the specimen. In order to observe internal crack patterns, the specimen was cut along the dashed lines shown on the top view in **Figure 8.2**. Section 1 shows internal crack pattern through the more corroded part and Section 2 shows internal crack pattern through the less corroded part of the rebar. The internal crack patterns appear similar for each case of the section. That is, internal cracks diagonally propagate toward the concrete surface and cause de-lamination on the concrete surface. In terms of internal crack length, the crack pattern through Section 1 shows longer internal cracks than the ones shown in Section 2.

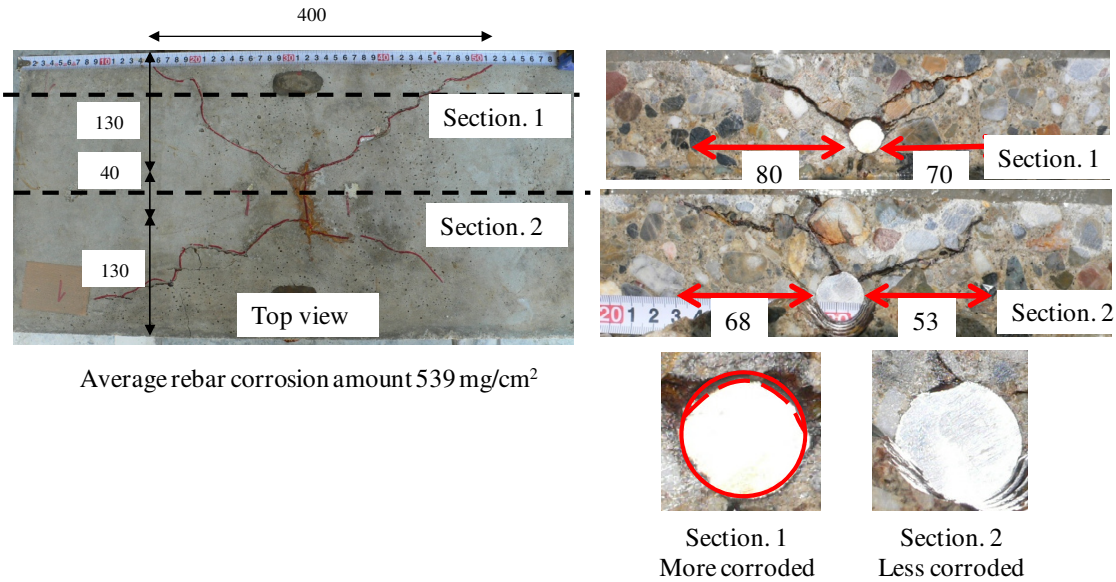

Figure 8.2. Crack patterns of specimen No. 1

Figure 8.3 shows surface crack pattern and internal crack patterns of specimen No. 2. The average corrosion amount of the rebar after the test was 624 mg/cm^2. In this case, surface crack pattern is also different from the normal cases presented in the previous chapters. That is, a part of surface was de-laminated from the concrete cover. The size of the delaminated part was about 200 mm x 110 mm. Outside the delaminated part, surface crack was very small as shown on the top view of the specimen. The specimen was also cut along the dashed lines shown on the top view to observe internal crack patterns. Section 1 shows internal crack pattern through the more corroded part and Section 2 shows internal crack pattern through the less corroded part of the rebar. Section 1 shows internal cracks reaching the concrete surface at both sides of the rebar which causes the de-lamination of the concrete surface. Section 2 shows internal crack also propagating from the rebar toward the concrete surface but the crack lengths are shorter than the ones in Section 1.

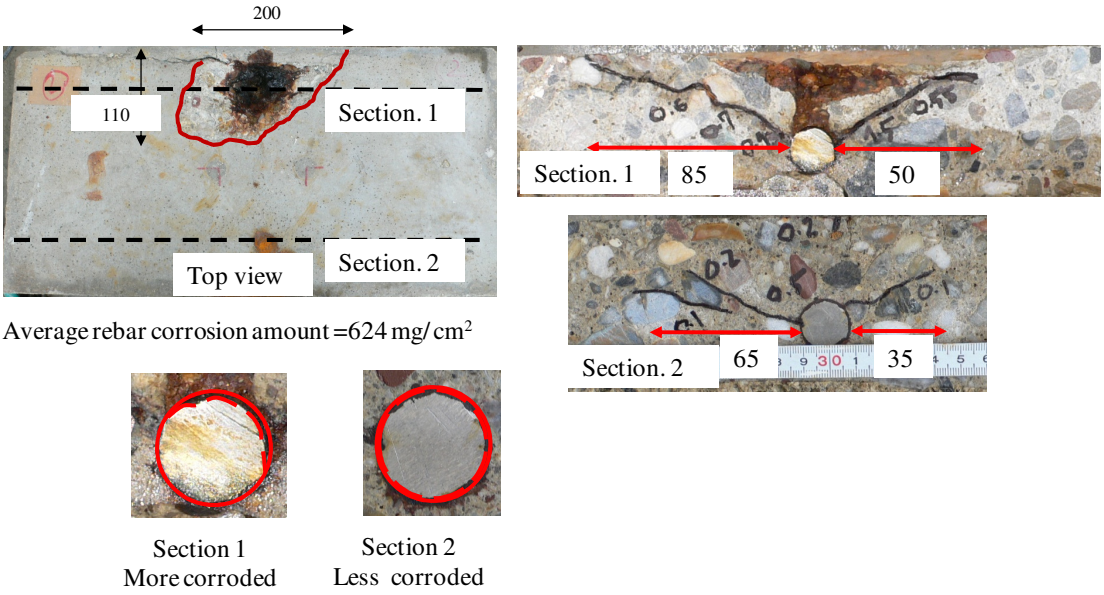

Figure 8.3. Crack patterns of specimen No. 2

Due to the different cases of the rebar longitudinal local corrosion, the surface crack patterns are different for each case and different from the uniform corrosion case presented in the previous chapters. In the case of longitudinal local corrosion of the rebar, the surface crack patterns are varied along the specimen's length. This is a three-dimensional behaviour of the crack propagation.

8.2.3 Simulation of longitudinal local corrosion

8.2.3.1 Modeling of specimen

As described above, the longitudinal local corrosion of rebar induces three-dimensional behavior of the crack propagation. Therefore, the proposed 3D-RBSM model is appropriate to simulate the cracking behavior in this condition. In the analysis, mesh sizes of the Voronoi particles are arranged with 15 mm mesh in the cover thickness crossing the specimen width and 40 mm mesh in the other areas as shown in **Figure 8.4**.

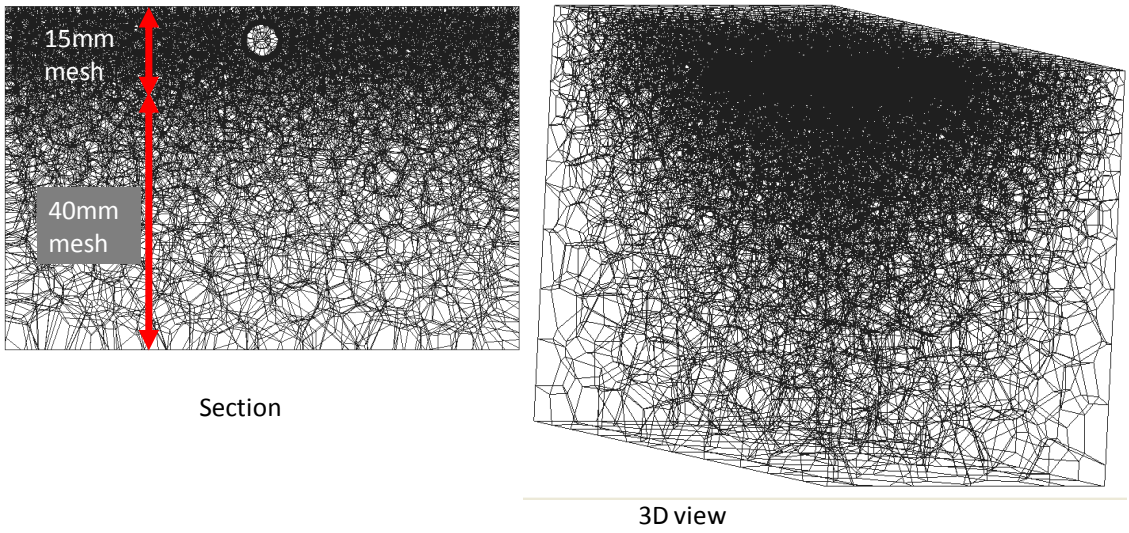

Figure 8.4. RBSM modeling of specimen

The longitudinal local corrosion appears that rebar corrosion amount is not uniformly distributed along the rebar length. In order to simulate the longitudinal local corrosion of the rebar, the corrosion amount of the rebar is re-distributed along the rebar length. Based on the observation from the experiment shown in **Figure 8.2** and **Figure 8.3,** two rebar corrosion patterns along the rebar length are assumed in this analysis for specimens No. 1 and No. 2 as shown in **Figure 8.5**.

The QUARTER local corrosion model is also assumed for the corrosion section of the rebar in the analysis .

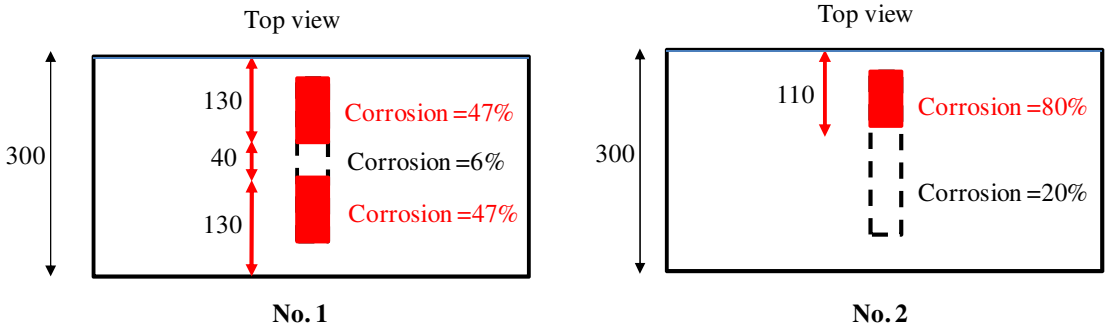

Figure 8.5. Assumed local corrosion pattern for simulation

8.2.3.2 Analytical results of specimen No.1

Figure 8.6 shows analytical results of specimen **No. 1** including the surface crack pattern top view and several sections showing internal cracks at the average corrosion amount 540 mg/cm^2. For clarity, only cracks at visible width are shown in the crack patterns in discussed in the previous chapters. On the top view of the specimen, the surface crack patterns appear similar to the experiment in **Figure 8.2**. That is, surface cracks widely distribute at two ends of the specimen and narrowly distribute in the middle of the specimen. Internal crack patterns are also obtained from the analysis and shown in Section 1 and Section 2 corresponding to the dashed lines shown on the top view. The analytical crack patterns show the similarity for each section. In each section, internal cracks propagate from the rebar toward the surface and the internal crack lengths are 84 mm and 72 mm on Section 1 and Section 2 respectively. The internal cracks, therefore, are reasonable agreement with the test results.

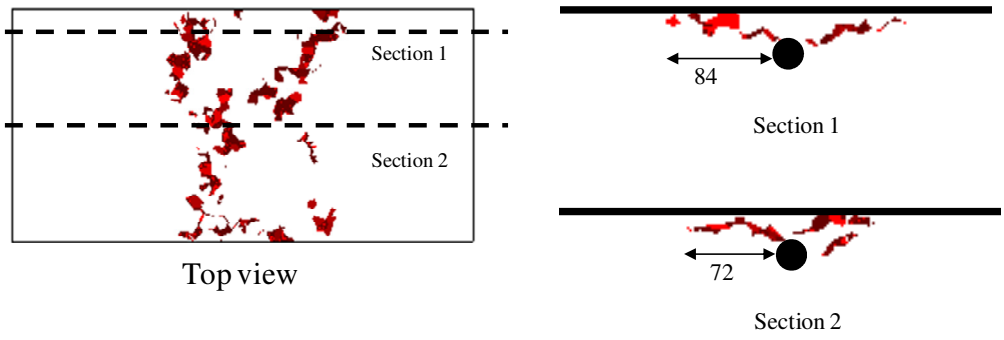

Figure 8.6. Analytical crack patterns of specimen **No. 1**

8.2.3.3 Analytical results of specimen No.2

Figure 8.7 shows analytical results of specimen **No. 2** including the surface crack

pattern top view and several sections showing internal cracks at the average corrosion amount 630 mg/cm^2. On the top view of the specimen, surface cracks appear in an area about 170 mm x 235 mm which is similar to the size of the delaminated part shown in the experiment in **Figure 8.3**. Outside the area 170 mm x 235 mm of the surface cracks, no visible crack is shown on the top view of the specimen. Internal crack patterns are obtained from the analysis and shown in Section 1 and Section 2 corresponding to the dashed lines shown on the top view. Section 1 shows internal cracks reaching the surface of the specimen at both sides of the rebar with the internal crack lengths about 80 mm – 95 mm. The internal cracks on Section 2 are shorter with the lengths about 50 mm. The internal cracks, therefore, are also reasonable agreement with the test results.

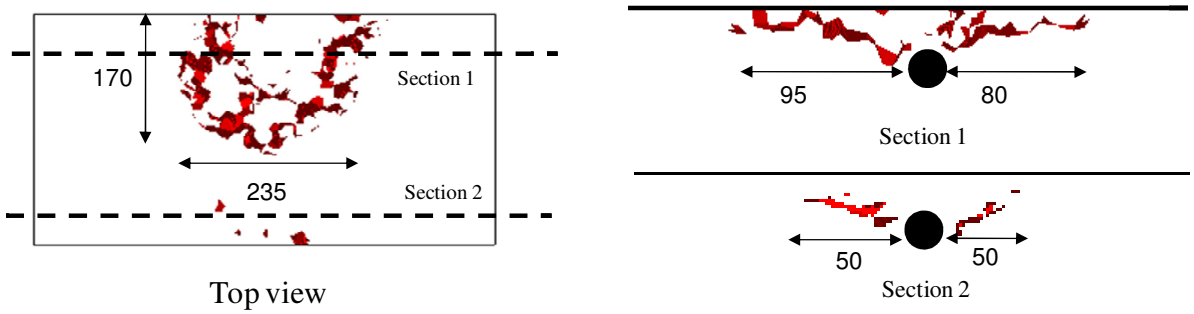

Figure 8.7. Analytical crack patterns No. 2 at corrosion amount 630 mg/cm^2

The simulation results show agreement with the experimental results in terms of surface crack patterns, delimitation area on the specimen surface, internal crack patterns and internal crack lengths. The analytical results show the merit of 3D-RBSM analytical method as it can reasonably simulate the 3D behavior of cracking due to the longitudinal local corrosion induced. It is clearly shows that 2D analytical method cannot simulate the cracking behavior in this case. It is also convenient to assume the

rebar longitudinal local corrosion directly in the analysis.

8.3 Simulation of de-lamination phenomenon of a real slab structure

8.3.1 Survey data

The surveyed concrete slab was a part of the slab structure of an expressway in Japan. The expressway concrete structure has been in service for 23 years. The maintenance process has been done in a period basis to monitor damage and degradation of the structure.

It was reported that no surface crack was found in the previous survey, however, in the recent investigation (in year 2010), a part of concrete surface was de-laminated from the slab surface.

Figure 8.8 briefly shows some survey data in this investigation. The de-lamination part was found on the bottom surface of the slab structure. The size of the de-lamination part is about 150 mm x 220 mm. The measured concrete cover is about 30 mm as shown **Figure 8.8**, the original rebar diameter was D19. Based on the observation of the corroded rebar, one part of the rebar length was significantly corroded rather than the other part of the rebar.

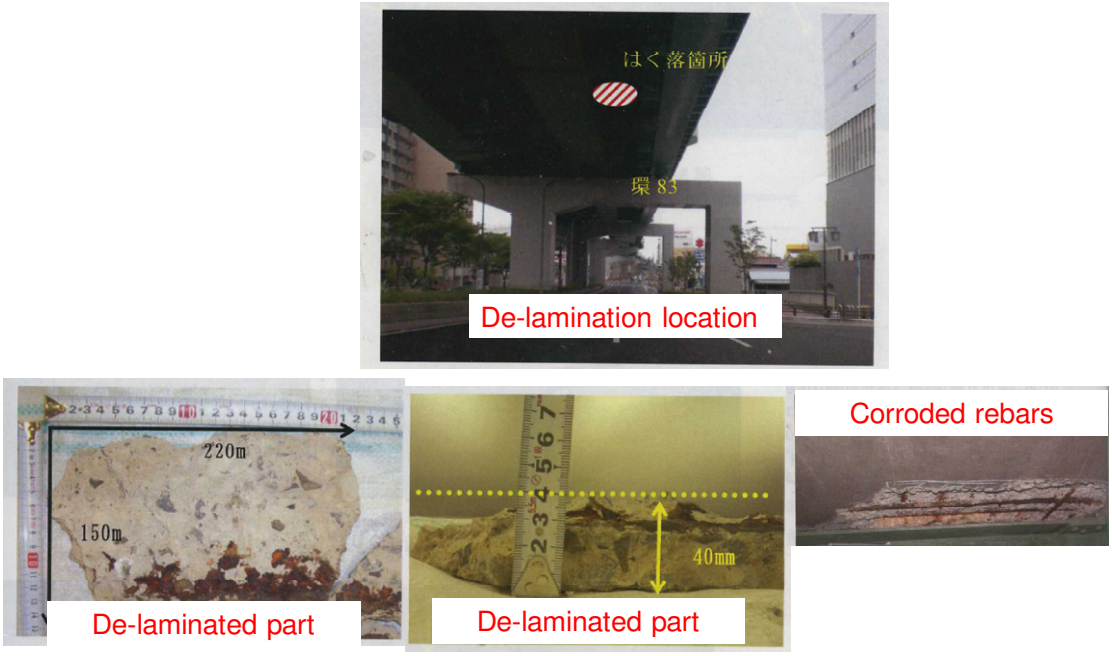

Figure 8.8. Survey results of the de-lamination of expressway slab structure

8.3.2 Analytical parameters

Based on the above survey data, it can be assumed that the de-lamination was caused by the corrosion of one rebar and only a part of the rebar length was corroded. This phenomenon appears similar to the longitudinal local corrosion along the rebar of the specimens in **Figure 8.2** and **Figure 8.3**.

In order to investigate the de-lamination caused by the rebar corrosion and effects on this phenomenon, the concept of longitudinal local corrosion model presented in **Figure 8.5** is applied and effects of cover thickness and local corrosion length are investigated. **Figure 8.9** shows the slab dimensions and parameters assumed in the analysis. The slab size is assumed 600 mm x 600 mm and the slab thickness is 230 mm based on the design document. The concrete compressive strength is assumed as 18.5 MPa in the analysis. The concrete cover thickness is assumed as 10 mm, 20 mm and 30 mm because the actual cover thickness may be varied due to the actual construction

condition. The rebar corrosion length is assumed as 100 mm, 200 mm and 600 mm (full length of the slab) because an actual corroded length of the rebar was unknown. In the analysis, 50 mm wide supports are given under the slab as shown in **Figure 8.9**.

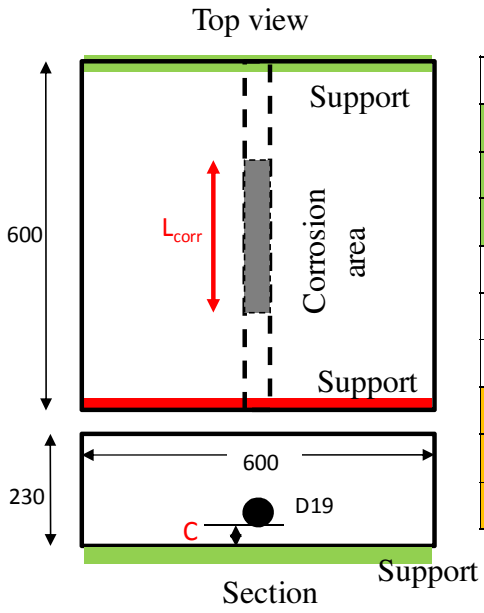

Case	C	L_{corr}
1	10	600
2		200
3		100
4	20	600
5		200
6		100
7	30	600
8		200
9		100

Figure 8.9. Analytical setting dimensions and parameters of slab

8.3.3 Effects of concrete cover thickness and local corrosion length

Figure 8.10 shows internal crack patterns at rebar corrosion amount 250 mg/cm^2 for various cover thicknesses (C) and various rebar local corrosion lengths (L_{corr}). The cross sections are obtained at the middle of the specimens or at the center of rebar. The internal crack pattern appears similar for each case. That is, the internal cracks diagonally propagate toward the surface and then cause de-lamination of the surface of the slab. Effect of variation of the concrete cover thickness can be understood on the internal crack patterns, that is, larger concrete cover thickness tends to induce longer internal cracks. This effect is evaluated quantitatively in the following part of this section.

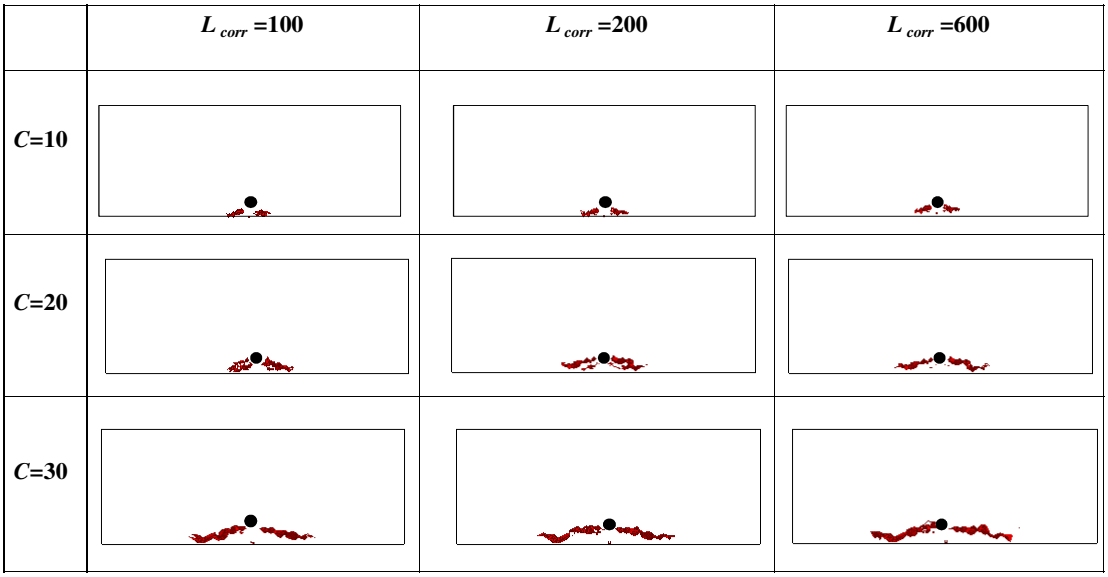

Figure 8.10. Analytical internal crack patterns of slab

Figure 8.11 shows propagation of internal crack length, which are measured from the rebar sides to the visible crack tips horizontally. The internal cracks initiate after the rebar corrosion amount about 50 mg/cm^2 and the rapidly propagate. In the later stage of the corrosion, internal crack lengths appear to converge to particular values. In each case of the same concrete cover thickness (C), the longer rebar corrosion length (L_{corr}) induces longer internal cracks but the difference is small. In the case of the same corrosion length (L_{corr}), the large concrete cover thickness induces longer crack lengths as clearly shown in **Figure 8.11**. With a longer rebar corrosion length L_{corr} = 600 mm, the concrete cover thickness C = 10 mm or C = 20 mm also induces shorter internal crack lengths than the ones induced by C = 30mm with even thought L_{corr} is only 200 mm. Therefore, the concrete cover thickness significantly affects the internal crack lengths.

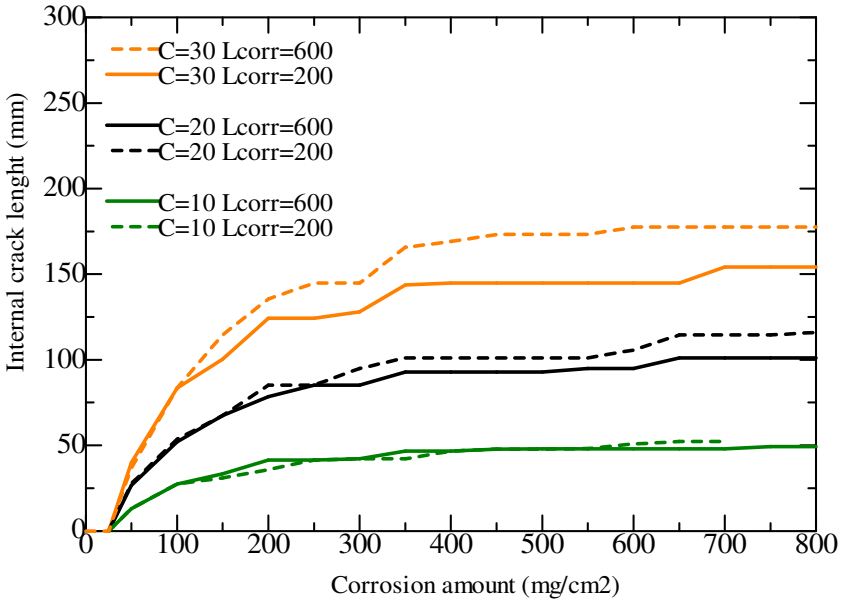

Figure 8.11. Propagation of internal crack length

Figure 8.12 shows surface crack patterns at rebar corrosion amount 500 mg/cm^2 for various cover thicknesses and various rebar corrosion lengths. Based on the surface crack patterns, the potential de-lamination area of the slab surface are estimated as also shown in this figure for each case. Basically, at the same value of C, longer L_{corr} induces longer surface area length. It is noted that in the case of L_{corr} = 600 mm (full length of the rebar), the maximum length of the surface crack area is limited between the supports given in the analysis as mentioned above. At the same value of L_{corr}, larger C induces wider surface crack area width. It can be seen that once rebar corrosion occurred, at the same level of rebar corrosion amount, the larger concrete cover thickness potentially induce a larger de-lamination (damage) area on the concrete cover. This behavior should be noted in the concrete design and the maintenance because the standards normally require large concrete covers in the design of structure in corrosive environments (Bentur, 1997). The effect of the rebar local corrosion length L_{corr} on the surface damage

area is also important as shown in the **Figure 8.12**. So, it is necessary to assume precisely local corrosion lengths of the rebar in the analysis.

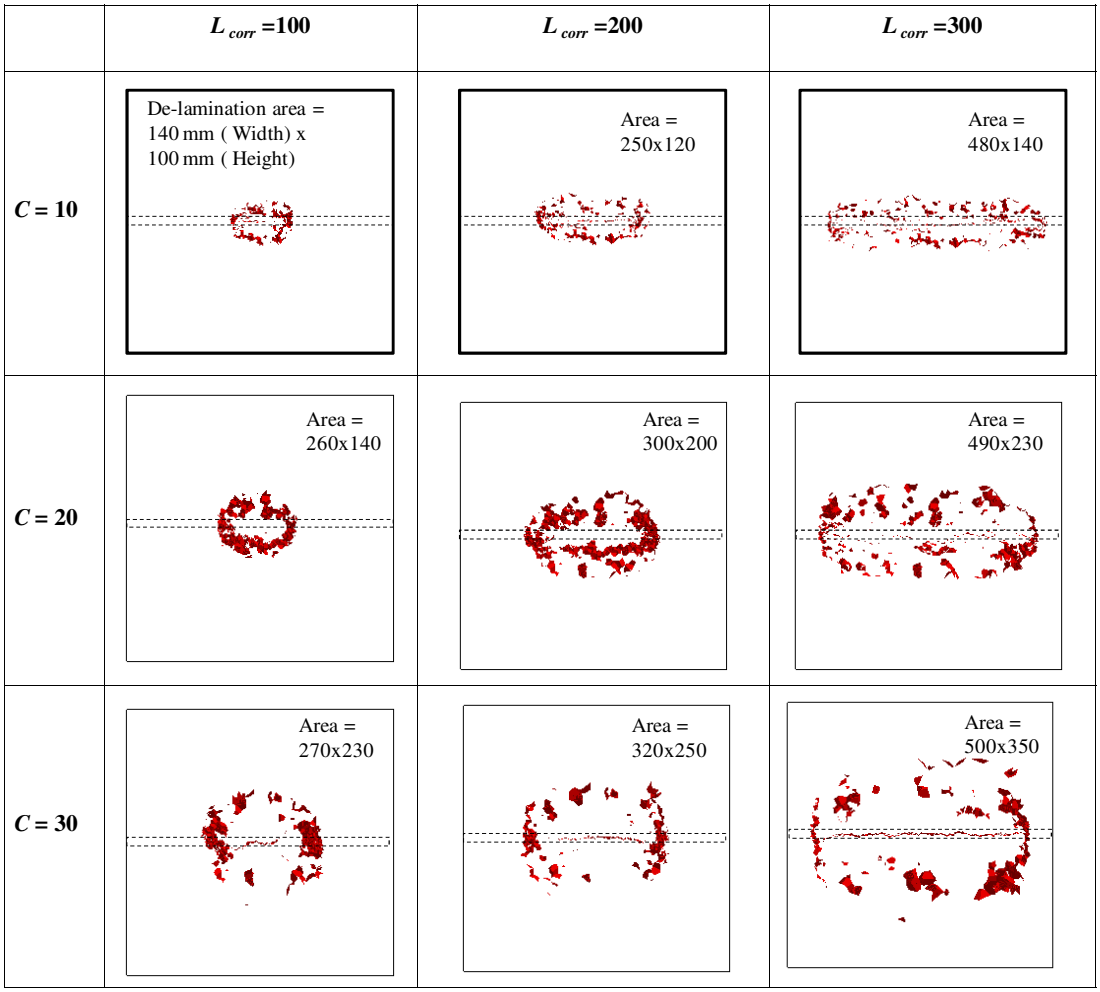

Figure 8.12. Surface crack area at rebar corrosion amount 500 mg/ cm^2

Figure 8.13 shows surface deformation of the specimens with the same corrosion length L_{corr} = 200 mm and various cover thicknesses C = 10 mm, 20 mm and 30 mm at rebar corrosion amount 600 mg/cm^2. Based on the 3D-deformation, the de-lamination phenomenon of the bottom surface of the slab can be observed. As shown in this figure, at the same value of L_{corr}, the concrete cover thickness C = 30 mm shows largest area of the de-lamination of the bottom surface of the slab.

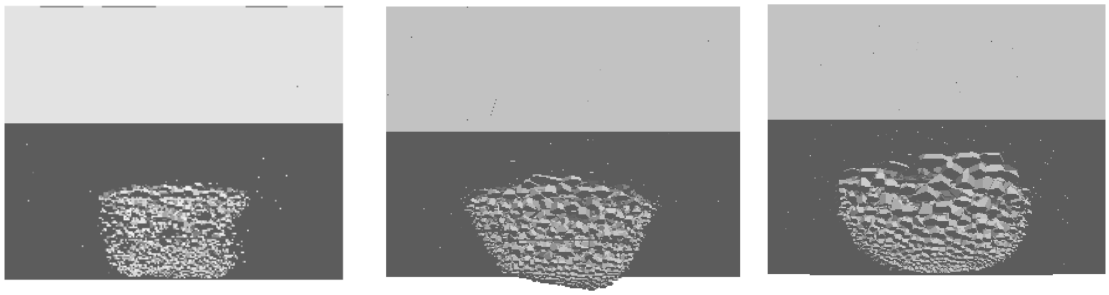

C =10 L_{corr} =200 | **C =20** L_{corr} =200 | **C =30** L_{corr} =200

Figure 8.13. Surface de-lamination of the slab

(magnification =30)

The analytical results show that the 3D-RBSM analytical model can reasonably simulate the de-lamination phenomenon of the slab structure. The 3D-RBSM analytical model clearly shows its advantage to simulate the cracking behavior in this condition.

8.4 Summary

This chapter investigated cracking behavior due to the longitudinal local corrosion o the rebar and de-lamination phenomenon of concrete cover based on the experiment and the analysis. The experiment in the laboratory condition and the survey data of the real slab structure were used to understand the cracking behavior in this case. The 3D-RBSM analytical model was applied to simulate the laboratory specimens and the real-slab structure and the analytical results are verified against the experimental results and the survey data. The following summary and conclusions were derived in this chapter.

(1) The longitudinal local corrosion along the rebar induced 3D behavior of crack propagation. That is, surface crack patterns and the internal crack propagation were varied along the specimen length. The 3D- RBSM analytical model is

necessary to simulate this behavior and it shows good agreement with the experimental results in the laboratory condition. The important note was derived that in the case of longitudinal local corrosion of the rebar, the internal cracks cannot be predicted from the surface cracking condition

(2) De-lamination phenomenon of the real-slab structure of the expressway structure was simulated and the simulation results appeared similar to the survey data of the slab structure.

(3) Based on the analytical results, the effects of concrete cover thickness and local corrosion length were clarified. That is, once rebar corroded, a larger concrete cover thickness potentially caused longer internal cracks and larger de-lamination areas on the slab concrete cover. This behavior should be noted in the design and maintenance processes. The local corrosion length affects the surface de-lamination area so it is necessary to precisely estimate local corrosion length of the rebar in order to evaluate the potential surface de-lamination.

9. CONCLUSIONS AND FUTURE RESEARCH

9.1 Summary and conclusions

The dissertation presented the study on cracking behaviour of concrete due to rebar corrosion. The study was conducted by using the experiment in laboratory condition and the numerical analysis. The following summary and conclusions are derived in the dissertation.

An experimental method of the electric accelerated corrosion test was developed in the laboratory condition. The experimental method included several advanced methods such as directly measuring surface crack width during the electric corrosion test; cutting, observing and measuring internal crack propagation directly; measuring specimen surface deformation precisely using laser equipment; observing and measuring specimens at several rebar corrosion amounts to investigate the crack propagation. Theses advanced experimental methods enabled to obtain the experimental results which are more fulfilled and precise than the previous ones reported in the literature.

Based on the experimental results, cracking behaviours of the specimens could be understood and the applicability of the proposed analytical model could be verified. Various specimen series designed for particular study purposes were tested using electric means. The experimental results of these specimen series presented the cracking behaviour of concrete due to rebar corrosion in various conditions. The contents of the experimental method and the specimen series conducted in this study were described in Chapter 2.

Chapter 3 presented the analytical method based on the 3D- RBSM method (as a structural analysis) combined with the three-phase corrosion material model including rebar, corrosion products layer and concrete. The internal expansion pressure due to rebar corrosion was proposed by applying the initial strain problem on the three-phase corrosion material model. Several corrosion models such as local corrosion model and penetration of corrosion products into cracks after cracking of concrete were also proposed in this chapter. It showed that the proposed RBSM method combined with the three-phase material model could simulate the corrosion induced cracking behaviour in several conditions reasonably.

In Chapter 4, the proposed analytical model was quantitatively and qualitatively verified against the experiment of the specimen series 150*150-C30. The values of the thickness and linear elastic modulus of corrosion products layer as of 1 mm and 500 MPa respectively were recommended for the analytical model. The local corrosion model on the rebar section was necessary to be applied in the analysis rather than the uniform corrosion model since it strongly influenced the internal crack patterns. The

effect of penetration of corrosion products into cracks was necessary to be considered because it quantitatively influenced the crack propagation. The penetration threshold value is a sensitive parameter in the model and it would require further studies to evaluate its values.

A cracking mechanism for this specimen series was developed and it showed that once rebar corroded, visible surface cracks initiated from the specimen surface and then propagated to the rebar. After that, the internal cracks initiated and propagated with the increase of the surface crack widths. A mechanism of the relationship between surface deformation, surface crack propagation, and internal crack propagation was clarified. That is, the surface crack width is dependent on the surface deformation value and the surface deformation area is related to the internal crack propagation. Therefore, in order to evaluate the surface crack propagation, the internal crack propagation also needs to be adequately evaluated.

Chapter 5 showed that the variation of rebar diameter significantly affected the initiation of surface cracks and internal cracks as well as the crack propagation after the initiation. Tsutsumi's k value significantly affected the crack pattern of the single-rebar specimen. However, when k value is between 2 and 2.5, a single crack also appeared and developed in the concrete cover which was lower than the threshold proposed by Tsutsumi. The variation of the width of internal expansion area influenced the crack propagation. However, the variation of the height of the internal expansion area did not affect the cracking behaviour. So, only the variation of the internal expansion area facing to the concrete cover influenced the cracking behaviour. It was necessary to determine which parameters are related to the crack propagation since k value or C/D

ratio did not have a clear relationship with the crack width propagation.

Chapter 6 investigated the crack propagation of single rebar specimens with various sizes experimentally and analytically. Based on this study, effects of specimen sizes were clarified. Internal cracks were dominant in comparison with surface cracks in large width specimens. Internal crack lengths developed rapidly after the crack initiation and the crack lengths tended to converge to a particular value; in this study, with the concrete cover thickness as 30 mm, the maximum internal crack length was about 90 – 100 mm. The internal cracks tended to propagate toward the concrete surface which caused a potential de-lamination area on the concrete surface. Cover thickness was important in the crack accumulation and the surface crack initiation while other dimensions did not have too much influence. Variation of the specimen width played an important role in the surface crack propagation and the internal crack propagation. That is, wider specimens resulted smaller surface cracks and longer internal cracks at the same level of rebar corrosion amount. Variation of specimen height did not influence the crack propagation, both surface cracks and internal cracks.

Chapter 7 simulated crack propagation due to the multi-rebar corrosion and investigated the effect of rebar spacing on the crack propagation. As a result, the cracking mechanism of multi-rebar corrosion specimens was clarified. The applicability of the analytical method in the case of multi-rebar corrosion was confirmed by the experimental results including crack patterns, surface crack propagation and internal crack propagation. In the case of multi rebar-corrosion, internal cracks joined together between the rebars and developed to large cracks earlier than the internal cracks in the

single-rebar corrosion. In the multi-rebar corrosion, internal crack propagated earlier than surface cracks. That is, when surface cracks could be observed, internal cracks had already developed. Rebar spacing significantly affected the crack patterns and the crack propagation in the case of the multi-rebar corrosion. The dominance and the propagation of internal cracks tended to cause de-lamination of the concrete cover in the multi-rebar corrosion.

Chapter 8 investigated cracking behavior induced by the longitudinal local corrosion phenomenon along the rebar. It included propagation of internal cracks and de-lamination phenomenon of concrete cover. The experiment in the laboratory condition and the survey data of the real slab structure were used to understand the cracking behavior and to verify the analytical results. The longitudinal local corrosion along the rebar induced a 3D behavior of the crack propagation. That is, surface crack patterns and the internal crack propagation were varied along the specimen length and a part of concrete surface was de-laminated. The 3D- RBSM analytical model, therefore, was necessary to simulate this behavior and it showed good agreements with the experimental results in the laboratory condition and the survey data of the real slab structure. The analytical results showed that once rebar corroded, a larger concrete cover thickness potentially caused a larger de-lamination area on the slab concrete cover. This behavior was necessary to be noted in the concrete design and the maintenance because the standards normally required large concrete covers in the design of structures in corrosive environments. The local corrosion length of the rebar significantly affected the de-lamination area of the slab surface. So, it is necessary to determine this parameter precisely in order to evaluate the damage due to rebar corrosion properly.

9.2 Comments to the maintenance process

Most of the current regulations in the concrete structure maintenance are based on surface condition of the structure. For example, Category A, B and C in the maintenance part of the JSCE specification 2001 (Takewaka and Kaneko, 2006) are based on visible deterioration on the structure, for example surface crack width, etc. However, the outcome of this study showed that the surface deterioration situation did not appear unique with the internal deterioration. That is, the surface crack propagation depended on the internal crack propagation, specimen sizes, rebar corrosion situation, etc. In some conditions, surface cracks were not observed but internal cracks already developed and caused de-lamination or spalling of concrete cover. So, the deterioration situation of structure cannot be adequately evaluated if it is only based on the surface condition. It is, therefore, necessary to also investigate other parameters such as rebar corrosion condition, rebar spacing, concrete cover thickness, etc in order to evaluate the structure deterioration more precisely in the maintenance process.

9.3 Suggestions for future research

Based on the outcome of the current study, some suggestions for future researches concerning the cracking behavior of concrete due to rebar corrosion are summarized as follows.

Regarding the three-phase material corrosion model, the current study includes several assumptions which need to be further developed. The thickness of corrosion layer products is kept to be constant as 1 mm during the analysis. This is a fictitious layer thickness and it is different from the real one which is increased during the corrosion process.

The corrosion products layer was assumed as linear elastic material in this study. Several researchers conducted direct compression tests on the corrosion products collected from the electric corrosion test and they found that the corrosion products behaved non-linearly after the peak. So, in future studies, the non-linear behavior of the corrosion products should be considered in the analysis.

The local corrosion model on the rebar section is an assumption in the analysis and it is necessary determine a unique corrosion model to be used in the analysis.

The threshold of penetration of corrosion products into cracks is just analytical assumption and it needs to be determined or confirmed by an experiment. Other factors such as corrosion penetration speed, penetration into concrete pores needs to be clarified.

Regarding behavior of concrete, the creep effect of the concrete needs to be considered since the cracking due to rebar corrosion process takes relatively long time to occur.

Factors to predict the crack propagation need to be formulated since the C/D ratio or the k value cannot present a relationship with the crack propagation.

Application of 3D behavior of the analytical model is limited in this study. It is necessary to verify the applicability of the analytical model against further 3D cracking behaviors.

Most of the specimens tested and simulated in this study are conducted in the laboratory condition with a high corrosion electric current density which may be different from the real structure corrosion condition with very small current density. Therefore, the analytical model will need to be applied on the real-structure condition in order to evaluate the crack propagation of the existing structures.